

**TRIPLET STATE DYNAMICS OF CHLOROPHYLLS
IN PHOTOSYNTHETIC REACTION CENTERS AND
MODEL SYSTEMS**

CENTRALE LANDBOUWCATALOGUS



0000 0213 7541

40051

Promotor: dr. T.J. Schaafsma
hoogleraar in de moleculaire fysica

NN08201, 1135

F.G.H. van Wijk

**TRIPLET STATE DYNAMICS OF CHLOROPHYLLS
IN PHOTOSYNTHETIC REACTION CENTERS AND
MODEL SYSTEMS**

Proefschrift

ter verkrijging van de graad van
doctor in de landbouwwetenschappen,
op gezag van de rector magnificus,
dr. C.C. Oosterlee,
in het openbaar te verdedigen
op vrijdag 1 mei 1987
des namiddags te vier uur in de aula
van de landbouwuniversiteit te Wageningen.

ISBN 259 457

*The road goes ever on and on
Down from the door where it began.
Now far ahead the Road has gone,
And I must follow, if I can,
Pursuing it with eager feet,
Until it joins some larger way
Where many paths and errands meet.
And whither then? I cannot say.*

*J.R.R. Tolkien
(from "The Lord of the Rings")*

STELLINGEN

1. De ladingsscheiding in gereduceerde fotosynthetische reactie centra via het z.g. radikaal-paar mechanisme, leidt in hoog magneetveld niet per definitie tot een uitsluitend T_0 -gepolariseerde electron donor triplet toestand, waarneembaar in het EPR $\Delta m = \pm 1$ triplet spectrum als een AEEAAE spin polarisatie patroon.

Dit proefschrift, Hoofdstukken II, IV, en V.

2. De relatieve amplitude van de Y-pieken in het $\Delta m = \pm 1$ triplet EPR spectrum van fotosynthetische reactie centra van purperbacteriën kan gebruikt worden om de nativiteit van het primaire acceptor ijzerchinoxon complex te bepalen.

Dit proefschrift, Hoofdstuk VI.

3. De tijdsresolutie van een EPR spectrometer wordt niet principieel beperkt door de frekwentie van 100 kHz, toegepast voor de magneetveld modulatie, zoals door sommige auteurs wordt beweerd.

M. Plato, und K. Möbius, Messtechnik 8 (1972) 224-234.
"Moderne Messtechnik und Datenverarbeitung in der Elektronenspinresonanz-Spektroskopie"

A.D. Trifunac, and R.G. Lawler, Magnet. Reson. Rev. 7 (1982) 147-174.

"Detection of transient paramagnetic intermediates by time-resolved magnetic resonance and related techniques"

4. De conclusie van Angerhofer et al. dat er tekenomkeer plaats vindt in de ODMR spectra van antennehoudende reactie centra preparaten, vergeleken met antenneloze reactie centra preparaten, is op grond van hun eigen waarnemingen niet gerechtvaardigd.

A. Angerhofer, J.U. van Schütz, and H.C. Wolf, Z. Naturforsch. 39C (1984) 1085-1090.

"Fluorescence-ODMR of reaction centers of Rhodospseudomonas viridis"

5. Bij het onderzoeken van de betrouwbaarheid van hun fluorescentielevensduurmetingen gaan DeWilton et al. ten onrechte voorbij aan neveneffecten van hoogvermogen laserpulsen op het monster.

A. DeWilton, L.V. Haley, and J.A. Koningstein, Can. J. Chem. 60 (1982) 2198-2206.

"Detection limitations of photomultiplier tubes in pulsed-laser emission spectroscopy: time-resolved fluorescence spectra of chlorophyll solutions"

6. De superfusie snelheid die Brodelius en Vogel toepassen bij de bestudering van plantecellen onder fysiologische condities, m.b.v. ^{31}P in-vivo NMR, is daarvoor te hoog, zodat deze cellen in een niet-fysiologische toestand van voortdurende substraat-uitputting verkeren.

P. Brodelius, and H.J. Vogel, J. Biol. Chem. 260 (1985) 3556-3560.
"A phosphorus-31 nuclear magnetic resonance study of phosphate uptake and storage in cultured Catharanthus roseus and Daucus carota plant cells"

7. Bij de polarografische bestudering van de binding van zware metalen aan polycarbonzuren, moeten Subramanian en Natarajan rekening houden met de verschillen in diffusiecoëfficiënten van de diverse speciës.

R. Subramanian and P. Natarajan, Ind. J. Chem. 24A (1985) 432-434.
"Complexation of Cu(II) with poly(acrylic acids) - A polarographic study"

8. Het systeem van de z.g. "No Claim" bonussen, gebruikt in de auto-verzekeringswereid, verhoogt het aantal gevallen waarin doorgere-den wordt na een ongeval, en dient daarom te worden ingeperkt.

9. Bij de discussies over de stimulering van het aantal geboorten in verband met het probleem van de 'vergrijzing' van de bevolking, realiseert men zich onvoldoende dat overbevolking een groter probleem is.

10. Bedrijven, instellingen, en/of diensten, waarvan het staats-eigen-dom geen algemeen belang dient, moeten worden geprivatiseerd.

11. Bedrijven die op commerciële basis opereren en waarvan de produkten en/of diensten de uitoefening van de algemeen belang dienende taken van de overheid bemoeilijken, moeten worden genationaliseerd.

12. Zoals vrijwel niemand, weten ook de meeste socialisten niet waarom de Dag van de Arbeid op 1 mei wordt gevierd.

Fred van Wijk

Triplet state dynamics of chlorophylls in photosynthetic reaction centers and model systems.

Wageningen, 1 mei 1987

Plan mijn Moeder

VOORWOORD

Alleen mijn naam staat op het omslag van dit proefschrift. Dat wil echter geenszins zeggen dat de inhoud slechts dankzij mij alleen tot stand is gekomen. Ik wil hier dan ook beginnen met alle medewerkers en studenten van de vakgroep Moleculaire Fysica te bedanken voor hun raad en daad, en vooral voor de uitstekende sfeer die een promovendus op de been houdt.

In het bijzonder wil ik Tjeerd Schaafsma bedanken voor zijn niet-aflatende inzet en de vrijheid die hij mij heeft gelaten in het onderzoek. Tjeerd, de discussies met jou waren altijd bijzonder stimulerend en brachten het onderzoek begripsmatig vaak een stap verder.

De inbreng van Peter Gast heeft zijn stempel duidelijk op dit werk achtergelaten. Peter, met jouw komst kwam het onderzoek naar de bacteriële fotosynthese in een ware stroomversnelling. Vele uurtjes vrije tijd bracht je op het lab door om mij te helpen met dit onderzoek. Jouw inbreng is voor mij van onschatbare waarde geweest.

Geavanceerde apparatuur willen gebruiken, en er liefst meer uithalen dan er in zit, was onmogelijk zonder de hulp van Adrie de Jager en Arie van Hoek. Promovendi komen en promovendi gaan, maar zonder jullie hulp zou hun het lachen snel zijn vergaan.

'Mijn' studenten Caroline Beijer en Riet van de Steeg, ook jullie dank ik voor de plezierige en de soms overstimulerende wijze waarop we hebben samengewerkt. Nu alleen de verslagen nog...

Raivo Tamkivi from Tartu was a great help for me during the early stages of this work. Dear Raivo, I thank you for the many useful discussions. Especially the tricks you taught me for analyzing complex kinetic schemes proved very useful throughout my research time.

I thank Peter Hore (Oxford) for sending me his preliminary results and the pleasant way we cooperated during the very last part of my research period in Wageningen.

Verder wil ik Jannie Bijl en Riet Mes bedanken voor hun geduld met mij en de tekstverwerker. Zonder Hennie van Beek zou er geen tech-

nische vooruitgang gerealiseerd zijn. Ruud Spruyt en Rob Koehorst waren mij meer dan eens behulpzaam met het 'natte' werk, waarvan helaas te weinig in dit proefschrift terecht is gekomen. Ulbert, de discussies met jou heb ik zeer gewaardeerd. Ook wil ik hier Raymond Verhaert noemen, die mij een hoop heeft geleerd van de 'nellecim'.

De mensen van de tekenkamer en de fotograaf hebben voortdurend garant gestaan voor een nette weergave van bijna alle figuren in dit boekje.

Elsevier Scientific Publishing Company gaf toestemming voor het reproduceren van een tweetal artikelen.

Ten slotte wil ik mijn vriendin Mieke bedanken voor haar bereidheid met mij mee te denken en menselijke steun. En het blijft jammer dat onze gezamenlijke EPR experimenten stopgezet moesten worden wegens het schrijven van onze proefschriften.

Nu zijn er nog steeds mensen die ik met name had willen bedanken, maar ik hoop dat zij het mij niet kwalijk nemen. Mijn dank is er niet minder om.

Fred van Wijk
2 februari 1987

CONTENTS

	page
I. GENERAL INTRODUCTION	1
1.1 photosynthesis	1
1.2 the photosynthetic reaction center of purple bacteria	3
1.3 the primary processes	8
1.4 the triplet state and its spin polarization	9
1.5 the radical pair mechanism	12
1.6 perspective and outline of this work	15
1.7 references	17
II. THEORETICAL ASPECTS OF STATIC AND DYNAMIC MAGNETIC INTERACTIONS IN SOME MULTI SPIN SYSTEMS	25
2.1 introduction	25
2.2 electron spin polarization and spin-lattice relaxation	27
2.3 a simple three electron spin model for P^F	29
2.4 references	43
III TIME-RESOLVING EQUIPMENT AND EXPERIMENTAL METHODS	47
3.1 introduction	47
3.2 a broad band tunable pulsed dye laser (Applied Optics (1987) in press)	50
3.3 the laser flash artefact in time-resolved EPR	58
3.4 microsecond time-resolution on a conventional EPR spectrometer using 200 kHz magnetic field modulation and phase-sensitive detection (Review of Scientific Instruments (1987) in press)	60
3.5 additional techniques and preparative methods	82

IV. STEADY STATE TRIPLET STATE SPIN POLARIZATIONS IN BACTERIAL REACTION CENTERS	85
4.1 introduction	85
4.2 interaction of a third spin with the radical pair in the photosynthetic bacterium <u>Rhodopseudomonas viridis</u> monitored by the donor-triplet electron spin polarization (Photobiochemistry & Photobiophysics 11 (1986) 95-100)	86
4.3 the relation between the electron spin polarization of the donor triplet state of the photosynthetic reaction center from <u>Rhodopseudomonas viridis</u> and the redox state of the primary acceptor (FEBS Letters 206 (1986) 238-242)	92
4.4 the electron spin polarization of the donor triplet state in native and modified reaction centers from <u>Rhodobacter sphaeroides</u> R-26 (submitted to Photochem. Photobiol.)	97
4.5 summary and conclusions	107
V. TRIPLET STATE SPIN DYNAMICS IN REACTION CENTERS FROM <u>RHODOPSEUDOMONAS VIRIDIS</u> AS STUDIED BY TIME-RESOLVED EPR	109
5.1 introduction	109
5.2 materials and methods	111
5.3 results	113
5.4 discussion	121
5.5 appendix	133
5.6 references	133

VI. PHOTO-ACTIVITY AND STABILITY OF THE REACTION CENTER PROTEIN FROM THE PHOTOSYNTHETIC BACTERIUM <u>RHODOPSEUDOMONAS</u> <u>VIRIDIS</u> IN REVERSED MICELLES	137
6.1 abstract	137
6.2 introduction	138
6.3 materials and methods	140
6.4 results	142
6.5 discussion	149
6.6 references	155
SUMMARY	159
SAMENVATTING	162

CHAPTER I

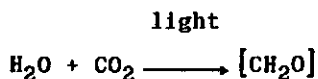
GENERAL INTRODUCTION

1.1 PHOTOSYNTHESIS

According to current scientific views, radiation from the sun has provided the energy to initiate and sustain all life on earth. The earliest forms of life were probably totally dependent on the breakdown of non-biologically formed energy-rich molecules for their survival. These organisms were strictly consumers of organic matter, not producers [1]. A major step forward in the evolution was the development of photosynthesis, which enabled living organisms to capture solar energy for the production of organic molecules. The impact of photosynthesis was overwhelming, e.g. it determined the composition of the earth's atmosphere, and provided enormous quantities of food for non-photosynthetic organisms, including man.

Photosynthesis is one of the most basic ecological and life-sustaining processes, and is therefore subject of wide scientific interest. During the last decades it has also been recognized that a basic understanding of the complexities of photosynthesis is required if we are to evaluate its true potential, and understand why it is such an efficient energy converting process. Such understanding could also provide clues to construct and improve artificial photosynthetic systems [2,3].

The major function of photosynthesis is to act as a pump transferring electrons and protons from a donor to an acceptor, using light as fuel. For plants and algae the donor is water, and carbondioxide is reduced and utilized to produce carbohydrates (e.g. sugars):



where CH_2O is the building-block of sugars.

Photosynthetic bacteria are not capable of oxidizing water, and use more reduced compounds. There are several types of photosynthetic bacteria, those that use reduced inorganic sulfur compounds as donor, such as H_2S (green and purple bacteria), and those that use non-sulfur donors (non-sulfur purple bacteria, e.g. Rhodospseudomonas viridis and Rhodobacter sphaeroides).

In 1905 Blackman [4] showed that the photosynthetic activity consists of a group of processes depending on light for their occurrence, and a second group which do not.

The majority of the light reactions involve a special class of pigment molecules: the chlorophylls (fig. 1). These pigments are embedded in specialized proteins, located in membranes of photosynthetic species. These chlorophyll-containing proteins can be divided into two types, according to their function. The first type catches photons (visible light) and transmits photon energy to a second type, a spe-

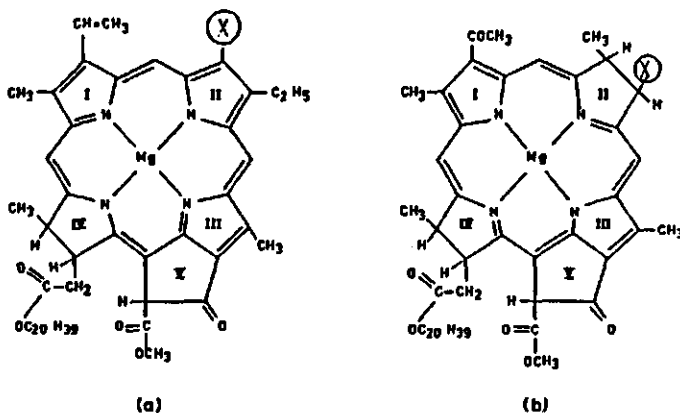


Figure 1.

Molecular structure of chlorophylls: a. $\text{X} = -\text{CH}_3$ for Chl-a, $\text{X} = -\text{CHO}$ for Chl-b;
 b. $\text{X} = -\text{C}_2\text{H}_5$ for BChl-a, $\text{X} = -\text{C}_2\text{H}_4$ for BChl-b.

cialized cluster of proteins: the reaction center (RC). The first type, "light-harvesters" or "antennas" make up the majority of the light-absorbing pigments: typically 100 - 300 antenna chlorophylls serve one RC.

After absorption of a photon the energy migrates from one pigment to another in the antenna system, and arrives in 10^{-11} s at the RC. In the RC the energy is trapped on a Chl-dimer (or BChl-dimer in bacteria), called the primary (electron) donor (P). The excited dimer ejects an electron to a nearby intermediary acceptor (I) in a few picoseconds. The electron on I is subsequently transferred to a primary acceptor, and then to a secondary acceptor, denoted Q_A , and Q_B , respectively. These processes make up the primary electron transfer reactions in the RC. The architecture of the RC and the primary photoreactions are described in more detail in the following paragraphs.

For more details on photosynthesis in general we refer to a number of recent reviews [5-13].

The present work is concerned with several processes in the RC's of Rps. viridis, Rb. sphaeroides, and Chromatium vinosum.

1.2 THE PHOTOSYNTHETIC REACTION CENTER OF PURPLE BACTERIA

The first photochemically active reaction center was isolated from Rb. sphaeroides R-26 in 1968 by Reed and Clayton [14]. From then on the isolation procedures have improved [15], culminating in the crystallization of purified RC's of Rps. viridis by Michel in 1982 [16], and later also of Rb. sphaeroides [17].

Although spectroscopic studies on the pigments in the RC's have revealed mutual distances and orientations of these chromophores [18-27], it lasted until 1984 before the first X-ray results provided unambiguous and accurate data on the absolute positions and orientations of almost all of the chromophores in the Rps. viridis RC [28-30]. Although during the crystallization step the primary and

secondary acceptors were at least partly lost [16], more recently improved methods resulted in fully photochemically active RC's [31,32], (with only half of the secondary acceptor lost during crystallization) [33]. Therefore the results from the crystal structure are believed to represent the native structure to a great extent. Also for Rb. sphaeroides R-26 RC crystals the photoactivity was demonstrated [34].

There is increasing evidence that the RC's from different purple bacteria are closely related, as reflected by large homologies in amino acid sequence [30], and almost identical pigment organization

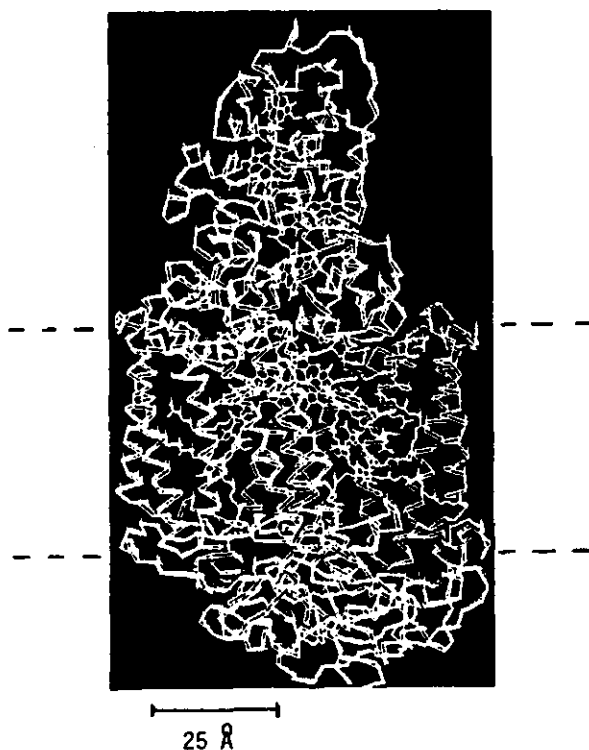


Figure 2.

Structure of the backbone of the reaction center protein complex of Rps. viridis as seen in the plane of the photosynthetic membrane (dashed lines). (From Ref. [30]).

[35-39,123]. Furthermore, it becomes more and more likely that the RC structure of purple bacteria probably resembles that of photosystem II in green plants (ignoring the oxygen evolving part of the latter) [40-42]. Thus, the elucidation of the RC structure from *Rps. viridis* bears a wide interest, and is a mile-stone in photosynthesis research.

The protein structure of the RC from *Rps. viridis* is shown in figure 2. It consists of four subunits, one of which is a c-type cytochrome, containing 4 heme groups. This cytochrome is tightly (but not covalently) bound to the actual RC, consisting of 3 subunits, labeled L, M, and H, corresponding to their relative molecular weight (low, medium, and high) [12,37]. The primary processes are all located within the LM complex. The outer dimensions of the RC-protein complex are roughly 30 x 70 x 130 Å³ [43]. The longest axis is perpendicular to the plane of the photosynthetic membrane. The cytochrome and the H-subunit protrude out of the membrane, and have polar amino acid

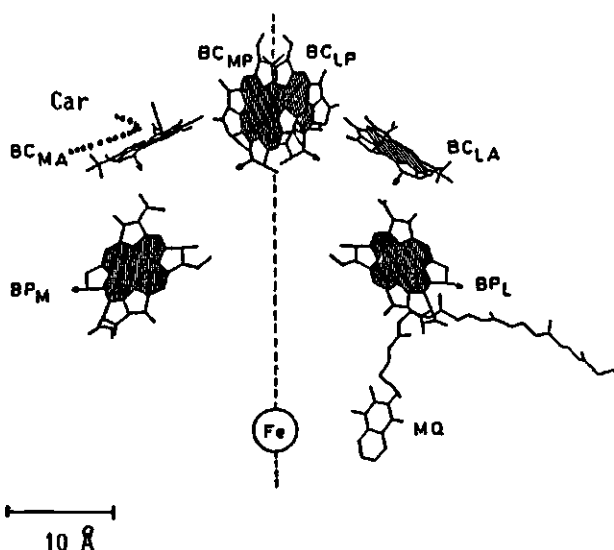


Figure 3.

Positions of the chromophores in the LM subunits of the reaction center from *Rps. viridis* as seen in the plane of the photosynthetic membrane. Car denotes the approximate position of the carotenoid [44]. Further details are given in the text (after ref [121]).

residues on their surface, whereas the LM part is buried in the membrane; its surface is apolar and covered with membrane lipids.

The positions of the chromophores in the RC are shown in figure 3. Note the C_2 -symmetry axis parallel to the long axis of the RC. The pigments are labeled L or M, corresponding to their location in the L or M protein subunit. The labels "P" and "A" denote the primary donor, and accessory pigment, respectively. The most likely position of the carotenoid in the RC [44] is very near the BC_{MA} . In Rps. viridis it is redundant.

The location of the accessory BChl (BC_{LA}) between the donor and intermediary acceptor I is puzzling, for its location seems to indicate its involvement in the early charge separation process. However, the spectroscopic results are contradictory with respect to the active role of BC_{LA} [45-51].

As the exact positions of the chromophores became resolved, the RC C_2 -symmetry seemed to suggest a dual electron transfer pathway. It was however demonstrated that only one of the two BP's was reduced on illumination [35,52-57], although delayed fluorescence measurements were explained invoking some participation of the other BP [58].

The acceptor side of the RC consists of a $Q_B-Fe^{2+}-Q_A$ complex [20, 36,59-67], where Q_A is the primary quinone acceptor (a menaquinone in Rps. viridis and C. vinosum [33,61,68], and ubiquinone in Rb. sphaeroides [61] and Q_B is the secondary quinone acceptor (a ubiquinone [33,69]). The structure of these quinones is shown in figure 4.

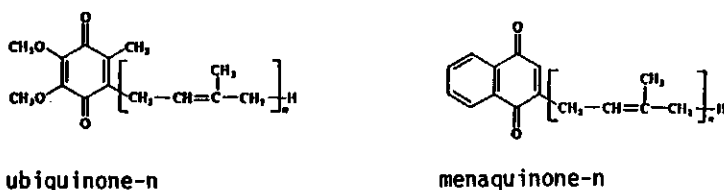


Figure 4.

Molecular structure of the ubiquinones and menaquinones (vit. k_2) as found at the acceptor side of bacterial reaction centers.

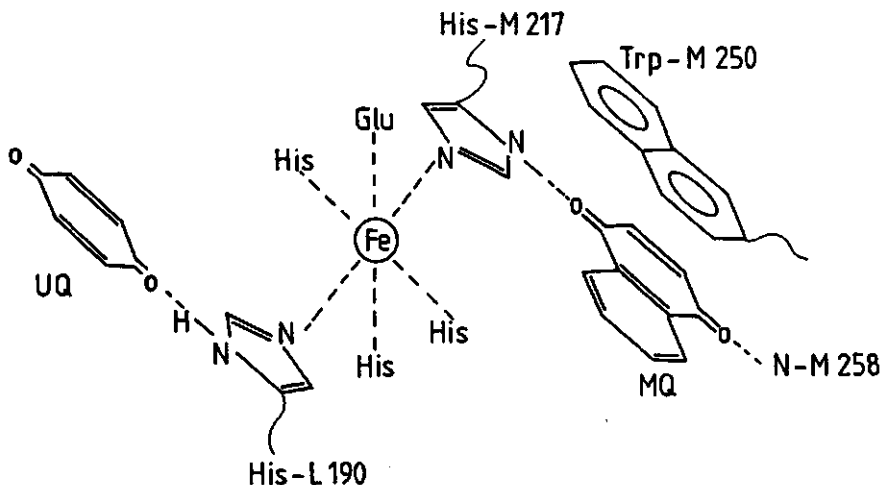


Figure 5. Schematic structure of the acceptor side of the reaction center from Rps. viridis, according to refs. [70,128]. Dotted lines indicate electrostatic interaction.

Since the acceptor side of the RC is of particular importance to the following chapters, it is more closely examined.

Lubitz and Plato [70] presented results, using the refined crystallographic data from Rps. viridis, demonstrating the electronic interactions between the Fe^{2+} , MQ, BP_L , and the surrounding amino acids, schematically shown in figure 5 (taken from [70] and [128]). From this figure it is seen that the Fe^{2+} and the quinones are not directly coupled [124], although a strong magnetic interaction between the electron spins of the singly reduced quinones and the high-spin Fe^{2+} has been measured [39,65,71]. (The spectroscopic behaviour of the quinone-iron complex is described in detail by Butler et al. [71,72].) The interaction between high-spin Fe^{2+} ($S=2$) and the reduced Q^- results in a characteristic shift of the EPR signal from Q_A^- to $g=1.83$, and $g=1.65$, first observed by McElroy [20,62,66,73]. Large anisotropic g - and dipolar effects are responsible for the shift and broadness of the Fe^{2+} EPR signal. This signal is only detectable below ~ 20 K. Rapid spin-lattice relaxation on the Fe^{2+} , due to its large

orbital momentum is thought to be responsible for the strong temperature dependence of the $g=1.8$ signal [65].

There is a second magnetic interaction involving Q^- , i.e. with reduced BP_L^- . The $Fe^{2+}-Q^-$ coupling strengths are ca 10^2 mT for various purple bacterial species, whereas the magnitude of the $Q^- - I^-$ interaction varies widely for different bacterial species (see e.g. Dutton et al.[20]). Relatively large couplings are observed when the primary acceptor is a menaquinone. Better π -electron orbital overlap of menaquinone with Trp-M250 [30] might be responsible for this observation, although no firm proof has been given yet. The magnetic interactions in the RC have recently been reviewed by Hoff [74].

1.3 THE PRIMARY REACTIONS

In this paragraph the dynamics and the redox properties of the components of the bacterial RC are considered in more detail.

Figure 6 shows the redox couples and lifetimes of the primary photoreactants. Upon exciting the primary donor (P-960 for Rps. viridis, P-870 for Rb. sphaeroides), e.g. by trapping the energy from a nearby excited antenna molecule, an electron is transferred from the excited donor to I. Various times have been reported for this process: 2.8 ± 0.2 ps [51], 4.0 ± 1.0 ps [49], or 7 ± 2 ps [48] in Rb. sphaeroides, and 6.0 ± 0.9 ps [75], 12 ± 2 ps [50], or < 8 ps [76] in Rps. viridis RC's. The electron leaves BP_L^- in approximately 200 ps to the primary quinone acceptor [45,59,76-78], the latter transfer stabilizing the charge-separated state. Although the individual redox properties of the primary reactants may differ for various species of purple bacteria, the kinetics of the primary steps show a remarkable resemblance, indicating a close structural relationship.

The time of the energy transfer step from a nearby excited antenna molecule to the primary donor is ca 1 ps [11,79,80]. This time is comparable to the time that an excitation remains on a particular antenna molecule [11,80]. Hoff argued [81] that 2.8 ps (or

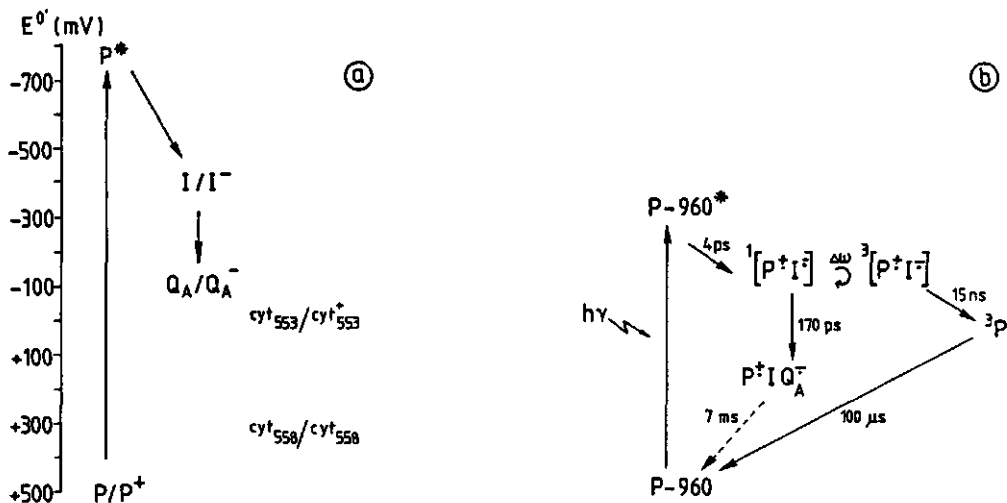


Figure 6.

a. Redox properties of the reaction center of Rps. viridis (after ref. [35,66]). b. The kinetics of the primary processes in Rps. viridis. Further details are given in the text.

more) is therefore an unlikely long time for the existence of P^* , especially for Rps. viridis, where the lowest excited state of P-960 is higher in energy than the corresponding state in the antenna, a curious phenomenon already known since the first characterization of the photosynthetic system of Rps. viridis [82]. Ultrafast spectroscopic methods have provided possible answers for the problem of the long life-time of the trapped excitation on P-960 [122,125-127]. A charge-separated state on P^* itself was postulated, which comes into existence only ~50 fs after excitation of P. It is not clear whether the accessory BChl's play a role in the latter process.

1.4 THE TRIPLET STATE AND ITS SPIN POLARIZATION

Much work has been carried out studying the triplet state of the primary donor (3P) in the photosynthetic RC [9,18,83-86]. The

advantage of studying this triplet state in photosynthetic RC's is that it may act as an internal magnetic probe, sensitive to its environment. 3P can be generated if the electron transfer step from BP_L^- to Q_A is blocked, e.g. because the primary acceptor Q_A was removed, or prereduced. Under these circumstances the P^+I^- state recombines to form : a) the excited donor, giving rise to delayed fluorescence [25,87-90], b) the singlet ground state of P + heat, or c) the triplet state 3P [9]. The yield of any of the recombination products depends on the temperature and other external conditions (e.g. magnetic field strength). At low temperature ($T < 20$ K) the triplet yield becomes close to unity, whereas at room temperature the triplet yield is about 15% [91].

When external magnetic fields are applied, the triplet yield drops considerably at room temperature, due to the increased separation between the $|T_+>$ energy levels and the $|S>$ state energy level in the P^+I^- state [92-94]. At low temperature however, there is no effect on the triplet yield by the magnetic field [92].

Since Dutton first measured the triplet state of P [95], EPR has proven to be a useful technique to study the primary processes in photosynthetic RC's. The dipolar zero field splitting parameters D and E obtained from $\Delta m = \pm 1$ triplet EPR, and ODMR spectra depend on the electronic structure of the molecule and characterize the observed triplet state, and thus contain information about the molecular frame on which the triplet state is located [96]. The donor triplet EPR spectrum exhibits an electron spin polarization (ESP) pattern, which was recognized as anomalous, i.e. this ESP pattern is inconsistent with the "normal" populating mechanism via intramolecular intersystem crossing [97,98]. The ESP patterns in triplet EPR powder spectra reflected a pure initial $|T_0>$ population in all canonical orientations, resulting in an AEEAAE ESP pattern (fig. 7). This pattern is observed in all photosynthetic RC's, including the plant photosystems I and II [95,98-101].

The explanation for this anomalous polarization was found in chemically induced magnetic polarization (CIMP) [92,102-106]. The

ERRATA

p. 25 8th line "Roelofs et al." should be:

"Chidsey et al."

p. 26 Table I, 1st line "0.01 - 0.05" should be:

"0.1 - 0.5"

p. 35 formula (9) " ... $\exp\{\frac{i}{\hbar}E_j t\}$... " should be:

"... $\exp\{-\frac{i}{\hbar}E_j t\}$..."

p. 40 11th line from bottom " $|S \rangle, |T_0 \rangle \dots$ " should be:

" $|S\alpha \rangle, |T_0\alpha \rangle \dots$ "

10th line from bottom " $|S \rangle, |T_0\beta \rangle \dots$ " should be:

" $|S\beta \rangle, |T_0\beta \rangle \dots$ "

p.115 1st paragraph "The transients at 100 K ..." should be:

"The transients in figure 1 at 100 K exhibit several differences with those obtained at 5 K."

p.125 8th line from above "(i.e. smaller τ_e)" should be:

"(i.e. longer τ_e)"

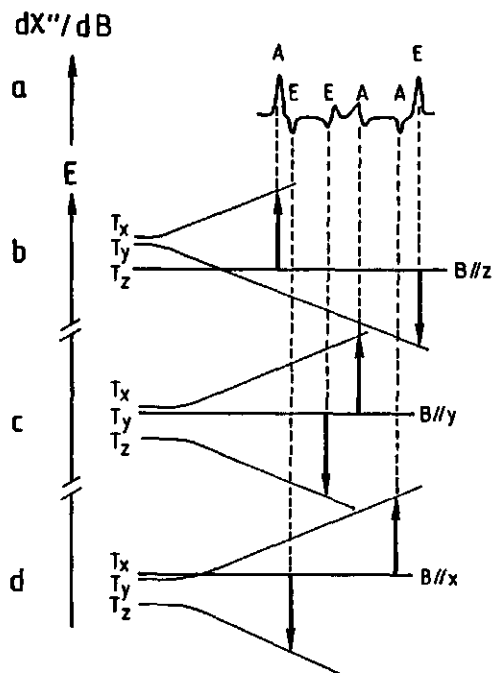


Figure 7.

The origin of an anomalously spin polarized first derivative $\Delta m=1$ triplet EPR spectrum (a). Emissive transitions are labeled E, A denotes absorption; b-d: Magnetic field dependence of the energies of the three spin levels of the triplet of the primary donor (3P), in which the magnetic field (B) is parallel to the z,y, and x zero field magnetic axes. The observed transitions are indicated by black arrows (after [106]). Note that in b-d only the middle sublevel ($m_s=0$) at high magnetic fields carries population, independent of the relative orientation of the magnetic field and the molecular frame.

magnetic field effect on the triplet yield [92-94] and the anomalous ESP can be explained by invoking the radical pair mechanism (RPM) for the triplet state formation in photosynthetic RC's [92,98].

1.5 THE RADICAL PAIR MECHANISM

Although the RPM was developed to explain the electron and nuclear spin polarization of the products of chemical reactions in solution [107,108], it could be successfully applied to the photosynthetic RC [92,102-106,109], which, especially at low temperature, is more like a solid.

In the following a RC in a state in which the primary acceptor (Q_A) has been removed is considered in the presence of a high magnetic field, i.e. much larger than the zero-field splittings of the donor triplet state.

After absorption of a photon the P^* state ejects an electron, producing the P^+I^- state. The two unpaired electrons on P^+ and I^- were highly correlated just before the charge separation, and at the time scale of this chemical reaction this correlation is preserved i.e. the net spin moment of the RP state remains zero during charge separation.

The basis set that describes this spin system consists of one singlet ($|S\rangle$) and three triplet RP-states ($|T_+\rangle$, $|T_0\rangle$, and $|T_-\rangle$). The Hamiltonian describing the RP is given by [110]:

$$H = g_1\beta\vec{S}_1 \cdot \vec{B} + g_2\beta\vec{S}_2 \cdot \vec{B} + \sum_i A_{1i}\vec{S}_1 \cdot \vec{I}_i + \sum_j A_{2j}\vec{S}_2 \cdot \vec{I}_j - J_{12}(\frac{1}{2} + 2\vec{S}_1 \cdot \vec{S}_2) + \vec{S}_1 \cdot \vec{D} \cdot \vec{S}_2 \quad (1)$$

where 1 and 2 denote the unpaired electrons on P^+ and I^- , respectively; g_i is the g-factor of electron i ; β the Bohr magneton; B denotes the external magnetic field; A_{kq} denotes the hyperfine tensor, which couples electron k with nuclear spin q ; I_q denotes the nuclear magnetic moment of the q th atom; J_{12} is the electron exchange interaction; and D is the dipolar interaction tensor. These terms are one by one discussed in more detail by Ogrodnik [110].

In the following, only isotropic interactions are considered, and it is assumed that $B=B_z$.

The external magnetic field causes each of the electron spins to precess around its axis. The difference in precession frequency ($\Delta\omega_{12}$) of

electrons 1 and 2 is given by [106,107,112]:

$$\Delta\omega_{12} = \frac{1}{\hbar} \left\{ \frac{1}{2} \beta H_z (g_1 - g_2) + \frac{1}{2} \sum_i A_{1i} m_{1i} - \frac{1}{2} \sum_j A_{2j} m_{2j} \right\} \quad (2)$$

where \hbar is Planck's constant over 2π , and m_{kq} denotes the magnetic nuclear quantum number of atom q on radical k ($k=P^+$, I^-).

Thus, the external magnetic field induces $|S\rangle - |T_0\rangle$ mixing by g -value differences and/or differences in the local magnetic field strengths at P^+ and I^- (see figure 8). The $|T_+\rangle$ and $|T_-\rangle$ states are hardly involved, for the Zeeman energy splitting (~ 300 mT for X-band EPR fields) is much larger than the exchange energy J_{12} , which causes the energy gap between $|S\rangle$ and $|T_0\rangle$. $|J_{12}|$ is ca. 0.1 mT [74,113,114]. (If there is no coupling at all between electron 1 and 2, the notion of a triplet state becomes meaningless.)

In the photosynthetic RC the RP state has a lifetime of about 200

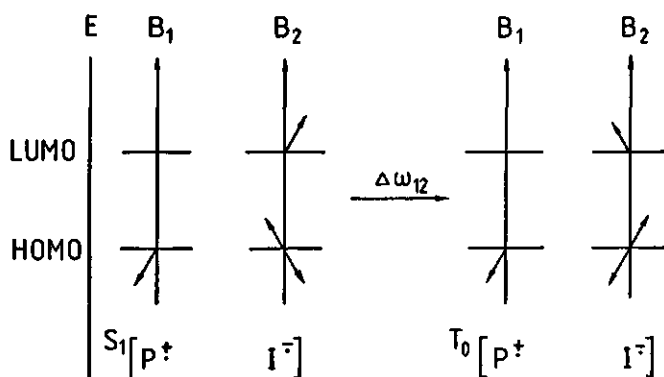


Figure 8.

Simplified view on the S - T_0 mixing in the radical pair mechanism. Because the local magnetic field strengths are different, the spins on I^- precess with a different frequency with respect to those on P^+ . After $\pi/\Delta\omega$ s the initial singlet state of the unpaired electrons of the RP is converted into the $m_s=0$ triplet state (" P^R "). Upon recombination of the RP, only the $m_s=0$ sublevel of 3P is populated (" P^R ").

ps when 'normal' forward electron transfer is allowed, and exists 10 - 20 ns [89,115,116], if Q_A has been removed (or prereduced), effectively blocking the forward electron transfer. Parson et al. [115] denoted this short-lived (20 ns) state " P^F ", and denoted the much more stable triplet state of the primary donor itself (3P) " P^R " (F stands for "fast decaying", and R stands for "remaining"). These notations will also be used in this work. In the 'normal' case, 200 ps is too short for the RP to develop any $|T_0\rangle$ character, because g-value and hyperfine differences are too small. However, under blocked conditions the triplet RP-state becomes observable.

Eq. 2 implies that the S- T_0 mixing is caused by either differences in g-values between P^+ and I^- , and/or differences in hyperfine coupling strengths. In the RC the g-values of P^+ and I^- differ only ~ 0.001 [117,118], which is insufficient to cause any substantial S- T_0 mixing during the 20 ns life time of P^F . Therefore the differences in hyperfine coupling strengths are considered responsible for the S- T_0 mixing. This was theoretically illustrated using the notion of one proton coupled to one of the electrons [111], replacing the two hyperfine terms in eq. 1 and representing the net hyperfine coupling.

So far the RC was considered without the presence of Q_A . In principle the same description is expected to apply when the primary quinone is prereduced, also blocking the forward electron transfer. But now there is an important difference. The unpaired electron on Q_A^- (or better, the $Q_A^- Fe^{2+}$ complex) can magnetically interact with the nearby spin on I^- as was realized by Roelofs et al. [119], and Hoff and Hore [120]. This resembles the description given above, i.e. of two electron spins in a RP interacting with one proton. However, now the Zeeman energy of the third electron spin on Q_A^- is a large factor in the three electron spin Hamiltonian (see Chapter II), in contrast to the relatively small contributions by the hyperfine term in the two electron spin-, one proton model. In the following chapters the $P^+I^-Q_A^-Fe^{2+}$ multi electron spin system is considered in much more detail for various bacterial species. In these

bacteria the magnitude of the magnetic interaction between the spins of the second electron on I^- (BP_L) and the third electron on Q_A varies considerably (from ~ 0.05 mT to ~ 20 mT).

1.6 PERSPECTIVES AND OUTLINE OF THIS WORK

In the previous sections a survey has been given of the photochemical reactions in the bacterial photosynthetic reaction center (RC) and the architecture of this RC. Both the structure of the RC and the sequence and time-scale of the events have been unraveled in great detail, so that research on primary processes in photosynthesis can now be focussed on the relation between structure and function. This is not straightforward as Hoff has pointed out recently [74], since the X-ray data give information on core electrons (in a molecular frame in a neutral ground state), whereas the spectroscopic data are sensitive to the properties of the outer electrons, dealing exclusively with charged and/or excited states.

Several basic questions remain to be answered: e.g. Why is the light-energy converting process so efficient in the RC? What is the role, if any, of the protein itself in the charge-separating and electron transfer process? Is there any reason for a dual electron path-way? And more detailed questions like: how exactly is the electron from P^* transferred to the intermediary acceptor? Do the tails of the chromophores play an active role in the electron transfer process? What is the function of the iron ion in the RC?

Many of these questions are being answered at this moment by the joined efforts of numerous workers in the field.

In our laboratory we were interested in the relation between structure of the photochemical device and the kinetics of electron and energy transfer processes in photosynthesis as well as biomimetic (artificial) systems [129-135]. The magnetic interactions between the involved reactants may provide a clue to understand the parameters determining the mechanism and kinetics of photosynthetic electron

transfer. Spectroscopic techniques provide the tools to study the above-mentioned relation.

This work focusses on the factors which determine the electron spin polarization (ESP) of the lowest triplet state of the primary electron donor (P^R) in photosynthetic bacterial RC's. One of the main results is that the magnetic interactions between the components of the RC in the acceptor region, which are related to the structural properties of the acceptor side, determine the ESP pattern of P^R at low temperature (e.g. liquid nitrogen temperature). On the other hand, the donor properties of the RC are reflected by the quantum yield of P^R .

In summary, EPR spectra of P^R contain structural information on both donor and acceptor side of the RC. We have applied this concept to model-systems containing bacterial RC's.

This study was triggered by the surprising observation that the ESP pattern of the primary donor triplet state EPR spectrum from Rps. viridis RC's depends on the temperature (see Chapter IV), leading to the question whether the well-established radical pair mechanism in photosynthetic RC's necessarily results in an AEEAAE ESP pattern in EPR spectra.

A simple theoretical approach, scouting various explanations for the observed temperature dependence of the ESP pattern of P^R is presented in Chapter II. In Chapter IV several experiments are described on RC's and chromatophores under steady state conditions. It was concluded from these experiments that a detailed knowledge about the dynamics of the triplet state is essential to further characterize the mechanism underlying the temperature dependence.

For that purpose a pulsed dye laser was constructed. Furthermore, an improved method for the detection of time resolved EPR was developed, both described in Chapter III. The results of the time-resolving experiments are reported in Chapter V. It was concluded that phonon-assisted transitions between P^F and P^R may explain the P^R relaxation behaviour. Finally, the profit of the use of the ESP pattern as moni-

tor for structural changes in the RC was demonstrated in Chapter VI, where the incorporation of RC's into reversed micelles is described.

1.7 REFERENCES

- [1] R.E. Dickerson, *Scientific American* 9 (1978) 62-78.
- [2] P. Mathis, *Photosynth. Res.* 8 (1986) 97-111.
- [3] See e.g. J.M. Kleijn, Thesis (1987) Wageningen Agricultural University, The Netherlands.
- [4] F.F. Blackman, *Ann. Botany* 19 (1905) 281-295.
- [5] J. Barber, *Rep. Progr. Phys.* 41 (1978) 1157-1199.
- [6] R.K. Clayton in "Light and Living Matter", vol. 1 (1970) pp. 1-3, R.E. Krieger Publ. Co., Huntington, New York.
- [7] A.N. Glazer, *Ann. Rev. Plant Physiol.* 36 (1982) 173-198.
- [8] A.N. Glazer, *Ann. Rev. Plant Physiol.* 52 (1983) 125-157.
- [9] A.J. Hoff in "Triplet State ODMR Spectroscopy" (R.H. Clarke, ed.) (1982) pp. 367-425, Wiley, New York.
- [10] Govindjee, and R. Govindjee in "Bioenergetics of Photosynthesis" (Govindjee, ed.) (1975) pp. 1-51, Acad. Press, New York.
- [11] R. van Grondelle, *Biochim. Biophys. Acta* 811 (1985) 147-195.
- [12] G. Drews, *Microbiol Rev.* 49 (1985) 59-70.
- [13] R.J. Cogdell, *Ann. Rev. Plant Physiol.* 34 (1983) 21-45.
- [14] D.W. Reed, and R.K. Clayton, *Biochem. Biophys. Res. Comm.* 30 (1968) 471-475.
- [15] G. Gingras in "The photosynthetic bacteria" (R.K. Clayton, and W.R. Sistrom, eds.) (1978) pp. 119-131, Plenum Press, New York.
- [16] H. Michel, *J. Mol. Biol.* 158 (1982) 567-572.
- [17] J.P. Allen, and G. Feher, *Proc. Natl. Acad. Sci. USA* 81 (1984) 4795-4799.
- [18] R.H. Clarke, R.E. Connors, H.A. Frank, and J.C. Hoch, *Chem. Phys. Lett.* 45 (1977) 523-528.
- [19] K. Sauer, *Acc. Chem. Res.* 11 (1978) 257-264.
- [20] P.L. Dutton, R.C. Prince, and D.M. Tiede, *Photochem. Photobiol.*

- 28 (1978) 939-949.
- [21] A. Vermeglio, J. Breton, G. Paillotin, and R. Cogdell, *Biochim. Biophys. Acta* 501 (1978) 514-530.
- [22] J.J. Katz, L.L. Shipman, and J.R. Norris in "Chlorophyll organization and energy transfer in photosynthesis", Ciba foundation symp. 61 (1979) pp. 1-40, *Excerpta Medica*, Amsterdam.
- [23] V.A. Shuvalov, and A.A. Asadov, *Biochim. Biophys. Acta* 545 (1979) 296-308.
- [24] Y.E. Erokhin, I.A. Abdourakhmanov, and I.R. Prokhorenko, *Proc. Photosynt. III* (G. Akoyunoglou, ed.) (1981) pp. 959, *Balaban Int. Sci. Services*, Philadelphia, PA.
- [25] J. Amesz, *Progr. Bot.* 43 (1981) 49-63.
- [26] J. Breton, and A. Vermeglio in "Photosynthesis: Energy conversion by plants and bacteria", vol. I (1982) pp. 153-194, *Acad. Press Inc.*
- [27] R.H. Clarke, R.E Connors, and H.A. Frank, *Biochem. Biophys. Res. Comm.* 71 (1976) 671-675.
- [28] J. Deisenhofer, O.Epp, K. Miki, R. Huber, and H. Michel, *J. Mol. Biol.* 180 (1984) 385-398.
- [29] J. Deisenhofer, and H. Michel in "Antennas and reaction centers from photosynthetic bacteria" (M.E. Michel-Beyerle, ed.) (1985) pp. 94-96, *Springer Verlag*, Berlin.
- [30] J. Deisenhofer, O. Epp, K. Miki, R. Huber, and H. Michel, *Nature* 318 (1985) 618-624.
- [31] P. Gast, M.R. Wasielewski, M. Schiffer, and J.R. Norris, *Nature* 305 (1983) 451-452.
- [32] W. Zinth, W. Kaiser, and H. Michel, *Biochim. Biophys. Acta* 723 (1983) 128-131.
- [33] P. Gast, T.J. Michalski, J.E. Hunt, and J.R. Norris, *FEBS Lett.* 179 (1985) 325-328.
- [34] P. Gast, and J.R. Norris, *FEBS Lett.* 177 (1984) 277-280.
- [35] T.L. Netzel, P.M. Rentzepis, D.M. Tiede, R.C. Prince, and P.L. Dutton, *Biochim. Biophys. Acta* 460 (1977) 467-479.
- [36] D.M. Tiede, and P.L. Dutton, *Biochim. Biophys. Acta* 637 (1981)

278-290.

- [37] J.P. Thornber, R.J. Cogdell, R.E.B. Seftor, and G.D. Webster, *Biochim. Biophys. Acta* 593 (1980) 60-75.
- [38] K.D. Philipson, and K. Sauer, *Biochemistry* 12 (1973) 535-539.
- [39] G. Feher, and M.Y. Okamura in "The photosynthetic bacteria" (R.K. Clayton, and W.R. Sistrom, eds.) (1978) pp. 349-386, Plenum Press, New York.
- [40] A.W. Rutherford, *Biochem. Soc. Trans.* 14 (1985) 15-17.
- [41] M.C.W. Evans, *Physiol. Veg.* 23 (1985) 563-569.
- [42] V.V. Klimov, and A.A. Krasnovkii, *Photosynthetica* 15 (1981) 592-609.
- [43] J. Deisenhofer, H. Michel, and R. Huber, *Trends Biochem. Sci.* 10 (1985) 243-248.
- [44] J. Deisenhofer, oral presentation at the CECAM Workshop on "The structure and dynamics of photoreaction centers in photosynthesis" (1986) Orsay, France.
- [45] C.C. Schenck, W.W. Parson, D. Holten, and M.W. Windsor, *Biochim. Biophys. Acta* 635 (1981) 383-392.
- [46] C. Kirmaier, D. Holten, and W.W. Parson, *Biochim. Biophys. Acta* 810 (1985) 49-61.
- [47] C. Kirmaier, D. Holten, and W.W. Parson, *FEBS Lett.* 185 (1985) 76-82.
- [48] V.A. Shuvalov, and A.V. Klevanik, *FEBS Lett.* 160 (1983) 51-55.
- [49] V.A. Shuvalov, and L.N.M. Duysens, *Proc. Natl. Acad. Sci. USA* 83 (1986) 1690-1694.
- [50] V.A. Shuvalov, J. Amesz, and L.N.M. Duysens, *Biochim. Biophys. Acta* 851 (1986) 327-330.
- [51] J.L. Martin, J. Breton, A.J. Hoff, A. Migus, and A. Antonetti, *Proc. Natl. Acad. Sci. USA* 83 (1986) 957-961.
- [52] R.K. Clayton, and T. Yamamoto, *Biophys. J.* 16 (1976) 222a, abstr. F-PM-D6.
- [53] E.W. Knapp, S.F. Fischer, W. Zinth, M. Sander, W. Kaiser, J. Deisenhofer, and H. Michel, *Proc. Natl. Acad. Sci. USA* 82 (1985) 8463-8467.

- [54] A.J. Hoff in "Molecular biology, biochemistry, and biophysics", vol. 35 (F.K. Fong, ed.) (1982) pp.80-151, Springer Verlag, Berlin.
- [55] D.M. Tiede, R.C. Prince, P.L. Dutton, *Biochim. Biophys. Acta* 449 (1976) 447-467.
- [56] D.M. Tiede, R.C. Prince, G.M. Reed, and P.L. Dutton, *FEBS Lett.* 65 (1976) 301-304.
- [57] V.A. Shuvalov, and V.V. Klimov, *Biochim. Biophys. Acta* 440 (1976) 587-599.
- [58] J.K. Hoerber, W. Goebel, A. Ogrodnik, M.E. Michel-Beyerle, and W.E. Knapp in "Antennas and reaction center of photosynthetic bacteria" (M.E. Michel-Beyerle, ed.) (1985) pp. 292-297, Springer Verlag, Berlin.
- [59] W.W. Parson, and R.J. Cogdell, *Biochim. Biophys. Acta* 416 (1975) 105-149.
- [60] R.E. Blankenship, and W.W. Parson, *Biochim. Biophys. Acta* 545 (1979) 429-444.
- [61] J.R. Bolton in "The photosynthetic bacteria" (R.K. Clayton, and W.R. Sistrom, eds.) (1978) pp. 419-429, Plenum Press, New York.
- [62] J.S. Leigh, and P.L. Dutton, *Biochem. Biophys. Res. Comm.* 46 (1972) 414-421.
- [63] A.W. Rutherford, and M.C. W. Evans, *FEBS Lett.* 100 (1979) 305-308.
- [64] A.W. Rutherford, and M.C.W. Evans, *FEBS Lett.* 104 (1979) 227-230.
- [65] G.C. Dismukes, H.A. Frank, R. Friesner, and K. Sauer, *Biochim. Biophys. Acta* 764 (1984) 253-271.
- [66] R.C. Prince, J.S. Leigh, and P.L. Dutton, *Biochim. Biophys. Acta* 440 (1976) 622-636.
- [67] R.J. Shopes, and C.A. Wraight, *Biochim. Biophys. Acta* 806 (1985) 348-356.
- [68] N.L. Pucheu, N.L. Kerber, and A.F. Garcia, *Arch. Microbiol.* 109 (1976) 301.
- [69] W.W. Parson in "The photosynthetic bacteria" (R.K. Clayton, and W.R. Sistrom, eds.) (1978) pp. 455-469, Plenum Press, New York.
- [70] W. Lubitz, and M. Plato, oral presentation at CECAM Workshop on

"The structure and dynamics of photoreaction centers in photosynthesis", 1986, Orsay, France.

- [71] W.F. Butler, R. Calvo, D.R. Fredkin, R.A. Isaacson, M.Y. Okamura, and G. Feher, *Biophys. J.* 45 (1984) 947-973.
- [72] W.F. Butler, D.C. Johnston, H.B. Shore, D.R. Fredkin, M.Y. Okamura, and G. Feher, *Biophys. J.* 32 (1980) 967-992.
- [73] J.D. McElroy, Thesis (1970) Univ. California, San Diego, La Jolla, USA.
- [74] A.J. Hoff, *Photochem. Photobiol.* 43 (1986) 727-745.
- [75] M.R. Wasielewski, and D.M. Tiede, *FEBS Lett.* 204 (1986) 368-372.
- [76] D. Holten, M.W. Windsor, W.W. Parson, and J.P. Thornber, *Biochim. Biophys. Acta* 501 (1978) 112-126.
- [77] M.G. Rockley, M.W. Windsor, R.J. Cogdell, and W.W. Parson, *Proc. Natl. Acad. Sci. USA* 72 (1975) 2251-2255.
- [78] K.J. Kaufmann, P.L. Dutton, T.L. Netzel, J.S. Leigh, and P.M. Rentzepis, *Science* 188 (1975) 1301-1304.
- [79] J.G.C. Bakker, R. Van Grondelle, and W.T.F. Den Hollander, *Biochim. Biophys. Acta* 725 (1983) 508-518.
- [80] M. Vos, R. Van Grondelle, F.W. Van Der Kooij, D. Van De Poll, J. Amesz, and L.N.M. Duysens, *Biochim. Biophys. Acta* 850 (1986) 501-512.
- [81] A.J. Hoff, oral presentation at CECAM Workshop on (The structure and dynamics of photoreaction centers in photosynthesis", 1986, Orsay, France.
- [82] A.S. Holt, and R.K. Clayton, *Photochem. Photobiol.* 4 (1965) 829-831.
- [83] T.G. Monger, R.J. Cogdell, and W.W. Parson, *Biochim. Biophys. Acta* 449 (1976) 136-153.
- [84] J.S. Leigh in "The photosynthetic bacteria" (R.K. Clayton, and W.R. Sistrom, eds.) (1978) Plenum Press, New York.
- [85] T.J. Schaafsma in "Triplet state ODMR spectroscopy" (R.H. Clarke, ed.) (1982) pp. 291-365, Wiley, New York.
- [86] H.J. Den Hollander, Thesis (1983) State Univ. Leiden, The Netherlands.

- [87] B.L. Strehler, and W. Arnold, *J. Gen. Physiol.* 34 (1951) 809-820.
- [88] V.I. Godik, and A.Y. Borisov, *Biochim. Biophys. Acta* 590 (1980) 182-193.
- [89] C.C. Schenck, R.E. Blankenship, and W.W. Parson, *Biochim. Biophys. Acta* 680 (1982) 44-59.
- [90] R. Van Der Werf, D. Zevenhuizen, and J. Jortner, *Chem. Phys.* 27 (1978) 319-329.
- [91] W.W. Parson, and T.G. Monger, *Brookhaven Symp. Biol.* 28 (1976) 195-212.
- [92] R.E. Blankenship, T.J. Schaafsma, and W.W. Parson, *Biochim. Biophys. Acta* 461 (1977) 297-305.
- [93] A.J. Hoff, H. Rademaker, R. Van Grondelle, and L.N.M. Duysens, *Biochim. Biophys. Acta* 460 (1977) 547-554.
- [94] M.E. Michel-Beyerle, H. Scheer, H. Seidlitz, D. Tempus, R. Haberkorn, *FEBS Lett.* 100 (1979) 9-12.
- [95] P.L. Dutton, J.S. Leigh, and M. Seibert, *Biochem. Biophys. Res. Comm.* 46 (1972) 406-413.
- [96] see e.g. S.P. Mc Glynn, T. Azumi, and M. Kinoshita "Molecular spectroscopy of the triplet state", Prentice-Hall, Inc., Englewood Cliffs, New Jersey.
- [97] T.J. Schaafsma, J.F. Kleibeuker, R.J. Platenkamp, and P. Geerse, *Mol. Spectros. Dense Phases* (1975) 491-494.
- [98] M.C. Thurnauer, J.J. Katz, J.R. Norris, *Proc. Natl. Acad. Sci. USA* 72 (1975) 3270-3274.
- [99] H.A. Frank, M.B. McLean, and K. Sauer, *Proc. Natl. Acad. Sci. USA* 76 (1976) 5124-5128.
- [100] A.W. Rutherford, D.R. Paterson, and J.E. Mullet, *Biochim. Biophys. Acta* 635 (1981) 205-214.
- [101] T. Swarthoff, P. Gast, and A.J. Hoff, *FEBS Lett.* 127 (1981) 83-86.
- [102] R. Kapteyn, *J. Amer. Chem. Soc.* 94 (1972) 6251-6262.
- [103] J.K.S. Wan, and A.J. Elliot, *Acc. Chem. Res.* 10 (1977) 161-166.
- [104] R. Friesner, G.C. Dismukes, and K. Sauer, *Biophys. J.* 25 (1979)

277-294.

- [105] J.B. Pedersen, "Theories of chemically induced magnetic polarization" (1979) Odense Univ. Press.
- [106] R.E. Blankenship, *Acc. Chem. Res.* 14 (1981) 163-170.
- [107] G.L. Closs, *J. Am. Chem. Soc.* 91 (1969) 4552-4554.
- [108] R. Kaptein, and J.L. Oosterhoff, *Chem. Phys. Lett.* 4 (1969) 195-197.
- [109] H.J. Werner, K. Schulten, and A. Weller, *Biochim. Biophys. Acta* 502 (1978) 255-268.
- [110] A. Ogrodnik, Ph.D. Thesis (1983) Tech. Univ. Munich, FRG.
- [111] R. Haberkorn, and M.E. Michel-Beyerle, *Biophys. J.* 26 (1979) 480-498.
- [112] F. Adrian, *J. Chem. Phys.* 54 (1971) 3912-3917.
- [113] A.J. Hoff, and P. Gast, *J. Phys. Chem.* 83 (1979) 3355-3358.
- [114] P. Gast, Ph.D. Thesis (1982) State Univ. Leiden, The Netherlands.
- [115] W.W. Parson, R.K. Clayton, and R.J. Cogdell, *Biochim. Biophys. Acta* 387 (1975) 265-278.
- [116] V.A. Shuvalov, and W.W. Parson, *Proc. Natl. Acad. Sci. USA* 78 (1980) 957-961.
- [117] J.D. McElroy, G. Feher, and D.C. Mauzerall, *Biochim. Biophys. Acta* 267 (1972) 363-374.
- [118] C.E.D. Chidsey, M.G. Roelofs, and S.G. Boxer, *Chem. Phys. Lett.* 74 (1980) 113-118.
- [119] M.G. Roelofs, C.E.D. Chidsey, and S.G. Boxer, *Chem. Phys. Lett.* 87 (1982) 582-588.
- [120] A.J. Hoff, and P.J. Hore, *Chem. Phys. Lett.* 108 (1984) 104-110.
- [121] W. Zinth, M. Sander, J. Dobler, W. Kaiser, and H. Michel in "Antennas and reaction centers of photosynthetic bacteria" (M.E. Michel-Beyerle, ed.) (1985) pp. 97-102, Springer Verlag, Berlin.
- [122] S.G. Boxer, T.R. Middendorf, and D.J. Lockhart, *FEBS Lett.* 200 (1986) 237-241.
- [123] A.W. Rutherford, I. Agalidis, and F. Reiss-Husson, *FEBS Lett.* 182 (1985) 151-157.

- [124] G. Feher, R.A. Isaacson, M.Y. Okamura, and W. Lubitz in "Antennas and reaction centers from photosynthetic bacteria" (M.E. Michel-Beyerle, ed.) (1985) pp. 174-189, Springer Verlag, Berlin.
- [125] S.G. Boxer, A. Kuki, D.J. Lockhart, T.R. Middendorf, and R. Moog, Proc. Vth Int. Seminar Energy Transfer Condensed Matter, 1985, (P. Pancoska, and J. Pantoflicek, eds.) (1985) pp. 108-115.
- [126] S.R. Meech, A.J. Hoff, and D.A. Wiersma, Chem. Phys. Lett. 121 (1985) 287-292.
- [127] S.G. Boxer, D.J. Lockhart, and T.R. Middendorf, Chem. Phys. Lett. 123 (1986) 476-482.
- [128] H. Michel, O. Epp, and J. Deisenhofer, EMBO J. 5 (1986) 2445-2451.
- [129] J. Hala, G.F.W. Searle, T.J. Schaafsma, A. Van Hoek, P. Pancoska, K. Blaha, and K. Vacek, Photochem. Photobiol. 44 (1986) 527-534.
- [130] U. Hofstra, R.B.M. Koehorst, and T.J. Schaafsma, Chem. Phys. Lett. 130 (1986) 555-559.
- [131] M.A. Bergkamp, J. Dalton, and T.L. Netzel, J. Am. Chem. Soc. 104 (1982) 253-259.
- [132] M.R. Wasielewski, and M.P. Niemczyk, J. Am. Chem. Soc. 106 (1984) 5043-5045.
- [133] B.A. Leland, A.D. Joran, P.M. Felker, J.J. Hopfield, A.H. Zewail, and P.B. Dervan, J. Phys. Chem. 89 (1985) 5571-5573.
- [134] M.R. Wasielewski, M.P. Niemczyk, W.A. Svec, and E.B. Pewitt, J. Am. Chem. Soc. 107 (1985) 1080-1082.
- [135] T.A. Moore, D. Gust, P. Mathis, J.-C. Mialocq, C. Chachaty, R.V. Bensasson, E.J. Land, D. Doizi, P.A. Liddell, W.R. Lehmann, G.A. Nemeth, and A.L. Moore, Nature 307 (1984) 630.

CHAPTER II

THEORETICAL ASPECTS OF STATIC AND DYNAMIC MAGNETIC INTERACTIONS IN SOME MULTI SPIN SYSTEMS

2.1 INTRODUCTION

Prerduced photosynthetic RC's contain a paramagnetic anion of the quinone type (Q^-). Recently several observations were reported, which were ascribed to the presence of the additional electron spin on Q_A^- [1-4]. Several groups [4,5] realized that it was necessary to consider the interaction of the third electron spin on Q_A^- with the unpaired electron spin on I^- in the P^+I^- radical pair (RP) state for a proper description of the magnetic interactions in the primary reactants of the charge-separating pathway. Roelofs et al. noted the possible consequences of electron spin relaxation within the $Q_A^-Fe^{2+}$ complex [4].

Generally, the lineshape, e.g. the ratio of the amplitudes of the X, Y, and Z transitions of the $\Delta m=1$ EPR spectrum of the donor triplet state, changes with temperature. In the more pronounced case, such as for Rps. viridis (see Chapter IV), even the sign of the Y-transitions may change. This is denoted as a change in electron spin polarization (ESP) pattern. This indicated some relation with the magnetic interaction between I^- and Q_A^- , which was known to be larger for Rps viridis. The magnitude of this interaction in various bacterial species and in plant photosystem II has been collected in Table I [6]. From this Table it is clear that a substantial magnetic interaction between I^- and Q_A^- is not rare in photosynthesis, although its effect on the electron transport process under physiological conditions, if any, is presently unclear.

Table I

Species	J_{23} (mT) ^a	ref.
<u>Rb. sphaeroides</u>	0.01 - 0.05	7 - 9
<u>Rps. gelatinosa</u>	8.3	10
<u>C. vinosum</u>	8.0	11
<u>Rps. viridis</u>	18.0	12
<u>T. Pfennigii</u>	6.8	13
PS-II	5.2	14 - 16

a: pH 7

The lineshape of the triplet spectrum is not only affected by the presence of a third electron spin, but it is also sensitive for intramolecular spin-lattice relaxation (SLR). SLR is monitored by EPR as an increase in decay rate of the triplet signal. To decide whether SLR can induce the observed changes in the ESP pattern, the kinetics of the relaxation process in the triplet state is considered in section 2.2 of this Chapter. It will be shown that this process cannot cause the observed temperature dependence of the ESP pattern of the donor triplet state in RC's from Rps. viridis. The temperature dependence of the observed decay rates of the EPR triplet signals is considered in more detail in Chapter 5.

In section 2.3 the effect of the presence of the third electron spin on the RP will be considered theoretically by a simple calculation in order to get qualitative insight in the physics of the spin levels of the recombination probabilities, which determine the populating rates of the donor triplet state, and thus its ESP pattern. For this purpose static magnetic interactions are quantum mechanically considered, resulting in the breakdown of exclusive S-T₀ mixing in the radical pair state P⁺I⁻.

Static interactions alone cannot explain a temperature dependence as observed in the EPR triplet spectra. Therefore the effect of rapid T₁ processes within the Q_A⁻Fe²⁺ complex on the spin dynamics of the

three-electron spin system is qualitatively discussed in the second part of section 2.3.

2.2 ELECTRON SPIN POLARIZATION AND SPIN-LATTICE RELAXATION

In this section we investigate whether the observed temperature dependence of the ESP of the donor-triplet state (P^R) of bacterial RC's (Chapters IV and V) is the result of spin-lattice relaxation (SLR).

SLR denotes any of three phonon-assisted processes, causing spontaneous transitions between any pair of the three spin levels of P^R , from which the Raman-process is most commonly encountered [17]. Depending on the nature of the relaxation process, temperature dependencies from T^2 to T^9 have been observed [17,18].

At low temperatures P^R in photosynthetic RC's is exclusively populated in its $m_s=0$ sublevel by the action of the radical pair mechanism [19,20]. The other sublevels may become populated by SLR. This will affect the ESP pattern as monitored by the $\Delta m=1$ triplet EPR powder spectrum. Especially when the SLR process is faster than the time resolution of the EPR spectrometer it may become impossible to discriminate between a temperature dependent change of the relative population rates of the three spin levels and of the relaxation process. If the SLR rate constants are much faster than the rate constants for decay from the observed triplet state, the ESP pattern of its EPR spectrum reflects a Boltzmann distribution over the three spin levels of P^R and exhibits inversion symmetry around its center [21]. On the other hand, in the absence of SLR, i.e. at sufficiently low temperature, the $\Delta m=1$ triplet EPR spectrum exhibits mirror symmetry around its center. Such mirror symmetry is also found if the spectrum is recorded during a time-span following the generation of the triplet state which is short with respect to the SLR time, e.g. when using a pulsed excitation source and time-gated boxcar detection. We denote this the initial spectrum, in contrast to the fully thermalized spectrum. In

both the fully relaxed and fully polarized states of P^R , the amplitudes of any pair of EPR peaks (i.e. low and high field transitions: X^+/X^- , Y^+/Y^- , and Z^+/Z^-) are very close to equal. In the intermediate situation, if SLR is of the same order as the spin level decay rates, the $\Delta m=1$ triplet spectrum loses all symmetry: the amplitudes of e.g. the X^+ and X^- peaks are different. Generally, the same holds for the Y^+/Y^- and Z^+/Z^- peak amplitudes.

In the following the radiative and radiationless decay of the spin levels of P^R is described by a single decay rate constant, since the phosphorescence quantum yield for chlorophyll-like compounds is extremely low [31,32].

For *Rps. viridis*, for which we first observed the change in the ESP patterns of P^R , two of the three decay rate constants are already near the time-resolution of the standard EPR spectrometer (i.e. 14, and 16 ms^{-1} [22]). Therefore our observation that the ESP pattern of P^R in the EPR $\Delta m=1$ triplet spectra changes with temperature, might be caused by temperature-dependent SLR.

We consider a T_0 -populated triplet state ($P_0 = 0$, $P_1 = 0$), with different SLR rate constants at high magnetic field, connecting any pair of sublevels (fig. 1). The ratio of such a pair of relaxation

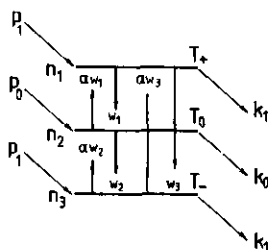


Figure 1.

Kinetic scheme for a triplet state in high magnetic fields. Only the T_0 -populating occurs ($P_1=0$), corresponding to the (two-spin) radical pair mechanism; w_1, w_2 , and w_3 denote relaxation rate constants, α denotes the Boltzmann factor $\exp\{-\Delta E/kT\}$. The energy-differences between T_+ and T_0 , and T_0 and T_- are assumed to be equal.

rates (w_{up}/w_{down}) is determined by the Boltzmann factor: $\exp -\Delta E/kT$ (α in fig. 1), where ΔE denotes the energy-difference between the pair of spin levels. It is assumed that $E_1 - E_2 = E_2 - E_3$, hence only a single factor α is required. Then, solving the set of first order differential equations for the steady state case, the following result is obtained:

$$\text{sign } \{n_1 - n_2\} = \text{sign} \{ (\alpha - 1) [\alpha w_1 w_2 + \alpha w_2 w_3 + \alpha^2 w_1 w_3 + w_1 k_1] - k_1 [(\alpha^2 + 1) w_1 + \alpha w_2 + k_1] \} \quad (1)$$

Since $0 < \alpha < 1$, and all rate constants are positive, both terms on the right hand side of eq. 1 are negative. Therefore $n_1 - n_2$ is negative for any set of parameters ($P_0, k_0, k_1, w_1, w_2, w_3$) at any temperature (α), indicating an absorptive EPR signal under all (steady state) circumstances. The observation that the absorptive Y^+ peak of P^R ($T < 20$ K) is converted into an emissively polarized transition at increasing temperature ($T > 20$ K) therefore cannot be caused by an intramolecular relaxation process.

2.3 A SIMPLE THREE ELECTRON SPIN MODEL FOR P^F

In the following we present a theoretical description of the magnetic interactions in the P^F state. Emphasis is on the populating probabilities of the high-field spin levels of P^R from the corresponding spin levels of P^F . By " P^F " we denote the total (three electron) spin system in the state $P^+ I^- Q_A^-$ in the (prereduced) photosynthetic RC.

Eigenstates of P^F

We must solve

$$H \Psi = E \Psi \quad (1)$$

where

$$H = \sum_{i=1}^3 g_i \beta \vec{S}_i \cdot \vec{B} - 2 J_{23} \vec{S}_2 \cdot \vec{S}_3 \quad (2)$$

and

$$\Psi = \sum_{k=1}^8 a_k \phi_k \quad (3)$$

H is the three-electron spin Hamiltonian, describing P^F ; Ψ and ϕ_k are three-electron spin functions 1, 2, and 3 denote the electron spins on P^+ , I^- , and Q_A^- , respectively; g_i is the electron g-value of electron i; β denotes the Bohr magneton; B is the external magnetic field of the EPR spectrometer; J_{23} denotes an exchange interaction - assumed to be isotropic - between spins 2 and 3. $\{\phi_k\}$ spans an orthogonal set of basis functions:

$$\begin{aligned} \phi_1 &= |\alpha\alpha\alpha\rangle & \phi_3 &= |\alpha\beta\alpha\rangle & \phi_5 &= |\alpha\beta\beta\rangle & \phi_7 &= |\beta\beta\alpha\rangle \\ \phi_2 &= |\alpha\alpha\beta\rangle & \phi_4 &= |\beta\alpha\alpha\rangle & \phi_6 &= |\beta\alpha\beta\rangle & \phi_8 &= |\beta\beta\beta\rangle \end{aligned}$$

We choose $\vec{B} = B_z \hat{z} = B$; and $J_{23} = J$

Solving (1) and setting the secular determinant to zero:

$$\det \{ H_{ij} - E S_{ij} \} = 0 \quad \text{and} \quad S_{ij} = \delta_{ij}$$

yields the secular matrix, given by:

$$\begin{vmatrix} d_{11} & & & & & & & & \\ & d_{22} & -J & & & & & & \\ & -J & d_{33} & & & & & & \\ & & & d_{44} & & & & & \\ & & & & d_{55} & & & & \\ & & & & & d_{66} & -J & & \\ & & & & & -J & d_{77} & & \\ & & & & & & & d_{88} & \end{vmatrix} = 0 \quad (4)$$

with

$$d_{11} = \Delta_1 + \Delta_2 + \Delta_3 - J/2 - E$$

$$d_{22} = \Delta_1 + \Delta_2 - \Delta_3 + J/2 - E$$

$$d_{33} = \Delta_1 - \Delta_2 + \Delta_3 + J/2 - E$$

$$d_{44} = -\Delta_1 + \Delta_2 + \Delta_3 - J/2 - E$$

$$d_{55} = \Delta_1 - \Delta_2 - \Delta_3 - J/2 - E$$

$$d_{66} = -\Delta_1 + \Delta_2 - \Delta_3 + J/2 - E$$

$$d_{77} = -\Delta_1 - \Delta_2 + \Delta_3 + J/2 - E$$

$$d_{88} = -\Delta_1 - \Delta_2 - \Delta_3 - J/2 - E$$

where

$$\Delta_1 = \frac{1}{2} g_1 \beta B, \text{ the Zeeman energy of spin 1.}$$

Solving (4), taking the g-values of the first and second spin to be equal (they differ ca. 0.001 [4,23]):

$$\Delta_1 = \Delta_2 = \Delta$$

and

$$C = (\Delta - \Delta_3)^2 + J^2$$

yields the energies and eigenfunctions of the eight eigenstates of P^E (Table II).

The eigenfunctions can be expressed in another basis set, e.g. in "RP-functions", which consist of the conventional singlet and triplet functions, describing spins 1 and 2, combined with the spin function of the third spin, either $|\alpha\rangle$ or $|\beta\rangle$. These "RP"-basis functions conveniently show the probability of populating any of the three triplet sublevels of P^R upon recombination.

Table II

Eigenfunctions and -energies of three-spin P^F

i	ψ_i^a	E_i
1.	$ aaa\rangle$	$2\Delta + \Delta_3 - J/2$
2.	$c_1 a\alpha\beta\rangle + c_2 \alpha\beta a\rangle$	$\Delta + J/2 + \sqrt{C}$
3.	$c_2 a\alpha\beta\rangle - c_1 \alpha\beta a\rangle$	$\Delta + J/2 - \sqrt{C}$
4.	$ \beta aa\rangle$	$\Delta_3 - J/2$
5.	$ \alpha\beta\beta\rangle$	$-\Delta_3 - J/2$
6.	$c_1 \beta\alpha\beta\rangle + c_2 \beta\beta\alpha\rangle$	$-\Delta + J/2 + \sqrt{C}$
7.	$c_2 \beta\alpha\beta\rangle - c_1 \beta\beta\alpha\rangle$	$-\Delta + J/2 - \sqrt{C}$
8.	$ \beta\beta\beta\rangle$	$-2\Delta - \Delta_3 - J/2$

$$a: c_1 = .J/[J^2 + (\Delta G - \sqrt{C})^2]^{1/2}; \Delta G = \Delta - \Delta_3$$

$$c_2 = (\Delta G - \sqrt{C})/[J^2 + (\Delta G - \sqrt{C})^2]^{1/2}; C = (\Delta G)^2 + J^2$$

The projection of the eigenfunctions into "RP" functions is given in Table IIIa. For completeness the inverse projection is given in Table IIIb.

The relative energy levels of the eigenstates are shown in Figure 2. In this figure these energy levels of P^F were calculated using the experimental values for J and ΔG ($\Delta - \Delta_3$) of Rps. viridis.

The eigenfunctions $\psi_{2,3,6}$ and ψ_7 are linear combinations of a singlet, T_0 , and T_+ or T_- RP function (see Table IIIa). This means that the probability that the P^F state recombines into a $|T_+\rangle$ or $|T_-\rangle$ P^R substate is non-vanishing at high field: the presence of a third electron spin, coupling to the second spin on I^- breaks the exclusive $S-T_0$ mixing which characterizes the "true two-spin" RP-mechanism in photosynthetic species [19,20].

Table III

Projection of eigenfunctions (ψ_j) into "RP"-functions (a) and the inverse (b)

IIIa	
i	ψ_i in "RP"-functions
1.	$ T_+\alpha\rangle$
2.	$c_2/\sqrt{2} S\alpha\rangle + c_2/\sqrt{2} T_0\alpha\rangle + c_1 T_+\beta\rangle$
3.	$-c_1/\sqrt{2} S\alpha\rangle - c_1/\sqrt{2} T_0\alpha\rangle + c_2 T_+\beta\rangle$
4.	$-1/\sqrt{2} S\alpha\rangle + 1/\sqrt{2} T_0\alpha\rangle$
5.	$1/\sqrt{2} S\beta\rangle + 1/\sqrt{2} T_0\alpha\rangle$
6.	$-c_1/\sqrt{2} S\beta\rangle + c_1/\sqrt{2} T_0\beta\rangle + c_2 T_-\alpha\rangle$
7.	$-c_2/\sqrt{2} S\beta\rangle + c_2/\sqrt{2} T_0\beta\rangle - c_1 T_-\alpha\rangle$
8.	$ T_-\beta\rangle$

For definition of c_1 and c_2 , see legend of Table II

IIIb	
"RP"-function	in eigenfunction ψ_i
$ S\alpha\rangle$	$c_2\psi_2 - c_1\psi_3 - \psi_4$
$ S\beta\rangle$	$c_1\psi_6 - c_2\psi_7 + \psi_5$
$ T_+\alpha\rangle$	ψ_1
$ T_+\beta\rangle$	$c_1\psi_2 + c_2\psi_3$
$ T_0\alpha\rangle$	$c_2\psi_2 - c_1\psi_3 + \psi_4$
$ T_0\beta\rangle$	$c_1\psi_6 + c_2\psi_7 + \psi_5$
$ T_-\alpha\rangle$	$c_2\psi_6 - c_1\psi_7$
$ T_-\beta\rangle$	ψ_8

For definition of c_1 , and c_2 , see the legend of Table II

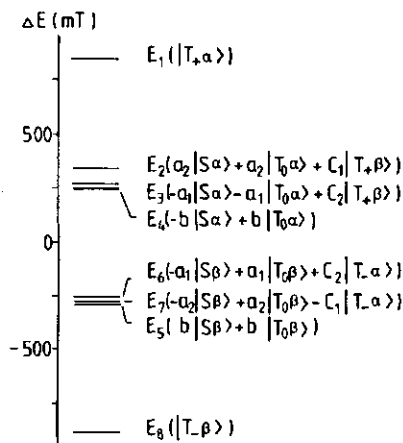


Figure 2.

Energy level scheme of the eight magnetic sublevels in the reaction center state P^F , as a result of the spin-spin interactions between the electrons on P^+ , I^- , and $Q_A^-Fe^{2+}$, defined by eq. (2). The coefficients c_1 and c_2 are given in the legend of Table II; $a_1=c_1/\sqrt{2}$, $a_2=c_2/\sqrt{2}$, $b=1/\sqrt{2}$; $|J_{23}|=20$ mT, $\Delta G=28$ mT.

Populating probabilities of P^R

In order to estimate the fraction of P^R that will be found in the $|T_{\pm}\rangle$ states, we consider the time-dependent eigenfunctions:

$$\psi_j(t) = \psi_j \cdot \exp\left\{-\frac{i}{\hbar} E_j t\right\} \quad (5)$$

$$j \in \{1, 2, \dots, 8\}$$

When the RP is born, at $t=0$, its spin configuration is in the singlet state. If we assume that at $t=0$ 50% of the net spin on Q_A^- exists as $|\alpha\rangle$, and the other 50% as $|\beta\rangle$, then the probability-coefficient of finding an eigenstate $|\psi_j\rangle$ at $t=0$ is given by:

$$c_{\psi_j}(t=0) = \langle S\alpha | \psi_j \rangle + \langle S\beta | \psi_j \rangle \quad (6)$$

Since the problem is symmetric for spins 3 being $|\alpha\rangle$ or $|\beta\rangle$, we proceed considering only the first term in eq. (6). The appropriate time-dependent eigenfunction then becomes:

$$\psi_j(t) = \langle S\alpha | \psi_j \rangle \langle \psi_j | \exp\left\{-\frac{i}{\hbar} E_j t\right\} \quad (7)$$

If we want to know how much T_0 character this eigenstate has (the calculation of the T_+ and T_- character is analogous):

$$[c_{T_0}(t)]_j = |T_0\alpha\rangle \langle S\alpha | \psi_j \rangle \langle \psi_j | \exp\left\{-\frac{i}{\hbar} E_j t\right\} \quad (8)$$

Hence the probability to observe the $|T_0\rangle$ state in this eigenfunction is given by:

$$|c_{T_0}(t)|^2 = \left| \sum_{j=1}^8 |T_0\alpha\rangle \langle S\alpha | \psi_j \rangle \langle \psi_j | \exp\left\{\frac{i}{\hbar} E_j t\right\} \right|^2 \quad (9)$$

The results for all 8 spin combinations are summarized in Table IV.

Table IV
Time-dependent probability to find the "RP" state ϕ_1 in P^F

ϕ_i	$ c_{\phi_1} ^2$
$ T_+\alpha\rangle$	0
$ T_+\beta\rangle$	$1/2 c_1^2 c_2^2 (1 - \cos \omega_{23}t)$
$ T_0\alpha\rangle$	$1/8 (1 + c_1^4 + c_2^4 + 2c_1^2 c_2^2 \cos \omega_{23}t - 2c_1^2 \cos \omega_{34}t - 2c_2^2 \cos \omega_{24}t)$
$ T_0\beta\rangle$	$1/8 (1 + c_1^4 + c_2^4 + 2c_1^2 c_2^2 \cos \omega_{67}t - 2c_1^2 \cos \omega_{56}t - 2c_2^2 \cos \omega_{57}t)$
$ T_-\alpha\rangle$	$1/2 c_1^2 c_2^2 (1 - \cos \omega_{67}t)$
$ T_-\beta\rangle$	0
$ S\alpha\rangle$	$1/8 (1 + c_1^4 + c_2^4 + 2c_1^2 c_2^2 \cos \omega_{23}t + 2c_1^2 \cos \omega_{34}t + 2c_2^2 \cos \omega_{24}t)$
$ S\beta\rangle$	$1/8 (1 + c_1^4 + c_2^4 + 2c_1^2 c_2^2 \cos \omega_{67}t + 2c_1^2 \cos \omega_{56}t + 2c_2^2 \cos \omega_{57}t)$

c_1, c_2 , and ΔG as defined in the legend of Table II.

$$\hbar\omega_{23} = J + 2\sqrt{C}; \quad \hbar\omega_{24} = \Delta G + J + \sqrt{C}; \quad \hbar\omega_{34} = \Delta G + J - \sqrt{C}; \quad \hbar\omega_{23} = J + 2\sqrt{C}$$

$$\hbar\omega_{56} = \Delta G - J - \sqrt{C}; \quad \hbar\omega_{57} = \Delta G - J + \sqrt{C};$$

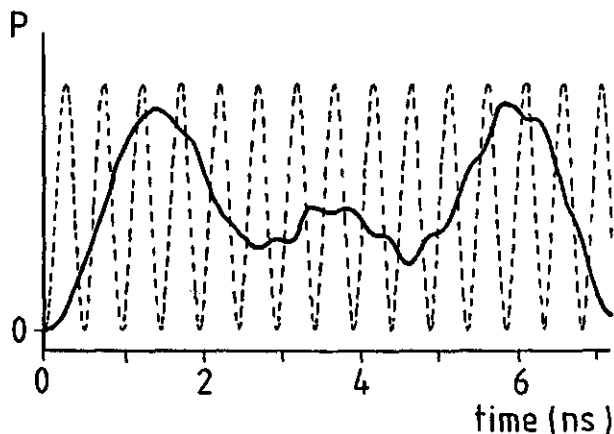


Figure 3.

Time-dependence of the probability P to detect the $|T_+\rangle$ or $|T_-\rangle$ state of spins 1 and 2 in the three spin system (dashed line), and idem to detect the $|T_0\rangle$ state (heavy line). In this figure the amplitudes are differently scaled: the maximum probability of the $|T_{\pm}\rangle$ states is ca 25 x smaller than for the $|T_0\rangle$ probability. $|J_{23}|/\Delta G = 0.43$.

There is a difference between the time-dependence of the probability for the $|T_{\pm}\rangle$ character in P^F , and that of the $|S\rangle$ and $|T_0\rangle$ character as is evident from figure 3. Using experimental values for *Rps. viridis* for J_{23} and ΔG , it is found that the frequency of the quantum beats for the $|T_{\pm}\rangle$ and $|T_-\rangle$ states is higher by a factor ~ 5 with respect to the overall-frequency of the $|T_0\rangle$ and $|S\rangle$ states in P^F . The maximum amplitude of the $|T_{\pm}\rangle$ probability beats is however much smaller than for the singlet and T_0 probabilities.

If a lifetime for P^F of τ ns is used, then the probability for recombination in the $|T_+\rangle$ substate of P^R (with the third spin in the state $|\alpha\rangle$ is given by:

$$|c_{T_+\alpha}|_{P^R}^2 = \left| \int_0^{\infty} \sum_{j=1}^8 |T_+\alpha\rangle \langle S\alpha| \Psi_j \rangle \langle \Psi_j| \exp\left\{-\frac{i}{\hbar} E_j t\right\} \cdot \tau \cdot \exp\left\{-\frac{t}{\tau}\right\} dt \right|^2 \quad (10)$$

Table V

Populating probabilities of p^R

ϕ_i	$ c_{\phi_i} ^2(p^R)$
$ T_+\alpha\rangle$	0
$ T_+\beta\rangle$	$c_1^2 c_2^2 [1 - (\omega_{23}^2 \tau^2 + 1)^{-1}]$
$ T_0\alpha\rangle$	$1/4 [1 + c_1^4 + c_2^4 + 2c_1^2 c_2^2 (\omega_{23}^2 \tau^2 + 1)^{-1} - 2c_1^2 (\omega_{34}^2 \tau^2 + 1)^{-1} - 2c_2^2 (\omega_{24}^2 \tau^2 + 1)^{-1}]$
$ T_0\beta\rangle$	$1/4 [1 + c_1^4 + c_2^4 + 2c_1^2 (\omega_{67}^2 \tau^2 + 1)^{-1} - 2c_1^2 (\omega_{56}^2 \tau^2 + 1)^{-1} - 2c_2^2 (\omega_{57}^2 + 1)^{-1}]$
$ T_-\alpha\rangle$	$c_1^2 c_2^2 [1 - (\omega_{67}^2 \tau^2 + 1)^{-1}]$
$ T_-\beta\rangle$	0

ω_{ij} as in the legend of Table IV; c_1, c_2 as in the legend of Table II.

Using that for the $p^F \rightarrow p^R$ process the spatial spin quantization is conserved, and assuming that there are no additional factors influencing the recombination in any of the three triplet states, we obtain the results summarized in Table V.

Because it is known that the triplet yield at low temperatures is near to unity [30], the recombination into a singlet state is neglected. We find about 95% $|T_0\rangle$, and ca. 2.5% $|T_+\rangle$ and $|T_-\rangle$. These populating rates do not cause a change of sign in the steady state EPR triplet spectrum, using the known [21] decay rates of p^R in Rps. viridis. This is in accordance with what is observed experimentally. At temperatures well below 10 K, the AE EAE ESP pattern is not affected, in spite of the presence of the third spin (see Chapter IV).

Several groups performed extended X-ray absorption fine structure (EXAFS) spectroscopy [33,34] and static magnetization measurements [35] on the iron site in RC's. From these results it was concluded that the Fe^{2+} is in a distorted octahedral environment. Bunker et al. [33] concluded that the Fe^{2+} is ligated to probably three histidine - nitrogens, and one oxygen (and indirectly to the primary and secondary quinone). This was confirmed by the crystallographic data from Michel et al. [36], further showing that the oxygen atom belongs to a glutamine amino acid residue (see also fig.5, Chapter I).

Calculations on the static interactions within the quinone-iron complex of Rb. sphaeroides RC's gave satisfactory fits for the experimental low temperature ($T < 5$ K) EPR spectra [28]. Only the predictions with respect to the third ($m_s^{\text{Fe}=0}$) Fe^{2+} energy level were not confirmed by the experimental results. This level is approximately 10 cm^{-1} (which is equivalent to ~ 15 K) above the second level. The difference between the calculated and experimental spectra was explained invoking fast spin relaxation, broadening the third level [28].

In the reduced quinone-iron complex, all Fe^{2+} energy levels are split into two, because of the magnetic interaction between the electron spins on Q_A^- and Fe^{2+} . At a magnetic field strength of 300 mT (X-band EPR) however, this splitting is small compared to the energy differences between the sublevels of the Fe^{2+} ground-state quintet, resulting in five $\text{Fe}^{2+}\text{-Q}_A^-$ doublets. Therefore, EPR only monitors transitions within one and the same $\text{Fe}^{2+}\text{-Q}_A^-$ doublet.

A distorted octahedral crystal field, as present around Fe^{2+} in the RC, reduces the Fe^{2+} orbital momentum [37], and thus the zero-field splittings within the ground state quintet. Such an effect has also been observed in MgO crystals, doped with paramagnetic Fe^{2+} [38-41]. Remarkably, in those samples some spectroscopic features (i.e. the quadrupole splitting in Mössbauer spectra) change also considerably at 14 K. This was suggested to arise from an Orbach SLR process [39], involving an excited Fe^{2+} spin state with an energy level

that was ca. 100 cm^{-1} higher than the observed level. However, static crystal-field theory predicted a nearest excited state level at 200 cm^{-1} . In this case the reduced observed energy-difference could be accounted for by invoking a dynamic Jahn-Teller effect, also quenching the spin-orbit coupling (SOC) [40] in MgO, but not destroying it.

The similarity between these observations and those in RC's may provide a clue to understand the SLR process in RC's. The residual orbital momentum of Fe^{2+} couples relatively strongly (with respect to that of Q_A^-) to the phonons in the protein matrix. Recently Bixon and Jortner [42] reported that the average vibrational frequency in proteins (i.e. the RC) is $\sim 100 \text{ cm}^{-1}$. Therefore, the protein matrix is capable of delivering phonons of required energy to the Fe^{2+} (by SOC), inducing rapid spin transitions. These phonon-induced spin flips are expected to become effective around 14 K (the energy separation in degrees K between the second and third spin level in the Fe^{2+} ground state quintet [28]), and will cause an important decrease in the electron spin correlation time (and thus of T_1) of Fe^{2+} .

When only the lowest two ground-state doublets of the $\text{Fe}^{2+}\text{-Q}_A^-$ complex are involved (i.e. $T < 8 \text{ K}$), an Orbach process on a μs timescale has been observed in RC's [43]. When the third -fast relaxing- doublet becomes energetically within reach, a substantial increase of the relaxation rate is expected, and may well be within the lifetime of P^F ($\sim 10 \text{ ns}$). The mechanistic order of the events, if separable at all, is schematically given in figure 4.

The effect of T_1 processes in the $\text{Q}_A^-\text{Fe}^{2+}$ complex

As pointed out in Chapter I, the primary acceptor is considered to be a magnetically coupled quinone-iron complex. Since the spin-lattice relaxation in the high spin Fe^{2+} ($S=2$) can be very rapid already at low temperatures ($10^{-8} - 10^{-9} \text{ s}$ at $\sim 20 \text{ K}$ [12,24]), the third spin on Q_A^- in the $\text{Q}_A^-\text{Fe}^{2+}$ complex will be forced to make concomitant spin transitions with the Fe^{2+} spins ($J_{\text{Fe}^{2+}\text{-Q}_A^-} = 130 \text{ mT}$

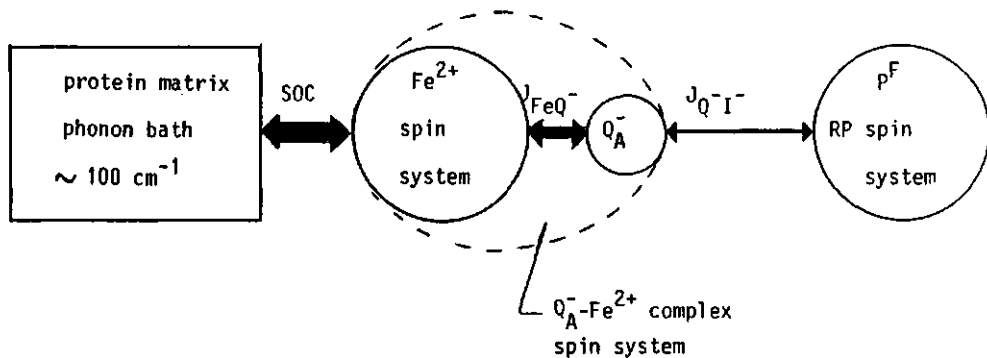


Figure 4.

Schematic diagram of the magnetic interactions determining the temperature dependence of the spin-dynamics within the RC state P^F . More details are given in the text.

[25]). Following Abragam [26] in such a system with a time-independent spin-spin interaction, a time-dependent spin operator $S_3(t)$ can be related to two different processes: Spin 3 may flip alone, but also, due to the exchange interaction between spins 2 and 3, simultaneously with spin 2. Table VI gives the transition probabilities between the eigenstates of P^F , if spin 3 flips. In figure 2 these transitions are indicated by thin vertical bars. From this figure and Table VI it is seen that transitions may occur between two groups of four eigenstates. One group connects $|S\rangle$, $|T_0\rangle$, $|T_{+\beta}\rangle$, and $|T_{+\alpha}\rangle$, the other connects the $|S\rangle$, $|T_0\beta\rangle$, $|T_{-\alpha}\rangle$, and $|T_{-\beta}\rangle$.

Figure 5 shows a model for a kinetic approach to investigate the effect of spin transitions on the populating rates of P^R from one of the two equivalent four-level groups. If the temperature increases, the electron spin correlation time of Fe^{2+} decreases, resulting in a concomitant shortening of the correlation time (τ_e) of Q_A^- in the quinone-iron complex. By this magnetic interaction with spin 2, this induces more transitions per unit time between the sublevels of P^F (see fig. 5). At relatively high temperatures P^F might be considered fully relaxed, i.e. all levels in each group of four levels are

Table VI

Probabilities P_{ij} for transitions $\psi_i \rightarrow \psi_j$ within P^F upon a flip of spin 3 (on $Q_A^-Fe^{2+}$).

$i \backslash j$	1	2	3	4	5	6	7
2	c_1^2						
3	c_2^2	$2-4c_1^2c_2^2$					
4	0	0	0				
5	0	c_2^2	c_1^2	0			
6	0	0	0	c_1^2	0		
7	0	0	0	c_2^2	0	$2-4c_1^2c_2^2$	
8	0	0	0	0	0	c_2^2	c_1^2

c_1 , and c_2 as in the legend of Table II.

equally populated by the fast equilibration between the four populations of P^F within the lifetime of P^F . In the limit of complete relaxation, considering both groups of four levels, the populating rates of P^R become, according to this model:

$$P_+ = P_- = k + kk_1 + kk_2$$

and

$$P_0 = 2(k/2 + kk_1/2 + kk_2/2) = P_+ = P_-$$

where k is the $P^F \rightarrow P^R$ decay rate constant.

Hence, the populating rates become equal at high temperatures, resulting in an inverted EPR spin polarization pattern for the Y-peaks. In fact, the ESP pattern of the X-peaks is predicted by this simple model to be inverted too, but anisotropic effects, which are obviously pre-

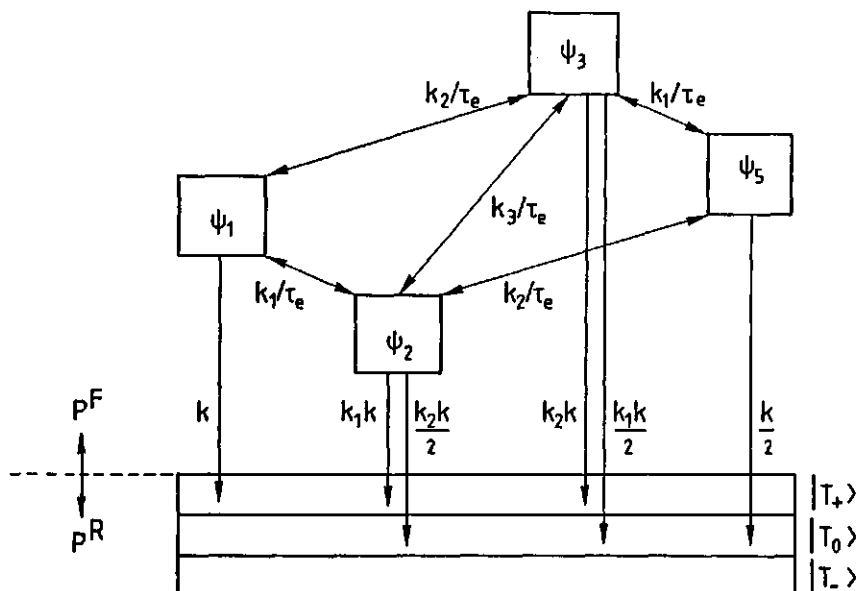


Figure 5.

One group of four (out of eight) magnetic sublevels of p^F , coupled by transitions induced by Fe^{2+} spin-lattice relaxation. k_1 , k_2 , and k_3 denote transition probabilities (see Table VI): $k_1=c_1^2$, $k_2=c_2^2$, $k_3=(k_1-k_2)^2$. c_1 and c_2 are defined in the legend of Table II. τ_e denotes the correlation time for $\alpha \leftrightarrow \beta$ transitions of spin 3 on Q_A^- in the $Q_A^-Fe^{2+}$ complex.

Vertical arrows denote transitions from the magnetic sublevels of p^F to the spin levels of p^R . k denotes the inverse lifetime of p^F .

sent in the system, have been neglected.

Upon a pulsed excitation the subsequent transient of an appropriate EPR transition within p^R is, according to the kinetic model of figure 5, expected to start at zero intensity, since there is no population difference between any pair of sublevels at $t \sim 0 \mu s$. The experimental results (see Chapter V) showed that this is the case for the Z-transitions. However, there was no effect of the presence of Q_A^- on the X-transitions, whereas the transients of the Y-transitions surprisingly showed that the $|T_+>$ and $|T_->$ sublevels of p^R are initially more populated than the $|T_0>$ sublevel.

Discussion

The kinetic approach presented above, based on the static three electron spin model, qualitatively illustrates the further break-down of the $S-T_0$ mixing (determined by the RP-mechanism) as the temperature (viz. the spin-lattice relaxation within P^R) increases. However, this approach is inadequate for understanding the observed preferential populating of the $|T_+\rangle$ and $|T_-\rangle$ substates of P^R for the Y^- and Y^+ transitions.

An explanation for the larger populating of the $|T_+\rangle$ states (for the Y^-/Y^+ transitions) may be sought in the different time-dependence of the probability beats, shown in figure 2, where it is seen that at short periods after the generation of P^R the $|T_+\rangle$ and $|T_-\rangle$ states are more probable than the corresponding $|T_0\rangle$ states.

The anisotropy which is observed in the temperature dependent EPR spectra cannot be explained by invoking an isotropic exchange interaction only in eq. 2. There are several explanations: 1) Dipolar and/or anisotropic exchange interaction between I^- and Q_A^- , as has been invoked to explain the shape of the split EPR signal from I^- [12] (due to its magnetic interaction with Q_A^-); 2) Dipolar and/or anisotropic exchange in the $Fe^{2+}-Q_A^-$ complex itself [28], giving rise to anisotropic relaxation of this complex; 3) Dipolar interaction between P^+ and I^- , or a combination of 1 - 3.

It is obvious that a more sophisticated treatment is necessary to fully understand the experimental results reported in Chapters IV and V of this work. Preliminary results from model calculations, based on the stochastic Liouville theorem [27], and including hyperfine, and dipolar interactions [29] are reported in Chapter V.

2.4 REFERENCES

- [1] V.A. Shuvalov, J. Ames, and L.N.M. Duysens, *Biochim. Biophys. Acta* 851 (1986) 327-330.
- [2] A. De Groot, E.J. Lous, and A.J. Hoff, *Biochim. Biophys. Acta* 808

- (1985) 13-20.
- [3] C.C. Schenck, W.W. Parson, D. Holten, and M.W. Windsor, *Biochim. Biophys. Acta* 635 (1981) 383-392.
 - [4] C.E.D. Chidsey, M.G. Roelofs, and S.G. Boxer, *Chem. Phys. Lett.* 74 (1980) 113-118.
 - [5] A.J. Hoff, and P.J. Hore, *Chem. Phys. Lett.* 108 (1984) 104-110.
 - [6] P.L. Dutton, R.C. Prince, and D.M. Tiede, *Photochem. Photobiol.* 28 (1978) 939-949.
 - [7] P. Gast, and A.J. Hoff, *Biochim. Biophys. Acta* (1979) 520-535.
 - [8] A.J. Hoff, and P. Gast, *J. Phys. Chem.* 108 (1984) 104-110.
 - [9] M.Y. Okamura, R.A. Isaacson, and G. Feher, *Biochim. Biophys. Acta* 546, (1979) 394-417.
 - [10] R.C. Prince, P.L. Dutton, B.J. Clayton, and R.K. Clayton, *Biochim. Biophys. Acta* 502 (1978) 354-358.
 - [11] D.M. Tiede, R.C. Prince, and P.L. Dutton, *Biochim. Biophys. Acta* 449 (1976) 447-467.
 - [12] R.C. Prince, D.M. Tiede, J.P. Thornber, and P.L. Dutton, *Biochim. Biophys. Acta* 462 (1977) 467-490.
 - [13] R.C. Prince, *Biochim. Biophys. Acta* 501 (1978) 195-207.
 - [14] V.V. Klimov, E. Dolan, E.R. Shaw, and B. Ke, *Proc. Natl. Acad. Sci. USA* 77 (1980) 7227-7231.
 - [15] V.V. Klimov, E. Dolan, and B. Ke, *FEBS Lett.* 112 (1980) 97-100.
 - [16] A.W. Rutherford, and P. Mathis, *FEBS Lett.* 154 (1983) 328-334.
 - [17] A. Abragam, and B. Bleaney, *Electron paramagnetic resonance of transition ions* (1970) pp. 541-584, Clarendon Press, Oxford.
 - [18] J.P. Gayda, P. Bertrand, A. DeVille, C. More, G. Roger, J.F. Gibson, and R. Cammack, *Biochim. Biophys. Acta* 581 (1979) 15-26.
 - [19] M.C. Thurnauer, J.J. Katz, and J.R. Norris, *Proc. Natl. Acad. Sci. USA* 72 (1975) 3270-3274.
 - [20] R.E. Blankenship, T.J. Schaafsma, and W.W. Parson, *Biochim. Biophys. Acta* 461 (1977) 297-305.
 - [21] J.F. Kleibeuker, and T.J. Schaafsma, *Chem. Phys. Lett.* 29 (1974) 116-122.
 - [22] H.J. Den Blanken, A.P.J.M. Jongenelis, and A.J. Hoff, *Biochim.*

- Biophys. Acta 725 (1983) 472-482.
- [23] J.D. McElroy, G. Feher, and D.C. Mauzerall, *Biochim. Biophys. Acta* 267 (1972) 363-374.
- [24] C.P. Scholes, R.A Isaacson, and G. Feher, *Biochim. Biophys. Acta* 244 (1971) 206-210.
- [25] G.C. Dismukes, H.A. Frank, R. Friesner, and K. Sauer, *Biochim. Biophys. Acta* 764 (1984) 253-271.
- [26] A. Abragam "The principles of nuclear magnetism" (1961) pp. 305-312, Oxford Univ. Press, Amen House, London.
- [27] see e.g. K. Blum "Density matrix theory and applications" (1981) Plenum Press, New York.
- [28] W.F. Butler, R. Calvo, D.R. Fredkin, R.A. Isaacson, M.Y. Okamura, and G. Feher, *Biophys. J.* 45 (1984) 947-973.
- [29] P.J. Hore, personal communication.
- [30] W.W. Parson, and T.G. Monger, *Brookhaven Symp. Biol.* 28 (1976) 195-212.
- [31] A.A. Krasnovskii Jr, N.N. Lebedev, and F.F. Litvin, *Dokl. Biophys. (Transl.)* 216 (1974) 39-42.
- [32] S.S. Dornikov, V.N. Knyukshto, K.N. Solovev, and M.P. Tsvirko, *Opt. Spectrosc. (USSR)* 46 (1979) 385-388.
- [33] G. Bunker, E.A. Stern, R.E. Blankenship, and W.W. Parson, *Biophys. J.* 37 (1982) 539-551.
- [34] P. Eisenberger, M.Y. Okamaru, and G. Feher, *Biophys. J.* 37 (1982) 523-538.
- [35] W.F. Butler, D.C. Johnston, M.B. Shore, D.R. Fredkin, M.Y. Okamura, and G. Feher, *Biophys. J.* 32 (1980) 967-992.
- [36] H. Michel, O. Epp, and J. Deisenhofer, *EMBO J.* 5 (1986) 2445-2451.
- [37] A. Abragam, and B. Bleaney "Electron Paramagnetic Resonance of Transition Ions" (1970) pp. 443-446, Oxford Univ. Press.
- [38] W. Low, and M. Weger, *Phys. Rev.* 118 (1969), 1119.
- [39] F.S. Ham, *Phys. Rev.* 160 (1967) 328.
- [40] F.S. Ham, W.M. Schwarz, and M.C.M. O'Brien, *Phys. Rev.* 185 (1969) 548.
- [41] J.Y. Wong, *Phys. Rev.* 168 (1968) 337.

- [42] M. Bixon, and J. Jortner, *J. Phys. Chem.* 90 (1986) 3795-3800.
- [43] R. Calvo, W.F. Butler, R.A. Isaacson, M.Y. Okamura, D.R. Fredkin, and G. Feher, *Biophys. J.* 37 (1982) (2 Pt 2) 111^a, Abstract M-PM-E7.

CHAPTER III

TIME-RESOLVING EQUIPMENT AND EXPERIMENTAL METHODS

3.1 INTRODUCTION

The experiments and the theoretical considerations described in this work aim at elucidation of the kinetic pathways involving the triplet state (P^R) in photosynthetic bacterial RC's. From earlier work [1-3] it is known that the populating rates of P^R are of the order of 10^8 s^{-1} , which is too fast to be detected by any EPR spectrometer. Therefore, the populating rates themselves cannot directly be measured by EPR, but one can measure the 'initial' spin polarization pattern. The initial ESP reflects the population distribution over the three spin levels of P^R before this distribution has changed appreciably due to spin-lattice relaxation between the spin levels, or due to decay to the ground state. Because the standard response time of the conventional X-band EPR spectrometer is limited to about $200 \mu\text{s}$ [4], which is long compared to reported lifetimes [5] and spin-lattice relaxation times [6,7] of P^R spin levels, it was necessary to improve the response time of the EPR spectrometer. However, since we are interested in the complete time evolution of the magnetic resonance signals of this triplet state, including the relatively long decay rates of P^R to the singlet ground state in one and the same experiment, a wide frequency-response is required.

Several light sources can be used to generate the triplet state and to determine its kinetics [6,8-10], from which a pulsed light source (i.e. a pulsed laser with sufficient energy per pulse) offers the most straightforward approach in view of the interpretation of the

experimental results [6,11]. If the duration of the light pulse is much shorter than the observed decay- and relaxation times, generally deconvolution methods are unnecessary. A disadvantage of most pulsed solid state lasers is the limited number of fixed wavelengths of the output light. The Q-switched Nd:YAG laser used in our experiments (1064 nm, 532 nm, and 355 nm), produces no radiation in the region of optical absorbance of the photosynthetic RC's (around 600 nm, and 780 - 1000 nm) [12]. Therefore a tunable dye laser was needed to shift the excitation wavelengths towards desired values.

In the next section (3.2) of this Chapter the design and construction of a high-gain pulsed dye laser system is described. This dye-laser makes use of the negligible reflection losses at optical boundaries when Brewster angles between light beam and optical boundary are used to obtain optimum efficiency for use in transient EPR spectroscopy. It allows excitation at wavelengths which are not available from the pump source.

When pulsed excitation sources are used in time-resolved EPR, e.g. lasers or pulsed beams of electrons [13], it is generally necessary to eliminate transient artefacts. Section 3.3 of this Chapter describes methods to reduce these artefacts.

In section 3.4 several aspects of time-resolved EPR are considered with respect to frequency response, time-resolution and fidelity of the detected transient, leading to a novel approach of wide-band phase-sensitive detection of EPR transients. This method combines wide frequency response with the high S/N ratio of phase-sensitive detection, and has therefore some advantages over the well-known "direct detection method" [14-17].

Finally, in section 3.5 other techniques and preparative methods relevant to this study are briefly described.

References

- [1] W.W. Parson, R.K. Clayton, and R.J. Cogdell, *Biochim. Biophys. Acta* 387 (1975) 265-278.
- [2] V.A. Shuvalov, and W.W. Parson, *Proc. Natl. Acad. Sci. USA* 78 (1980) 957-961.
- [3] C.C. Schenck, R.E. Blankenship, and W.W. Parson, *Biochim. Biophys. Acta* 680 (1982) 44-59.
- [4] A.D. Trifunac, and R.G. Lawler, *Magnet. Reson. Rev.* 7 (1982) 147-174.
- [5] H.J. Den Blanken, and A.J. Hoff, *Biochim. Biophys. Acta* 725 (1983) 472-482.
- [6] P. Gast, and A.J. Hoff, *FEBS Lett.* 85 (1978) 183-188.
- [7] A.J. Hoff, and I.I. Proskuryakov, *Chem. Phys. Lett.* 115 (1985) 303-310.
- [8] J.F. Kleibeuker, Thesis (1977) Wageningen Agricultural Univ., The Netherlands.
- [9] J.F. Kleibeuker, and T.J. Schaafsma, *Chem. Phys. Lett.* 29 (1974) 116-122.
- [10] A.J. Hoff, P.Gast, and J.C. Romijn, *FEBS Lett.* 73 (1977) 185-190.
- [11] C.J. Winscom, *Zeitschrift Naturforsch.* 30a (1975) 571-582.
- [12] G. Feher, and M.Y. Okamura in "The Photosynthetic Bacteria" (R.K. Clayton, and W.R. Sistrom, eds.) (1978) pp. 349-386, Plenum Press, New York.
- [13] M.S. Matheson, and L.M. Dorfman "Pulse radiolysis" (1969) M.I.T. Press, Cambridge.
- [14] S.I. Weissman, *Annu. Rev. Phys. Chem.* 33 (1982) 301.
- [15] W.J. McGann, and H.A. Frank, *Chem. Phys. Lett.* 121 (1985) 253-261.
- [16] S.S. Kim, and S.I. Weissman, *J. Magnet. Reson.* 24 (1976) 167-169.
- [17] S. King Wong, *J. Magnet. Reson.* 47 (1982) 500-503.

A. van Hoek and F.G.H. van Wijk

Agricultural University, Department of Molecular Physics,
De Dreijen 11, 6703 BC Wageningen, The Netherlands.

This paper describes the construction of a simple dye laser to be pumped by a Q-switched Nd:YAG laser. This system is used to create excited states at a time scale of ca. 10 ns, to be detected by means of time resolved EPR [1] or transient absorption spectroscopy. Neither of these techniques requires the spectral bandwidth of the dye laser to be particularly narrow, but spurious wavelengths must remain absent. For our applications multi-mode variations within the spectral envelope from shot to shot are not important and the dye laser was not designed to minimize these variations (e.g. a long cavity), which would have been necessary if applied to CARS for instance [2]. Recently a pulsed dye laser was reported [3] with a conversion efficiency of up to 20%, however tunability was achieved by changing the dye and/or its solvent. We preferred continuous tunability within the spectral range of the dye used.

Apart from the main wavelength, the output of a short cavity pulsed dye laser contains a background of spurious wavelengths, originating from spontaneous emission [4], in particular when pumped with high energy pulses from a Q-switched Nd:YAG laser (e.g. at 20 pulses per second: 100 mJ at 532 nm, 60 mJ at 355 nm). Therefore, the concept of an oscillator amplifier dye laser was used.

In order to gain maximum throughput efficiency of the dye laser, use was made of the polarized nature of the pump laser output by employing optical elements with such a geometry that all faces of these elements have the Brewster angle with respect to the laser beam.

This results in 100% deflections at the air-glass boundary. Also, 100% internal reflections were used. Fused silica Brewster cut elements were preferred because they have a long life expectancy and are relatively inexpensive as compared to many different customer specified high power mirrors (up to 100 MW/cm²). In the dye laser, described in this communication, only a few standard broadband mirrors were required.

The output of the Nd:YAG laser is horizontally polarized at all wavelengths (1064 nm, 532 nm using a 90° quartz rotator, and 355 nm). A gull wing prism wavelength separator is used to extract the desired output wavelength. The input and output faces of the two prisms are about at Brewster angle, resulting in negligible reflection losses. The output of the pump laser is directed towards the dye laser by two fused silica Brewster cut prisms (figure 1).

To pump the oscillator stage in the dye laser a small part of the

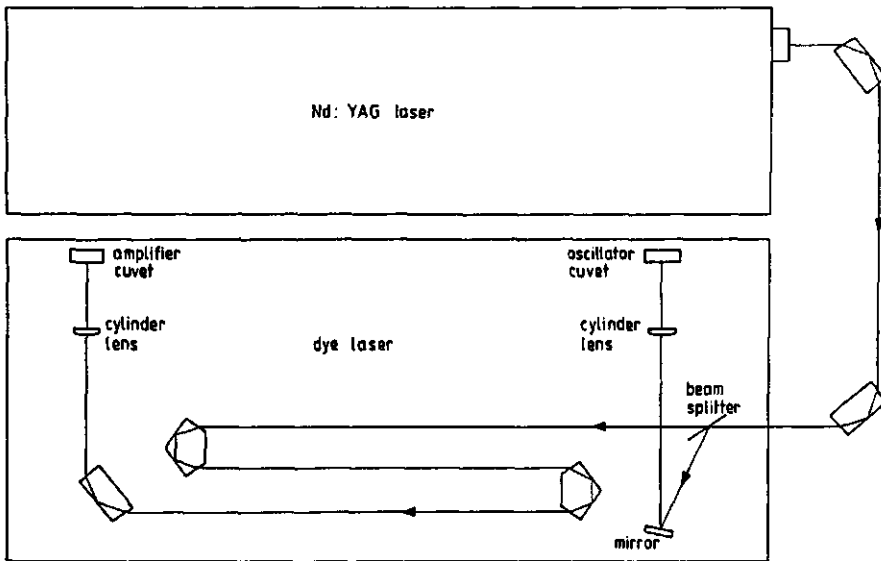


Figure 1.
Lay-out of the pump scheme.

main beam is split off, using a thin optical flat substrate (fused silica), which is tilted somewhat from Brewster angle. The percentage of reflectance of this beam splitter is controlled by changing the angle of the substrate with respect to the direction of the main beam [5]. During alignment, the excitation power of the oscillator stage was chosen as low as possible, but high enough to assure stable operation (ca. 1% of the incoming pump beam power).

The oscillator pump beam is directed to the oscillator cuvette through a fused silica cylindrical lens ($f=100$ mm), using a standard broadband mirror (Melles Griot, type 08MLB 003/341 or /343). The axis of the cylindrical lens could be rotated to control the overlap of the thin vertical image of the pump beam and the path of the dye laser beam in the cuvette. The focus line could also be adjusted.

The part of the pump beam that is not split off towards the oscillator stage, is deflected towards the amplifier stage via an optical delay line, using fused silica Brewster cut elements. The time delay

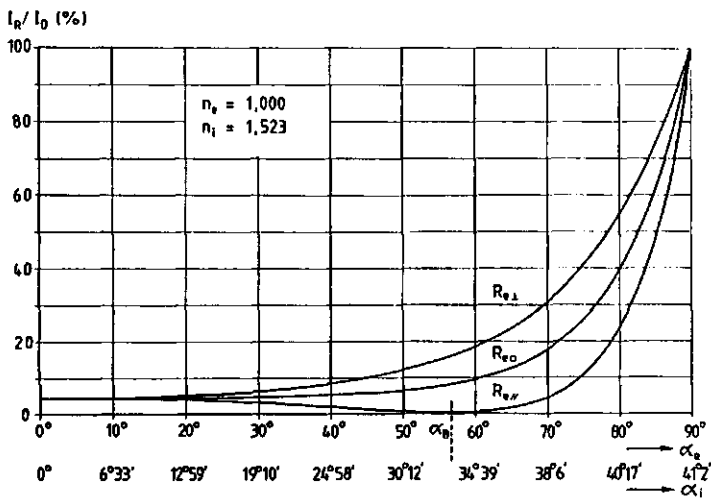


Figure 2. Reflected fractions of light on the surface boundary of an air/glass transition for unpolarized light (R_{e0}), and light polarized with the electric vector parallel ($R_{e//}$) and perpendicular ($R_{e\perp}$) to the plane of incidence. α_B is the Brewster angle.

of the amplifier pump pulse is necessary to compensate for the time delay, caused by building up laser action in the oscillator stage [6]. The optical delay line could be optimized by changing the position of the reflecting elements.

Just as in the oscillator cuvette, a thin vertical image is focussed in the amplifier cuvette by a cylindrical lens (lens and cuvette are identical to that in the oscillator stage). The cuvettes, the cylindrical lenses and the Brewster cut elements are all uncoated. Standard flow cuvettes were used (Hellma 134F QS, 10x4 mm).

The Brewster angle (α_B) for the optical elements was calculated from $\alpha_B = \arctan \mu$, where μ denotes the refractive index from air to fused silica [7]. To calculate the Brewster angle of the elements in the pump scheme, a theoretical wavelength of 420 nm was chosen as a compromise between the refractive indices [8] at 355 nm and 532 nm of the Nd:YAG laser output. The reflection losses introduced by this mismatch between theoretical and practical excitation wavelength were still very small, for the region of close to zero reflection around the Brewster angle is rather broad (figure 2). Further, the angle of the elements with respect to the light beam could be optimized for minimal reflection.

The oscillator stage of the dye laser consists of a standard broadband mirror (Melles Griot, type 08 MLB 003/343 or/341), four fused silica Brewster cut dispersion prisms [6], a flow cuvette and an output coupler (Zeiss FPE 015 nm, 30% reflectance, wedge 3%). The dye cuvette is about at the Brewster angle as a compromise for different optical boundaries. The cavity was kept as short as possible (ca. 20 cm, resulting in about 1.5 ns roundtrip time), and arranged in such a way that the laser beam passes the cuvette vertically (figure 3).

A shorter cavity results in more roundtrips during the 12 ns pump pulse, decreasing the bandwidth of the output. In general, also a lower output percentage of the cavity will increase the spectral purity. The reflectivity of the output mirror and the pump power to the oscillator were determined experimentally by using output mirrors with various percentages of reflection, and by varying the pump power: 30%

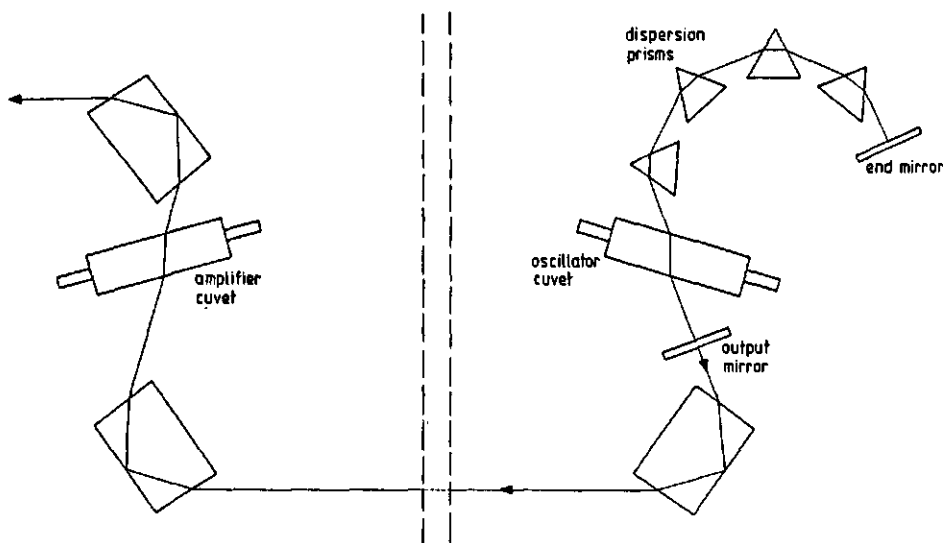


Figure 3.
Lay-out of the oscillator-amplifier scheme.

reflectivity and about 1% pump power resulted in reliable operation using a 12 ns width of the pump pulse and a 1.5 ns roundtrip time in the cavity.

Using the dispersion theory for multiple prism arrays as discussed by Duarte and Piper [9,10] a theoretical linewidth of the dye laser output of ≈ 1.5 nm/mrad was calculated. Thus, with an intra-cavity beam divergence of some mrad a linewidth of a few nm is expected; the exact value depending on multipass effects, beam geometry, etc.

The polarization direction of the oscillator light is forced to be horizontal in the cuvette (like the pump beam) by the many faces at Brewster angle within the cavity. Thus, an optimum condition is created for dye molecules with transition dipole moments of excitation and stimulation (and stimulated emission) along the same axis [6].

Rotation of the excited dye molecules will reduce the stimulated emission. However, the width of the pump pulse, the roundtrip time in the cavity, and the rotation correlation time of the dye molecules dissolved in an alcohol (which is estimated to be less than some tens

of picoseconds) make this process negligible at given photon flux.

The output beam from the oscillator was directed towards the amplifier cuvette using two Brewster cut elements. In the second cuvette the light path through the dye solution is vertical again. After passing this dye cuvette the amplified laser beam is deflected horizontally, again using a Brewster cut element, turning the output polarization to vertical. All Brewster angles in the oscillator amplifier were calculated using a refractive index of silica at 520 nm as a compromise between the blue and red dyes.

The dispersion prisms were mounted together at one block and were pre-aligned. The oscillator wavelength could be tuned by the end mirror controls. In this way, tuning is uncalibrated, but for most applications this is only a small disadvantage, because once running, the laser system is operated for a long period at the same wavelength. With minor modifications calibrated wavelength selection is possible. The output wavelength was measured using a beam splitter and a 0.25 m monochromator.

Of the deflection elements in the pump scheme only those just before the cylindrical lenses have a two-axis adjustment. All other elements are only partly adjustable. The two 90° deflection elements between pump laser and dye laser were mounted on prism tables. All components of the dye laser and pump scheme were attached to 10 mm thick anodized alumina plates, assembled perpendicularly.

The dye solution was circulated through both cuvettes by means of a centrifugal pump and was cooled by a glass heat exchanger and 2 l stock water at ambient temperature.

Testing the dye laser, several dyes were used, all of which were dissolved in methanol. Most frequently, a mixture of Rh 6G and Rh 640 (1:1) was used (Lambda Physik), lasing around 610 nm. With this dye mixture, pumping at 532 nm, 33 mJ/pulse and 21 Hz repetition rate from a JK Laser HY200, a conversion efficiency of over 10% was reached, quite comparable with values from commercial dye lasers. The amplification of the light pulse from the oscillator was found to be about 200 times. The bandwidth at 609 nm was 3 nm FWHM, as measured with a

SPEX minimate 0.25 m monochromator (resolution 1 nm), in good agreement with the theoretical expected value. No attempts were made to measure the percentage of amplified spontaneous emission [11-13]. The dimensions of the assembled dye laser are 30 x 20 x 120 cm (width, height and length, respectively). For the dye laser described here, all fused silica (Suprasil I) components were custom made by the Optics Group of the University of Amsterdam.

Mr. M. Groeneveld from the University of Amsterdam is kindly acknowledged for grinding the specially designed fused silica components. Mr. H.E. van Beek is acknowledged for the construction of all mechanical parts of the dye laser. We thank Prof. Dr. T.J.Schaafsma for carefully reading the manuscript.

REFERENCES

- [1] P.A. de Jager and F.G.H. van Wijk, "Microsecond time resolution on a conventional EPR spectrometer using 200 kHz magnetic field modulation and phase-sensitive detection," Rev. Sci. Instrum. (submitted), 1987.
- [2] D.A. Greenhalgh and S.T. Whittley, "Mode noise in broadband CARS spectroscopy," Appl. Optics 24, 907, 1985.
- [3] D. Klick, M.A. Akerman, H. Tsuda and D. Supurovic, "High-power broadband dye laser for manufacturing applications," Proc. Int. Conf. on Lasers 1985, (Ed. C.P.Wang) pp.531-538, (STS Press, McLean, VA, 1986
- [4] T.W. Hänsch in "Dye lasers" (Ed. F.P. Schäfer), Springer Verlag, New York, 194, 1973.
- [5] A. van Hoek and A.J.W.G. Visser, "Beam-splitter mount for efficient monitoring of mode-locked and synchronously pumped dye lasers," Rev. Sci. Instrum. 54, 1145, 1983.
- [6] F.P. Schäfer in "Dye Lasers" (Ed. F.P. Schäfer), Springer Verlag, New York, 1, 1973.
- [7] R.W.Ditchburn, "Light", Acad.Press, London, par. 12.4., 1976.
- [8] "Optics Guide 3," Melles Griot, Zevenaar, The Netherlands,

Irvine, CA., 1973.

- [9] F.J. Duarte and J.A. Piper, "Dispersion theory of multiple-prism beam expanders for pulsed dye lasers," *Opt. Commun.* **43**, 303, 1982.
- [10] F.J. Duarte and J.A. Piper, "Generalized prism dispersion theory," *Am. J. Phys.* **51**, 1132, 1983.
- [11] F.J. Duarte and J.A. Piper, "A double-prism beam expander for pulsed dye lasers," *Opt. Commun.* **35**, 100, 1980.
- [12] T.J. Mckee, J. Lobin and W.A. Young, "Dye laser spectral purity," *Appl. Optics* **21**, 725, 1982.
- [13] L.G. Nair and K. Dasgupta, "Amplified spontaneous emission in narrow-band pulsed dye laser oscillators- Theory and experiment," *IEEE J. Quant. Electr.* **QE-21**, 1782, 1986.

3.3 THE LASER-FLASH ARTEFACT IN TIME-RESOLVED EPR

It is a well known experience, that a short, high-power laser flash irradiating a sample in an EPR cavity, generates a spurious transient in time-resolved EPR [1-4]. This artefact represents a serious problem, because in many cases it forces the instrumental conditions, such as microwave power and amplifier gain to be set to less than optimal values. Therefore the obtained S/N ratio is often appreciably smaller than would have been possible otherwise.

Since the transient artefact is coherent with the light-pulse, it must be subtracted from the transient signal of interest, decreasing the obtained S/N ratio. Weak EPR transients may be completely obscured, even after careful subtraction, due to residual noise on the difference-signal. A novel time-resolving EPR technique, using the concept of broad-band phase-sensitive detection, as described in section 3.4, accomplishes the subtraction procedure automatically. Even so, it is crucial to minimize the artefact at forehand as much as possible. A considerable reduction of the laser-flash artefact was achieved when we observed that especially the side-walls of the E-231 (TE_{102} mode) rectangular EPR cavity (Varian), used in our experiments, are sensitive to irradiation by (scattered) high-power laser light.

A piece of carbon paper was brought into the cavity with the black side facing the scattered light, and completely covering the side-walls. The backside of the cavity, connected to the iris and wave guide was partly covered, leaving a hole for the microwaves. The inside front part of the cavity was left uncovered. This approach reduced the light-induced artefact by about a factor 10. The carbon paper introduces a broad, structureless, but light-independent EPR signal. This background signal was subtracted during the time-resolved experiments. Although the Q-factor of the cavity was reduced by introducing the carbon paper, the net improvement of the S/N ratio was ca. a factor 2 - 5, depending on the incident laser pulse power. It should be noted that this method is only advantageous if the amplitude of the flash artefact is much larger than the amplitude of the EPR

signal.

Another method, lacking the disadvantage of a reduced cavity Q, but less effective, employed a cylindrical glass light guide with flat top and bottom, snugly fitting into the EPR sample tube. The light guide was pressed down into the sample tube containing the liquid sample (ethylene glycol suspension of RC's) until no air remained between the bottom of the light guide and the liquid, and subsequently frozen. The sample was illuminated by focussing the laser beam on the top of the light guide. By this method the artefact was almost completely eliminated, and only a minor spurious dark signal around $g=2$ was introduced. Unfortunately, this method was less efficient, since the effective illumination of the sample was found to be rather poor, resulting in low EPR signal intensity.

References

- [1] S.S. Kim, and S.I. Weissman, Rev. Chem. Intermed. 3 (1979) 107.
- [2] R. Furrer, F. Fajara, C. Lange, D. Stehlik, H.M. Vieth, and W. Vollmann, Chem. Phys. Lett. 75 (1980) 332.
- [3] R. Furrer, F. Fajara, C. Lange, D. Stehlik, and W. Vollmann, Chem. Phys. Lett. 76 (1980) 383.
- [4] D. Von Beckert, and K. Mehler, Experimentelle Technik Physik 33 (1985) 73.

3.4 MICROSECOND TIME RESOLUTION ON A CONVENTIONAL EPR SPECTROMETER USING 200 kHz MAGNETIC FIELD MODULATION AND PHASE-SENSITIVE DETECTION

P.A. de Jager and F.G.H. van Wijk

Department of Molecular Physics, Agricultural University,
De Dreijen 11, 6703 BC, Wageningen, The Netherlands.

ABSTRACT

A method is developed to detect Electron Paramagnetic Resonance (EPR) transient signals with frequency components in the range from dc to 1 MHz and a low initial signal-to-noise ratio (e.g. 0.1 after one sweep). This method uses 200 kHz magnetic field modulation on a conventional EPR spectrometer, using a modified lock-in detector: the tuned amplifier is replaced by a broadband preamplifier with a high pass filter and the low pass filter of the lock-in detector is replaced by a broadband amplifier. The transients are generated incoherently from the magnetic field modulation, and subsequently averaged. The function of the (removed) low pass filter is taken over by the averaging. An instrumental response time of less than 1 μ s is obtained. This was determined by measuring the rise time of the triplet state of the photosynthetic reaction center of Rhodospseudomonas sphaeroides R-26 at 165 K. This method, direct detection and high frequency (1-2 MHz) modulation are discussed. The S/N ratio of the method described in this paper is similar to that of the other two methods. However, when large linewidths ($> .5$ mT) are met, it gives a superior S/N ratio as compared to high frequency (1-2 MHz) modulation methods, due to the higher maximum modulation amplitude. When the transients of interest contain frequency components in the low frequency noise regime (dc - 50 kHz), the described method is to be preferred over direct detection, because of its better S/N ratio.

INTRODUCTION

Time-resolved electron paramagnetic resonance (EPR) can be used to obtain relaxation times of short-lived radicals or metastable paramagnetic species, such as triplet states /1-4/. The power of the technique depends strongly on its time resolution. A serious problem related to the commercially available EPR spectrometers, is the built-in limited time resolution of about 200 μ s, due to narrow band filtering in the lock-in detector, operating at 100 kHz magnetic field modulation. The time resolution has been improved to 20 - 100 μ s by modifying the lock-in detector /4-9/. In the literature the time resolution and modulation frequency have been related to each other in a rather confusing way /1,9-14/, i.e. one might get the impression that the time resolution is limited by the modulation itself. This is incorrect, as will be shown in this paper. The presence of 100 kHz modulation has been taken as 'the principal barrier' /1/ to decrease the response time below 20 - 100 μ s. To overcome this putative problem, solutions were found by increasing the modulation frequency to 1 - 2 MHz /12,15,16/ or skipping the field modulation, using direct detection of the microwave absorption or emission /2,8,11,17/. Direct detection is to be preferred when exclusively fast transients are met. However, when e.g. fast increasing and slow decaying signals are met /18/, the signal of interest contains also low frequency components, and one needs a technique with a wide bandwidth (i.e. from dc - 1 MHz).

Since sophisticated averagers have become available, with 100% duty cycle in combination with high power, short pulse excitation sources, both with relatively high repetition rate, the time resolution of the EPR experiment could substantially be further increased. The limitation to the time resolution is then determined by the conventional EPR spectrometer itself (i.e. bandwidth of the cavity, crystal detector and preamplifier). In the following we show that, when the transient signals are averaged, a moderate field modulation frequency (i.e. 100 - 400 kHz) suffices to obtain at least microsecond

time resolution, with a good signal to noise (S/N) ratio. Further, we will compare this technique with the high frequency (1 - 2 MHz) modulation method and the direct detection method.

1. REQUIREMENTS

We want our method to meet the following requirements:

1. Detection of transients with frequency components in the range from dc to 1 MHz.
2. Detection of signals with a low initial S/N ratio must be possible. Therefore special attention must be paid to maximize the signal, and to minimize the noise and pulsed excitation artefact.
3. Use of an available conventional EPR spectrometer. The modification must result in an easy to operate apparatus. We prefer to use commercially available components, and the modification must be within a limited financial budget.
4. The modified spectrometer must remain available to conventional EPR spectroscopy.

From the first requirement it is concluded that standard EPR spectrometers can not be used to detect transient signals in the required time regime without modification. The third requirement excludes the superheterodyne EPR spectrometer /19/, and electron spin echo techniques.

Direct detection, in which no magnetic field modulation is applied and the signal from the microwave detector is directly fed into a signal processor (e.g. an averager or boxcar integrator), meets the requirements 1,3 and 4. However, it has the disadvantage of a low S/N ratio, caused by the presence of low frequency noise. This extra noise, which is superimposed on the white noise, is an instrumental problem, and originates from the microwave detector (1/f noise), preamplifier (1/f noise), microphonics in the cavity (e.g. building vibrations and sound waves), mains interference, and hum. A well known effective way in discriminating against this low frequency

noise is the use of a lock-in amplifier system. This uses magnetic field modulation with a frequency much higher than the frequencies in the abovementioned noise.

The amplitude of the signal in a lock-in detection system is proportional to the amplitude of the magnetic field modulation, and also, in a complicated way, to the linewidth of the signal. The amplitude of the signal that is observed by the direct detection method is about 2 times larger than that is obtained with optimal amplitude of the field modulation. However, to suppress artefacts the direct detection method requires the subtraction of the on - and off resonance signals. The subtraction procedure reduces the obtained S/N ratio per unit experimental time with a factor $2/\sqrt{20}$. The artefact is caused by the pulsed excitation source that generates the transient EPR signal. This spurious transient signal is added to the "true" EPR transient.

Suppression of this light-induced artefact can be achieved automatically when lock-in detection is applied, since the artefact signal is not dependent on the magnetic field position (within the modulation amplitude) and is therefore not modulated. Suppression of the spurious transient is obtained during the summation process. The artefact can only be eliminated, if it does not cause overload of the electronics (in any method). This overload produces a long dead time, caused by overload recovery.

An additional advantage of field modulation techniques is that, a first derivative spectrum is obtained, which is often more readily interpretable than the absorption signal that is provided by direct detection.

From the abovementioned arguments we have adopted the method of lock-in detection. In the following paragraph we will show that lock-in detection, with some modifications, also satisfies the first requirement.

II. FREQUENCY RESPONSE OF A LOCK-IN DETECTOR

Several authors suggested that the frequency of the modulation

itself is the limiting factor of the time resolution, or formulated the limitations to the time resolution of a lock-in detected EPR signal in a confusing way /1,9-14/. Since the above mentioned argument is erroneous, we will take a closer look at the operation of a lock-in detection system, and evaluate its frequency response in more detail.

A lock-in detector system improves the S/N ratio by reducing the bandwidth and by shifting the signals of interest to a less noisy part of the spectrum (out of the low-frequency regime). This shift is accomplished by modulating the experiment with a known frequency (f), generated by the oscillator (fig. 1). The reference unit converts the signal from the oscillator into a square wave (reference signal R in fig. 1). The phase-sensitive detector (PSD) is a double balanced mixer in which the input signal I in figure 1 is multiplied by R . The output signal $O = I \times R$. After the PSD a low pass filter reduces the bandwidth (Δf) and thus the noise. Because signal R is a square wave, the PSD also monitors signals and noise with frequency components at odd harmonics of the modulation frequency (i.e. $3f, 5f, \dots$), but with a sensitivity of inverse proportion to the order of the harmonics. When sine wave modulation is applied (as in the EPR experiment), these

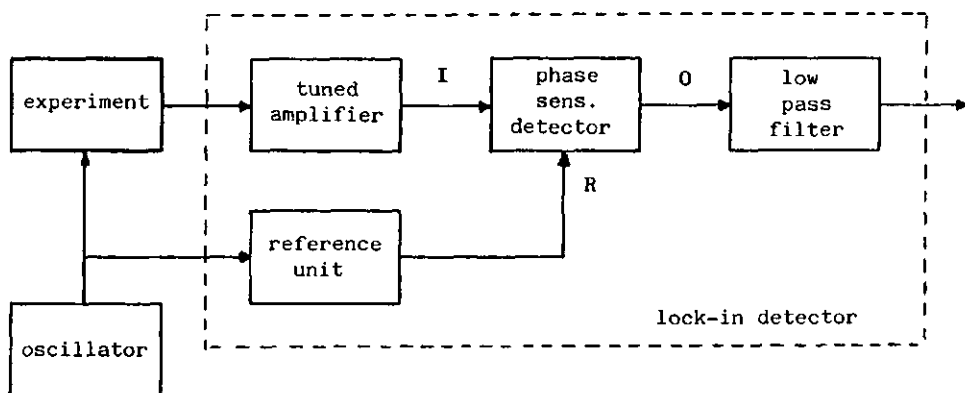


Figure 1.
Block diagram of a lock-in detector system.

higher harmonics only contain noise, and must be eliminated. This is achieved at forehand by the tuned amplifier.

The bandwidth (Δf), and timeconstant (τ) which are used in this article are defined in the Appendix. The bandwidth of the lock-in detector can be enlarged by replacing both the tuned amplifier and the low pass filter with broadband amplifiers with $\Delta f > 1$ MHz. Then the overall bandwidth becomes limited by the bandwidth of the remaining parts of the experimental set up. In the following a B-PSD denotes a broadband lock-in detector. Thus, the frequency response of a B-PSD is in principle equal to that of direct detection, as shown in figure 2. In this figure we consider a theoretical experiment with a kinetic response with zero rise time and an ideal B-PSD. The experiment is modulated with a sine wave with amplitude A (fig. 2a). The transient response of the experiment, shown in figure 2c, to the input U(t) is:

$$U(t) \cdot A \cdot \sin(2\pi ft + \phi) \quad (1)$$

where ϕ denotes the phase angle of the modulation at the time that the transient in fig. 2b (a unit step) is born, and A is small compared to the linewidth of the experiment. Since there is no phase difference between the reference square wave and the signal, the B-PSD converts the signal into a full wave rectified sine function (fig. 2d):

$$U(t) \cdot A \cdot \left[\frac{2}{\pi} - \frac{4}{3\pi} \cos 2(2\pi ft + \phi) - \frac{4}{15\pi} \cos 4(2\pi ft + \phi) - \dots \right] \quad (2)$$

where U(t) still denotes the transient signal, here the unit step function. Note the rise time at $t = 0$ in figures 2c and 2d. During the averaging process the phase angles ϕ_i will be different for each successive sweep i ($0 \leq \phi_i < 2\pi$), and the full wave rectified sine functions add to a unit step with a normalized amplitude $2/\pi$ (fig. 2e):

$$\lim_{n \rightarrow \infty} \sum_{i=1}^n U(t) A \left[\frac{2}{\pi} - \frac{4}{3\pi} \cos 2(2\pi ft + \phi_i) - \dots \right] = n \frac{2}{\pi} U(t) \cdot A \quad (3)$$

The total number of sweeps n necessary to eliminate the cosines in eq.

(3) is independent of the modulation frequency (f); in practice 100 - 1000 sweeps are sufficient. Thus, the averaging process smoothes the rectified sinewaves (fig. 2d). This is normally performed by the low pass filter in a (narrow band) lock-in detector. Since the low pass filter has been removed to improve the transient response, the averaging process must be incoherent with the modulation frequency.

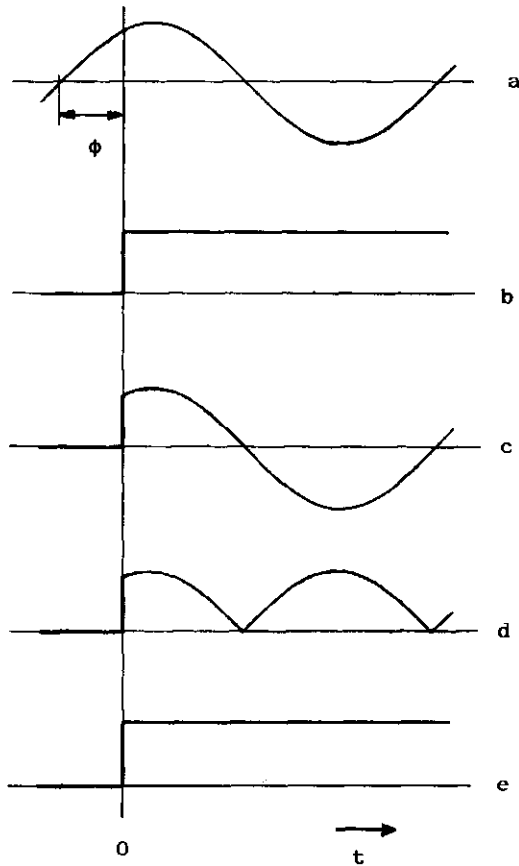


Figure 2.

Transient response of an ideal PSD with infinite bandwidth to a unit step. Figures a-d represent the same (single) sweep. a. modulation of the experiment; b. input of the experiment; c. output of the experiment; d. output of the PSD; e. output of the averager after many sweeps with random phases ϕ .

If the amplitude of the modulation (A in eqs. 1-3) is increased with respect to the linewidth, higher harmonics are generated. " $A \cdot \sin(2\pi ft + \phi)$ " in eq. 1 should then be replaced by the sum over the harmonics created by convoluting the field modulation with the line shape /28/. Eqs. 2 and 3 hold as well, and it is recognized that the (odd) harmonics present in the transient signal cause no trouble even though they pass the B-PSD.

A practical solution obtaining different phase-angles (ϕ_i) is employing two free-running oscillators: one for the pulsed excitation, the second for the field modulation. Another, more elaborate method, is to couple both oscillator frequencies, but introducing discrete phase-jumps.

Until now, an analog B-PSD was considered. A more elegant procedure is averaging in combination with digital phase sensitive detection: the modulated response of the experiment (eq. 1) is fed directly into the computer and real-time processed. After many sweeps the result $U(t)$ (eq. 3) is obtained. The advantage is the elimination of the analog B-PSD, in practice still limiting the bandwidth. In this way the field modulation and the pulse repetition rate (which can be seen as a second 'coding') are decoded simultaneously. This is possible because the order of decoding is immaterial, which is implicit in eqns (1) to (3). From eq. (3) it is also clear that the value of the modulation frequency f does not show up in the result after averaging (the right-hand side of eq. 3).

It is crucial that in the B-PSD no tuned amplifier, nor a low pass filter is used to block the odd harmonics of the signal (fig. 2c) or to smooth the rectified sine wave (fig. 2d), respectively. These components deteriorate the transient response and their function is taken over by the averaging process, without deteriorating the transient response. Because the step function (containing all frequencies) is detected without distortion, any transient signal will be detected with high fidelity.

III. EFFECT OF THE HIGH PASS FILTER

In order to eliminate the low frequency noise in a B-PSD a high pass filter must be applied at position I in figure 1. The effect of a high pass filter on the transient response to a unit step function is given in figure 3. The damped oscillation $D(t)$ is approximately described by:

$$D(t) = -c \cdot \cos(2\pi ft) \cdot e^{-t/\tau_{HP}} \quad (4)$$

τ_{HP} is the time constant of the high pass filter and f is the modulation frequency. c is a proportionality constant. $D(t)$ also depends on the phase setting of the B-PSD. The optimum value of τ_{HP} can be found by considering the spectral density of the low frequency and white noise. This implies a -3 dB point of the high pass filter f_{HP} between 10 kHz and 100 kHz, depending on the experimental system. In addition, to minimize the amplitude c of the distortion $D(t)$, the modulation frequency f must be higher than f_{HP} , because:

$$c \sim \frac{f_{HP}}{f} \quad \text{if } f \gg \frac{1}{(2\pi\tau_{HP})} = f_{HP} \quad (5)$$

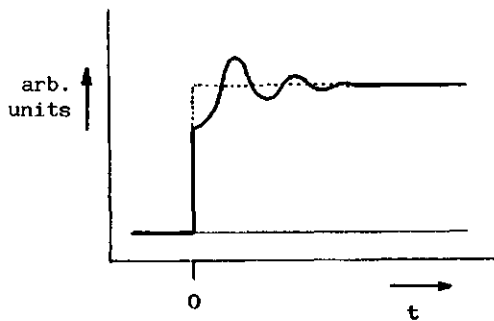


Figure 3.

Transient response of an ideal B-PSD equipped with a high pass filter after many sweeps (compare with fig. 2e).

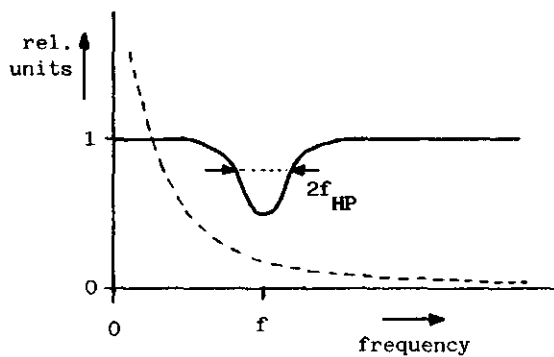


Figure 4.

The solid curve represents the overall amplitude frequency response of a B-PSD equipped with a high pass filter. The dashed curve represents the Fourier transform of the unit step function.

From equation (5) it is evident that the best transient response is obtained with the highest modulation frequency ($c \rightarrow 0$). The effect of this high pass filter on the overall frequency response of the B-PSD is given in figure 4. For simplicity the phase frequency response is not shown. The response of this B-PSD to a unit step (figure 3) is the inverse Fourier transform of the product of the two functions in figure 4. From this it is also clear that a higher modulation frequency results in a less distorted response. The dip in the amplitude frequency response has a depth of 50%, due to the fact that only one half of the information is lost by the action of the high pass filter. The other half of the information is detected around $2f$. It will be obvious that deconvolution methods /10/ can be applied to obtain an undistorted signal. This reduces the S/N ratio, but the low frequency noise still remains absent, because low frequency components are not used in this deconvolution process.

IV. APPLICATION ON EPR

In the EPR spectrometer the modulation is applied on the magnetic field. On a conventional spectrometer the modulation frequency is 100 kHz. From the preceding paragraph it was found desirable to increase the modulation frequency as much as possible. In the past several MHz has been reported /12,15,16/ although band pass filters and low pass filters were used, degrading the transient response. For these high modulation frequencies the modulation amplitudes are instrument limited to rather small values (i.e. ≤ 0.4 mT peak to peak). When large linewidths are met, as e.g. in biological triplet states, this small maximum modulation amplitude becomes an annoying limitation to the S/N ratio. On the other hand, when small linewidths are met, these high modulation frequencies give rise to undesirable sidebands. Furthermore, high modulation frequencies are difficult to handle and mean high capital investment or technical skill, since major modifications are necessary /21/. Another disadvantage of the application of high modulation frequencies is that, with a normal cavity a lower S/N ratio is obtained, as compared to moderate modulation frequencies, due to the limited bandwidth of the cavity (See Appendix). Therefore, we have chosen for a modulation frequency that is a compromise between S/N ratio and transient fidelity: 200 kHz.

As is discussed above, the bandwidth of a B-PSD is not necessarily the limiting factor in the experimental set up. For the EPR spectrometer (also in direct detection mode) the bandwidth is determined by the preamplifier (e.g. 1.5 MHz) and the cavity (See Appendix).

V. DESCRIPTION

Figure 5 gives the block diagram of the experimental set up. A Varian E-6 EPR spectrometer was used, equipped with an E-101 microwave bridge, and E-231(TE₁₀₂ mode) rectangular cavity. The cavity was

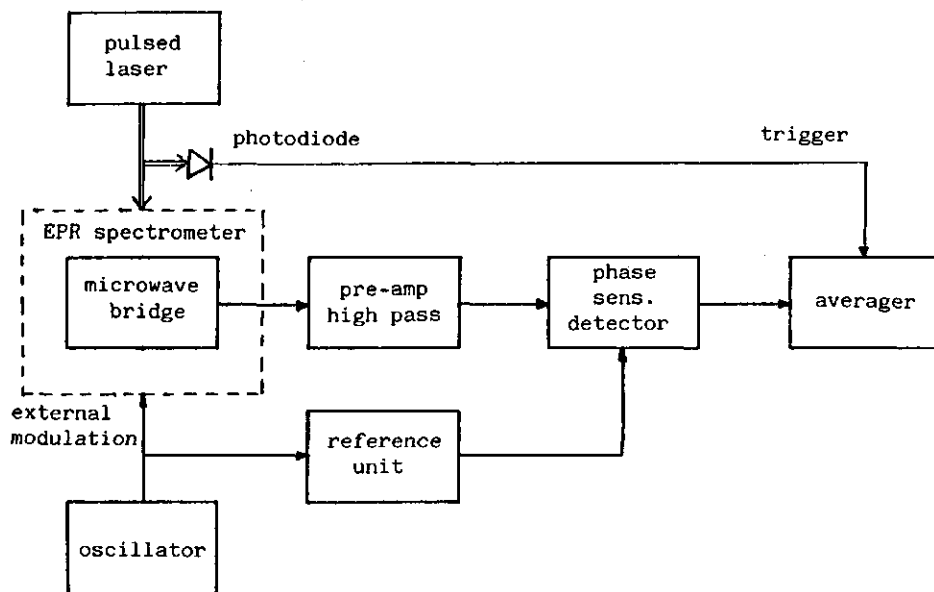


Figure 5.
Block diagram of the experimental set-up.

modified. The cavity modulation coils were connected in parallel aiding /12/, which allowed a higher modulation amplitude. These coils were brought into series resonance with an appropriate capacitor in the cavity tuning assembly (Varian pub. no. 87-125-732) /22/. The standard modulation amplifier was used. The output of the external oscillator (Hewlett-Packard 3310A) is connected to the input of the modulation amplifier. The field modulation amplitude is determined with an ac voltmeter /22/.

The front of the cavity was replaced by a light tube from an optical transmission cavity E-234 to obtain 100% optical transmission of the excitation pulse. The excitation source is a 12 ns (FWHM) laser flash from a homebuilt tunable dye laser /23/, pumped by a Q-switched Nd:YAG laser, JK Lasers HY 200. The broadband output (E16) of the E-101 absorption reference arm accessory was used (Varian pub. no. 87-125-795) instead of the "bridge signal out" output, because the signal from the latter is affected by the 70 kHz AFC notch filter and

a 300 kHz low pass filter.

The B-PSD system consists of a preamplifier with high and low pass filters (Brookdeal 452, Brookdeal, Bracknell, Berks, England), a reference unit (Brookdeal 422), and a modified phase sensitive detector (Brookdeal 411). The modification consists of a broadband amplifier (fig. 6) with a 50 ohm output. This output is connected to an averager (LeCroy signal analyser 3500, equipped with a 6102 amplifier/trigger unit, TR 8818 transient recorder, and MM 8103A memory). The highest sampling frequency of the averager is 100 MHz, although in practice a lower sampling frequency suffices. The averager is triggered by a fast photodiode. This averager allowed recording of transient signals with 100% duty cycle with a repetition frequency of the laser (up to 50 Hz) using 1024 data points and 160 ns (or 40 ns) dwell time and has a pretriggering facility. Aliasing of noise with $f > 3.12$ MHz (160 ns dwell time) is avoided, because the modified B-PSD has a bandwidth $\Delta f = 300$ kHz. No additional filtering is applied. EPR transients were recorded with minimal 70 kHz AFC modulation amplitude to avoid an increase in the noise level at 70 kHz, 140 kHz and higher harmonics interference at the input of the B-PSD.

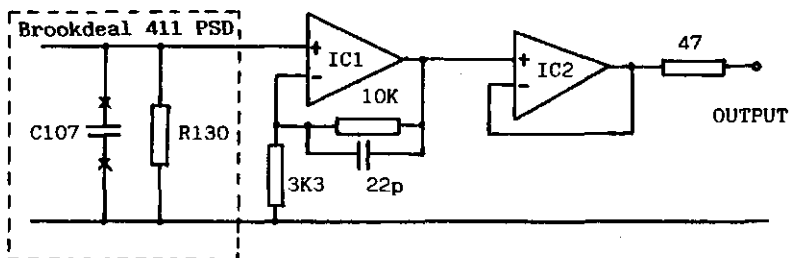


Figure 6.

Schematic diagram of the modification of the Brookdeal 411 PSD. Capacitor and resistor values are in Farads and Ohms, respectively. The ± 15 V supply voltages are not shown, they are obtained from the 411 supply voltages and are decoupled to ground with 100 n. C107 is removed to improve the transient response. IC1 and IC2 are LF351 National Semiconductor.

VI. RESULTS AND DISCUSSION

The transient response of the B-PSD was tested by applying a gated sine wave with $f = 200$ kHz. The rise time of the gate circuit was less than 200 ns (not shown), this input of the B-PSD compares to fig. 2c. Figure 7a shows a typical response after one sweep. A small leakage of the reference signal (200 kHz square wave) is visible. This leakage originates from the imperfectness of the B-PSD, and is independent of the input signal. This implies that a small signal is distorted by a relatively high leakage. At $t > 0$ the full wave rectified sine wave with a strong frequency component of 400 kHz is observed (see also fig. 2d). The effect of averaging 1000 sweeps is shown in figure 7b (which compares to fig. 2e). The spurious 200 kHz and 400 kHz signals disappeared to a large extent. The rise time of the step function in figure 7b was found to be $\tau = 610 \pm 20$ ns. (The error represents 90 % confidence of the fit). The effect of a 100 kHz high pass filter before the B-PSD is shown in figure 7c (which compares to fig. 3). The rise time was found from fitting a single exponential function, yielding $\tau = 900 \pm 100$ ns. Although a high pass filter was used, the output unit step signal does not show any sagging.

In our laboratory we are interested in triplet states of biological (photosynthetic) species /24/. The response of the X^+ peak of the $\Delta m = \pm 1$ EPR spectrum of the donor triplet state (P^R) of the isolated reaction center protein from the bacterium Rhodospseudomonas sphaeroides R-26 (depleted from its ubiquinone acceptors) at 165 K is given in figure 8. The donor triplet state is photochemically generated in less than 20 ns /25/. This provides a means to determine the response time of the total experimental set up. The transient of figure 8 is the result of 16,000 sweeps off-resonance, subtracted from 16,000 sweeps on-resonance. The subtraction procedure improves the fidelity of the transient, because the small fraction of the laser flash artefact that leaks through the B-PSD and remains present in the transient, is subtracted. However, this additional subtraction

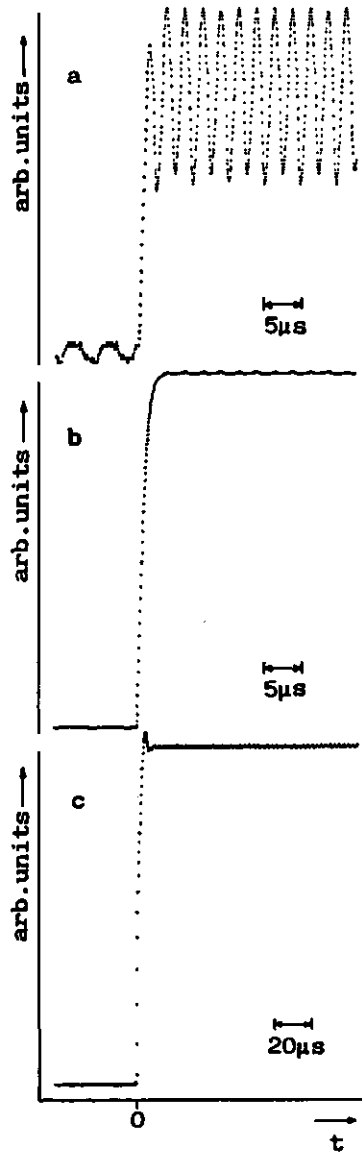


Figure 7.

Experimental transient response of the modified Brookdeal 411 PSD (-3dB point 300 kHz) and the LeCroy 3500 averager. The input signal is a gated sine wave simulating a unit step function modulated with a sine function with a frequency of 200 kHz. 1 K data points, pretrigger $\frac{1}{4}$ sweep, no digital filtering. a. single sweep, bandwidth not limited by filtering, dwelltime 40 ns; b. 1000 sweeps, further identical to a; c. 1000 sweeps, -3 dB points of the preamp are 100 kHz and 1 MHz, dwelltime 160 ns.

procedure, that unfortunately reduces the overall S/N ratio, is in general only necessary when very small signals (with respect to the flash artefact) are met. The EPR signal from the photosynthetic species was very weak under the chosen experimental conditions (e.i. low microwave power, and relatively high temperature). The microwave field

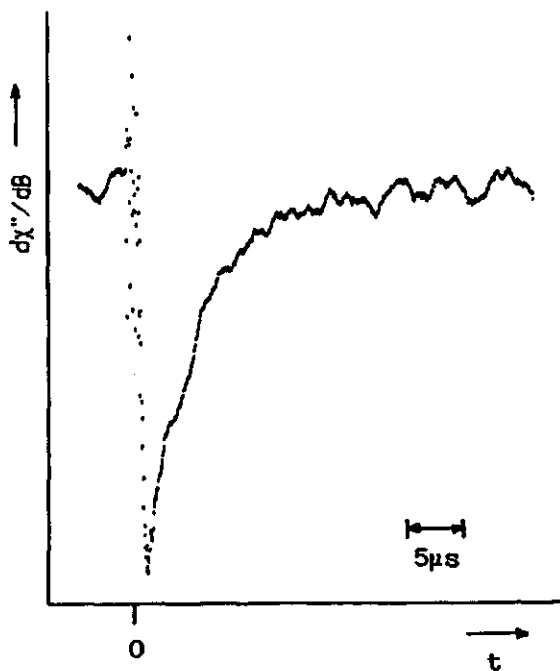


Figure 8.

Emissively polarised transient of the X^+ peak of the donor triplet (p^R) EPR spectrum of the reaction center protein (ubiquinone depleted) isolated from the photosynthetic bacterium Rhodospseudomonas sphaeroides R-26 detected at 165 K. The position of the X^+ peak was determined by recording a boxcar spectrum using the B-PSD. The sample was in a standard 4 mm quartz tube. Excitation: 612 nm, 2mJ/pulse, pulse width 12 ns FWHM, repetition frequency 21 Hz. EPR settings: 200 μ W, 200 kHz field modulation with 1.85 mT_{pp} amplitude. Detection: 16,000 sweeps off-resonance subtracted from 16,000 sweeps on-resonance, -3 dB points of the preamp 100 kHz and 1 MHz, -3dB point of the B-PSD is 300 kHz, dwelltime 40 ns, 1 K data points, pretrigger 1/8 sweep, no digital filtering.

strength was kept very low ($B_1 < 1\mu T$) /26/ to make sure that the shape of the transient signal is not affected by the microwaves or the field modulation (no stimulated relaxation or rapid passage effects /27/ were observed).

The pulse repetition rate of the experiment was 21 Hz. This seems to be low with respect to the obtained S/N ratio per unit time, since the observed transient has a decay time of ca. 5 μs . However, one does not observe the relaxation process from the triplet state to the singlet ground state. This process has a much longer decay time. The pulse repetition time must be determined by the time that the system has relaxed back to the initial state, thus, preventing build up of an excited steady state.

A theoretical comparison between the 200 kHz and the 2 MHz modulation method is possible using the 2 mT linewidth of the EPR peak in the powder spectrum of the detected triplet state (fig. 8). The transient of this figure was detected using 1.85 mT_{pp} modulation amplitude. The 2 MHz field modulation technique is experimentally limited to 0.1 - 0.4 mT_{pp} /12, 15, 16/, resulting in a S/N ratio that is a factor 2.5 (using 0.4 mT_{pp}) to 10 (0.1 mT_{pp}) lower /28/ than is obtained by applying 200 kHz modulation. In this calculation we did not account for further decrease in S/N ratio due to the limited bandwidth of the cavity.

An experimental comparison of the noise levels in the frequency bands 100 Hz - 1 MHz and 100 kHz - 1 MHz yields a factor ~ 10 more noise in the broader band. If these frequency bands are used for direct detection, and broadband phase sensitive detection at 200 kHz, respectively, the frequency response of the latter method extends to 0 Hz, and the direct detection to 100 Hz and has a ca. 3 times lower S/N ratio. When rapid transients (frequency components > 100 kHz) are to be detected, the noise level of both approaches is about the same (-3dB point at 100 kHz in direct detection), yielding ~ 3 times higher S/N for the direct detection /28/.

We paid attention not to overload the B-PSD with the artefact, to prevent the electronics to enter the non-linear region. This impro-

ves the fidelity of the resulting transient in the time that the artefact is present, but unfortunately permitting more noise and leakage of the reference square wave. When the fidelity of the transient in the first microseconds is not important, a gate circuit is preferred. It blocks the intense artefact, and permits an increase of the gain, improving the observed S/N ratio.

When a normal (not time resolved) spectrum or slower kinetics are measured ($\tau > 10 \mu\text{s}$), the S/N ratio can be improved with 10-15 % by filtering out the noise at odd harmonic frequencies with a tuned amplifier.

The fit of two exponential functions to the experimental data of figure 8 yields a rise time of $\tau_1 = 0.5 \pm 0.4 \mu\text{s}$, and a decay time of $\tau_2 = 4.8 \pm 0.4 \mu\text{s}$. The large relative error in τ_1 is caused by the residual distortions due to the flash artefact. The flash artefact consists of the light induced cavity artefact and radio frequency interference (the pulse laser is within 2m range of the EPR spectrometer). Nevertheless, the rise time is, within experimental error, equal to the rise time of the B-PSD system (fig. 7c), indicating that the bandwidth of the B-PSD in the EPR spectrometer limits the time resolution. The "true" τ_2 will be a fraction shorter than the observed $4.8 \mu\text{s}$ (an educated guess yields $4.6 \mu\text{s}$).

Comparing the experimental results of the broadband phase-sensitive detection method with the abovementioned requirements, it is concluded that

1. Microsecond time resolution is easily obtained. For the determination of τ -values of transients shorter than ca. $2 \mu\text{s}$ deconvolution methods will be necessary. This is currently implemented. It is estimated that a lower limit of ca. 200 ns can be achieved with the method applied to time resolved EPR. If this method is applied with 2 MHz modulation frequency, or direct detection is used, this lower limit of ca. 200 ns can be obtained without deconvolution methods.
2. Detection of signals with low initial S/N ratio (≈ 0.1) is possible as has been illustrated (fig.8). This is due to the modulation

procedure in combination with a high pass filter, suppressing low frequency noise and the excitation pulse artefact. This results in at least a similar S/N ratio as compared to high frequency (1 - 2 MHz) modulation.

However, when large linewidths (> 0.5 mT) are met, the 200 kHz method has a superior S/N ratio over high frequency modulation methods, due to a higher modulation amplitude. Only when the signals of interest contain frequency components in the low frequency noise regime (dc - 50 kHz), the broadband phase-sensitive detection method gives a better S/N ratio than direct detection. When using direct detection, artefact signals are generally suppressed by going on and off resonance at a low frequency and subtracting the results. In the scheme presented here, artefact signals are suppressed by going on and off resonance at a high frequency (i.e. 200 kHz field modulation frequency). In an ideal world both methods are fully equivalent. In the presence of low frequency instrumental instabilities, the high frequency strategy offers advantages.

3. Commercially available components were used. A modification in the phase-sensitive detector was necessary. Although we have applied 200 kHz modulation, the described method can be used with other modulation frequencies e.g. the 100 kHz modulation and PSD of a standard EPR spectrometer together with a 50 kHz high pass filter. In this case the ultimate time resolution is still determined by the bandwidth of the PSD, and deconvolution methods might be necessary when decay times faster than ca. 4 μ s must be measured.
4. The EPR spectrometer is still available to the conventional work. In our case it is a matter of a simple switch between the 100 kHz oscillator of the spectrometer and an external function generator operating at 200 kHz. There is one extra procedure, the modulation coils must be tuned to 100 or 200 kHz.

VII. APPENDIX

The bandwidth (Δf) of a first order system is the frequency where the amplitude of the sinusoidal signal is 3 dB lower with respect to the amplitude at zero frequency (as in a low pass filter), or at resonance frequency (tuned amplifier and cavity resonator). The bandwidth is given by:

$$\Delta f = \frac{1}{2 \pi \tau} \quad (\text{A1})$$

τ denotes the time constant of the first order system.

The bandwidth of the cavity (Δf_c) is under matched condition given by:

$$\Delta f_c = \frac{f_\mu}{2Q_L} \quad (\text{A2})$$

f_μ denotes the microwave frequency ($f_\mu = 9$ GHz), and Q_L denotes the loaded quality factor of the cavity (typically $2000 < Q_L < 6000$). A higher Q_L results in a higher S/N ratio ($S/N \sim \sqrt{Q_L}$) but in a smaller bandwidth.

VIII. REFERENCES

1. A.D. Trifunac and R.G. Lawler, Magn. Reson. Rev. 7, 147 (1982).
2. W.J. McGann and H.A. Frank, Chem Phys. Lett. 121, 253 (1985).
3. A.J. Hoff and I.I. Proskuryakov, Chem. Phys. Lett. 115, 303 (1985).
4. C.D. Buckley and K.A. McLauchlan, Mol. Phys. 54, 1 (1985).
5. J.R. Norris, EPR Lett. 1, 2 (1980).

6. P.B. Ayscough, T.M. English and D.A. Tong, *J. Phys. E* 9, 31 (1976).
7. A.R. McIntosh and J.R. Bolton, *J. Magn. Reson.* 32, 167 (1978).
8. O. Gonen and H. Levanon, *J. Chem. Phys.* (1986). In the press.
9. A.J. Hoff, P. Gast and J.C. Romijn, *FEBS Lett.* 73, 185 (1977).
10. T.M. Chiu, A. Siemiarczuk, S.K. Wong and J.R. Bolton, *J. Phys. Chem.* 89, 3343 (1985).
11. S.K. Wong, *J. Magn. Reson.* 47, 500 (1982).
12. G.E. Smith, R.E. Blankenship, and M.P. Klein, *Rev. Sci. Instr.* 48, 282 (1977).
13. P.J. Hore, K.A. McLauchlan, S. Frydkjaer, and L.T. Muus, *Chem. Phys. Lett.* 77, 127 (1981).
14. P.J. Hore in *Nato ASI Series*, vol. 85, no. Primary Photo-Processes in Biology and Medicine, 131 (1985).
15. P.W. Atkins, K.A. McLauchlan, and A.F. Simpson, *J. Phys.* E3, 547 (1970).
16. B. Smaller, J.R. Remko, and E.C. Avery, *J. Chem. Phys.* 48, 5174 (1968).
17. A.D. Trifunac, M.C. Thurnauer, and J.R. Norris, *Chem. Phys. Lett.* 57, 471 (1978).
18. F.G.H. van Wijk, Thesis, Wageningen, The Netherlands (in press) (1987).
19. G. Thirup and S. Frydkjaer, *J. Phys. E* 13, 1214 (1980).
20. D. Beckert, K. Mehler, *Exper. Technik. Physik.* 33, 73 (1985).
21. J.R. Norris, *EPR Letters (Varian)* 1, 2 (1980).
22. P.A. de Jager, and H.J.L. Bremer, *Rev. Sci. Instr.* 53, 1102 (1982).
23. A. van Hoek, and F.G.H. van Wijk, *Appl. Opt.*, in press (1987)
24. T.J. Schaafsma, G.F.W. Searle, C. Dijkema, L. Nedbal, A. van Hoek, P. Gast, and F.G.H. van Wijk. *Vth International Seminar on Energy Transfer in Condensed Matter, Proceedings, Prague 1985*, p. 163 (1986).
25. A.J. Hoff in Triplet State ODMR Spectroscopy (R.H. Clarke, Ed.) Wiley & Sons, New York, p. 367 (1982).

26. M.A. Hemminga, F.A.M. Leermakers, and P.A. de Jager, J. Magn. Reson. 59, 137 (1984).
27. R. Friesner, J.L. McCracken, and K. Sauer, J. Magn. Reson. 43, 343 (1981).
28. C.P. Poole, Jr., Electron spin Resonance, Interscience Publ., New York, (1967), pp 387-425.

ACKNOWLEDGEMENTS

We thank prof.dr. T.J. Schaafsma for initiating this project. C.B. Beyer is acknowledged for preparing the ubiquinone-depleted photochemical reaction center protein.

3.5 ADDITIONAL TECHNIQUES AND PREPARATIVE METHODS

Absorption measurements

Absorption measurements were carried out using a Uvikon 810 (Kontron) spectrophotometer for measurements with $200 \text{ nm} < \lambda < 700 \text{ nm}$. For measurements with $\lambda \leq 900 \text{ nm}$ a Shimadzu UV-200 spectrophotometer was used; and for measurements with $\lambda > 900 \text{ nm}$ a Beckman DU G-2400 (single beam) spectrophotometer was employed.

The absorption-difference spectrometers are referred to in sections 4.4 and 6.2.

Emission measurements

Room temperature fluorescence measurements, described in section 6.3 were carried out using a Perkin-Elmer LS-5 Luminescence spectrometer. Fluorescence measurements at cryogenic temperatures were carried out using the FDMR equipment (see below).

FDMR

Fluorescence detected magnetic resonance (FDMR) measurements were carried out employing either a homebuilt apparatus described by Van Der Bent et al. [1,2], or another homebuilt apparatus, described by Benthem [3]. In both cases the emission was detected using a Varian 152-A photomultiplier, which was sensitive in the NIR ($\lambda \leq 1150 \text{ nm}$).

Preparative methods

Photosynthetic bacteria were a kind gift by U. Smith at Argonne National Laboratory, USA (Rps. viridis and Rb. sphaeroides R-26), and dr J. Amesz at State University Leiden, The Netherlands (C. vinosum) and were anaerobically grown according to refs. [4,5]. RC's from Rb. sphaeroides R-26 and chromatophores from C. vinosum were obtained as described in [4]; RC's from Rps. viridis were purified as described in [6], with a slight modification as described in [7].

Iron was removed from isolated RC's of Rb. sphaeroides R-26 as described in [8].

Ubiquinone was removed from isolated RC's of Rb. sphaeroides R-26 as described in [9].

Quinone reconstitutions were carried out as described in [9]. A series of menaquinones (vitamine k2) were a kind gift from F. Hoffmann-La Roche & Co, switzerland.

No special precautions were made to remove oxygen from samples used in EPR measurements.

Further experimental details are given in Chapters 4 - 6.

References

- [1] S.J. Van Der Bent, P.A. De Jager, and T.J. Schaafsma, Rev. Sci. Instrum. 47 (1976) 117-121.
- [2] S.J. Van Der Bent, Thesis (1977) Wageningen Agricultural Univ., The Netherlands.
- [3] L. Benthem, Thesis (1984) Wageningen Agricultural Univ., The Netherlands.
- [4] C.A. Wraight, Biochim. Biophys. Acta 548 (1979) 309-327.
- [5] D. Budil, Argonne Natl. Lab., USA, personal comm.
- [6] H.J. Den Blanken, and A.J. Hoff, Biochim. Biophys. Acta 681 (1982) 365-374.
- [7] see Chapter 6 of this Thesis, section 2.
- [8] D.M. Tiede, and P.L. Dutton, Biochim. Biophys. Acta 637 (1981) 278-290.
- [9] M.Y. Okamura, R.A. Isaacson, and G. Feher, Proc. Natl. Acad. Sci. USA 72 (1975) 3491-3495.

CHAPTER IV

STEADY-STATE TRIPLET STATE SPIN POLARIZATIONS IN BACTERIAL REACTION CENTERS

4.1 INTRODUCTION

As pointed out in previous Chapters, the radical pair mechanism, determining the electron-spin dynamics in the RC-state P^+I^- in high magnetic fields, predicts an AEEAAE electron spin polarization (ESP) pattern in the $\Delta m=1$ EPR powder spectra of the donor triplet state (P^R), resulting from recombination of charges in the radical pair P^+I^- . Until now, this ESP pattern has been exclusively observed in preparations containing photochemically active RC's. For this reason, this pattern is generally accepted as evidence for the integrity and photochemical activity of the investigated RC's.

We were therefore surprised to find a deviating ESP pattern at temperatures higher than several tens of degrees Kelvin in photochemically active RC's of Rps. viridis. Further experiments demonstrated that this observation is not unique for Rps. viridis. Also for C. vinosum, and Rb. sphaeroides R-26 a change in the lineshape of the $\Delta m=1$ triplet EPR spectrum at increasing temperature was observed, although to a very different extent.

This Chapter describes various experiments verifying the hypothesis that the temperature-dependence of the lineshape of the RC triplet EPR spectra results from the transmission of a rapid spin-lattice relaxation of Fe^{2+} at the acceptor side via a quinone as relaxation carrier to the P^+I^- radical pair state in the RC.

Interaction of a third electron spin with the radical pair in the photosynthetic bacterium *Rhodopseudomonas viridis* monitored by the donor-triplet electron spin polarization

F.G.H. van Wijk, P. Gast and T.J. Schaafsma

Agricultural University, Department of Molecular Physics, De Dreijen 11, 6703 BC Wageningen, The Netherlands

(Received July 29, 1985)

(Revised February 17, 1986)

(Accepted February 28, 1986)

Summary

$\Delta m = \pm 1$ triplet EPR spectra of reaction centers and chromatophores from *Rhodopseudomonas viridis* were studied in the temperature range 8–270 K. The AEEAAE spin polarization pattern changes into AEAEAE above 19 ± 3 K. A similar effect was found in chromatophores from *Chromatium vinosum*. This phenomenon is ascribed to the exchange interaction between the electron spin on bacteriopheophytin (I), which is part of the radical pair P^+I^- (P denotes the primary donor), and a third electron spin on the reduced iron-quinone complex.

bacterial photosynthesis; reaction center; *Rhodopseudomonas viridis*; triplet state; EPR; electron spin polarization

Introduction

In the reaction centers (RCs) of photosynthetic bacteria and plant photosystems the primary donor triplet state has been found to give rise to strongly polarized $\Delta m = \pm 1$ EPR spectra at low temperature [1–4]. A unique electron spin polarization (ESP) pattern AEEAAE (A = enhanced absorption, E = emission) is observed which has been shown to be incompatible with intersystem crossing through spin-orbit coupling [5,6], but can be explained by invoking the formation of a

donor-acceptor (D^+A^-) radical pair (RP) [7,8]. Upon illumination the RP is created initially in a singlet state, and subsequently evolves into a triplet RP by differences in hyperfine interactions and g values between D^+ and A^- (in bacterial photosynthesis D^+ and A^- denote the cation of the bacteriochlorophyll dimer (P^+) and the anion of bacteriopheophytin (I^-), respectively). At sufficiently large magnetic fields, only the $m_s = 0$ triplet RP state is formed, giving rise to a donor triplet state, which carries only population in the corresponding $m_s = 0$ state, resulting in the abovementioned, unique spin polarization pattern.

In bacterial RCs the donor triplet state (P^R) can be observed when the first iron-quinone complex ($Fe^{2+}Q$) is reduced. This paramagnetic complex is coupled to the electronic spin on I^- of the RP by exchange and/or dipolar interactions [9-13], and therefore the system $P^+I^-(Fe^{2+}Q^-)$ should be considered a coupled three-spin system [14], very similar to a RP containing one proton [15].

The presence of a third electronic spin is expected to affect the EPR triplet state polarization pattern due to simultaneous spin-transitions in I^- and $Fe^{2+}Q^-$. Also, the $Fe^{2+}Q^-$ electronic spin may exhibit temperature-dependent relaxation at a time scale compatible with that of the RP lifetime. A dependence of the magnetic field effect of the P^R triplet yield on $Fe^{2+}Q^-$ has been proposed [16], but no direct effect of its presence on $\Delta m = \pm 1$ EPR triplet spectra has been reported, although spin polarization transfer of I^- to Q^- has been demonstrated [12,13]. Note, however, that these experiments were done with *Rhodospseudomonas spheroides* RCs, where the exchange coupling J_{I-Q^-} is rather small (0.2-0.5 mT) [11-13].

We have monitored the P^R state in RCs and chromatophores where the coupling is much larger (~ 10 mT), i.e. in *Chromatium vinosum* and *Rps. viridis* [9,10]. For *Rps. viridis* the AEEAAE ESP pattern changes to AEAEAE at $T > 19 \pm 3$ K, whereas the zero field splitting parameters $|D|$ and $|E|$ remain almost unchanged over a wide temperature range (8-270 K). In chromatophores, the change of the ESP pattern can be inhibited by SDS treatment, which uncouples the iron atom from Q [10].

Materials and Methods

Chromatophores from *C. vinosum* and *Rps. viridis* were obtained by sonicating for 10 min. *Rps. viridis* RCs prepared according to Ref. 17 with $A_{830} \approx 30$ were a kind gift from Dr. A.J. Hoff. Incubation of the chromatophores with 1% SDS was done at room temperature using a suspension with $A_{1015} \approx 80$ in 50 mM deoxygenated Tris, pH 8. For measurements at $T = 7-180$ K standard 4 mm quartz tubes were used; RCs and chromatophores were diluted three times in ethylene glycol to obtain transparent samples at low temperature. For temperatures above 180 K the RCs were immobilized in a poly(vinylalcohol) film and mounted on a quartz rod. The primary iron-quinone acceptor was photochemically reduced by illumination at low temperature.

EPR spectra were recorded on a Varian E-6 spectrometer equipped with a helium

flow cryostat (Oxford Instruments E-6) or a nitrogen flow cryostat. The EPR spectrometer was modified to obtain a response time of 20–30 μ s. Light minus dark spectra were obtained using a 150 W xenon lamp (Eimac R 150-7A) modulated at 25–5000 Hz and phase-sensitive detection (PAR Lock-in Analyser 5204). Spectra were accumulated using a PAR 4203 signal averager connected to a MINC-11 minicomputer.

Results

$\Delta m = \pm 1$ triplet EPR spectra using light modulation of *Rps. viridis* RCs recorded at various temperatures are shown in Fig. 1. At 8 K (Fig. 1a) an AEEAAE ESP pattern of P^R is observed. The Y-transitions are rather weak and broadened. $|D|$ and $|E|$ values of $(160.3 \pm 0.7) \times 10^{-4}$ and $(38.6 \pm 0.8) \times 10^{-4}$ cm^{-1} , respectively, agree with reported values [18]. At $T > 19 \pm 3$ K the Y-transitions reverse sign (Fig. 1b, c) and the ESP pattern becomes AEAEAE (Fig. 1d). At increasing temperatures the $|D|$ and $|E|$ values exhibit a small increase (160.5×10^{-4} and

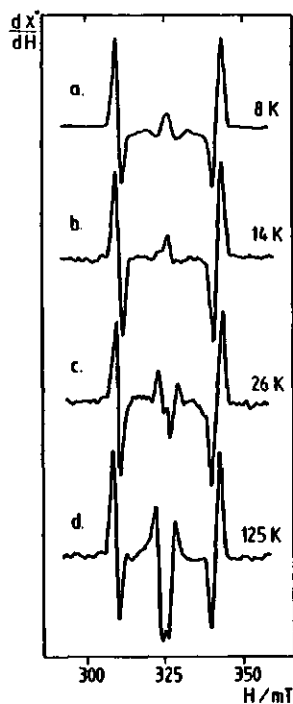


Fig. 1. Light minus dark triplet EPR spectra of P^R in *Rps. viridis* RCs at different temperatures ($A_{R30} = 10$). All samples contained 1 mM sodium ascorbate and were frozen in the dark. Relative amplifications: a: 1, b: 3, c: 6, d: 10. Light modulation frequency: 400 Hz; microwave power: 500 μ W in a, b and c, and 1 mW in d; 100 kHz magnetic field modulation: 1.6 mT.

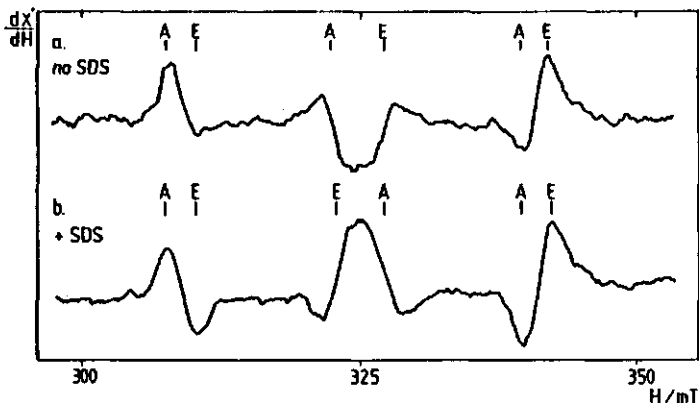


Fig. 2. Effects of SDS treatment on ESP pattern of P^R in chromatophores from *Rps. viridis* ($A_{1015} = 30$) at 125 K. a. No SDS added, ESP pattern: AEAEAE; b. 1% SDS added, incubated for 4 h, ESP pattern: AEEAAE. Light modulation frequency: 1 kHz; microwave power: 800 μ W; other conditions as in Fig. 1.

$39.0 \times 10^{-4} \text{ cm}^{-1}$ at 40 K; 162.0×10^{-4} and $39.6 \times 10^{-4} \text{ cm}^{-1}$ at 125 K) similar to results for *Rps. spheroides* [19]. This sign-reversal was also observed under continuous illumination. No $\Delta m = 2$ signal was found between 8 K and 125 K.

The same change in the ESP pattern is observed in chromatophores from *Rps. viridis* (Fig. 2a). Treatment with SDS inhibits the polarization inversion of the Y-transitions (Fig. 2b). At the same time an emissive spin-polarized $g = 2$ signal was observed (not shown; in Fig. 2 this signal is overmodulated), indicating that the iron atom is uncoupled from Q and that polarization transfer from I^- to Q^- occurs [12]. For chromatophores from *C. vinosum*, the 10 K triplet EPR spectrum exhibits an AEEAAE ESP pattern. At increasing temperature the amplitude of the Y-transitions decreased and disappeared completely at $T \approx 23$ K. Differently from the observations in *Rps. viridis* the amplitude of the Y-transitions remained zero up to 80 K.

Using phase-sensitive detection and light modulation [20] at $T = 100$ K we studied the phase dependence of the amplitudes of all six $\Delta m = \pm 1$ triplet transitions in *Rps. viridis* RCs as a function of the modulation frequency. We found that the Z- and X-transitions have different decay rate constants, showing that spin-lattice relaxation between the spin levels of the P^R triplet state does not dominate the kinetics. This conclusion is also supported by the observation that the sign of all transitions persists up to at least 240 K. At 100 K, the Y-transitions exhibit the same phase dependence as the Z-transitions.

Discussion

For many years it has been accepted, that the radical pair mechanism in bacterial photosynthesis invariably gives rise to a $\Delta m = \pm 1$ EPR triplet spectrum exhibiting an AEEAAE ESP pattern. Therefore, our assignment of a triplet spectrum with a

deviating polarization pattern to P^R needs firm proof. This assignment is supported by the following observations: Firstly, up to 40 K, the values of $|D|$ and $|E|$ agree with reported values for P^R of *Rps. viridis* [18], and are very different from the zero-field splittings for BChl-*b* in vitro [22]. Secondly, the RC preparations are highly purified and do not contain any appreciable amounts of antenna, free, or desintegrated BChl-*b*. If present at all, triplets in these impurities are not expected to give rise to a large EPR signal amplitude, since they are formed via normal intersystem crossing. Furthermore, the change of the ESP pattern is not caused by the isolation procedure, as chromatophores at 125 K exhibit the same polarization pattern as RCs (Fig. 2a).

From the mirror symmetry in all observed triplet spectra, including those with an AEAEAE ESP pattern, spin-lattice relaxation between the spin states of P^R can be ruled out as the mechanism that is responsible for the polarization change. Also intersystem crossing from the excited singlet donor state to the triplet state is unlikely, since no donor triplets are detected when the electron transfer is blocked by reducing I [9,10,23].

The effect of SDS treatment (Fig. 2) is an indication that the change of the polarization pattern is induced by the strong exchange and/or dipolar interaction between I^- and the third electron spin on the iron-quinone complex. In a coupled $P^+I^-Fe^{2+}Q^-$ spin system, rapid spin-lattice relaxation of the high spin iron [24] can be transmitted to the P^+I^- radical pair via the exchange coupling between Fe^{2+} and Q^- (128 mT [24]) and between Q^- and I^- (≈ 10 mT [9,10]). Thus, Fe^{2+} spin-lattice relaxation is expected to have a strong, temperature dependent influence on the spin-conversion mechanism in the P^+I^- radical pair, an effect which is normally neglected in calculations.

Further evidence for this role of $Fe^{2+}Q^-$ follows from the observation that similar effects were found in *C. vinosum*. In both species the coupling between I^- and $Fe^{2+}Q^-$ is much larger than in *Rps. spheroides* [9-11], where the ESP does not change with temperature [19]. Since the observed effect is strongly anisotropic (only the *Y*-peaks change), dipolar interactions probably contribute to the $I^-Fe^{2+}Q^-$ coupling [10]. The AEEAAE ESP pattern is unique for exclusive $S-T_0$ mixing [5], so effective population of the $T_{\pm 1}$ triplet levels is an absolute condition to give rise to the observed AEAEAE ESP pattern. Preliminary calculations (unpublished results) taking into account the coupling of the third electron spin on $Fe^{2+}Q^-$ to I^- indeed show that the $T_{\pm 1}$ triplet spin states of P^R can be populated. Spin-lattice relaxation of the high-spin Fe^{2+} may induce spin transitions within the three-spin system via the $I^-Fe^{2+}Q^-$ interactions during the lifetime of the $P^+I^-Fe^{2+}Q^-$ state of the RC, causing the observed temperature dependent change in the triplet spectra (Fig. 1). This is supported by the observations of Dismukes et al. [25] that no EPR spectrum could be observed above 20 K from $Fe^{2+}Q^-$ due to spin-lattice relaxation of the iron.

Concluding, we have demonstrated that the $S-T_0$ selection rule for P^R population is broken in reduced RCs and chromatophores from *Rps. viridis* and, to a

smaller extent, also in *C. vinosum* chromatophores. $T_{\pm 1}$ population of P^R is likely to be due to the magnetic coupling between $Fe^{2+}Q^-$ and I^- .

Acknowledgements

We thank Dr. A.J. Hoff for a generous gift of reaction centers of *Rps. viridis* and fruitful discussions. Experiments together with Drs. J.S. Norris and M.C. Thurnauer have drawn P.G.'s attention to the phenomenon of polarization inversion in *Rps. viridis*.

References

- 1 Dutton, P.L., J.S. Leigh and M. Seibert (1971) *Biochem. Biophys. Res. Commun.* 46, 406-413.
- 2 Frank, H.A., M.B. McLean and K. Sauer (1979) *Proc. Natl. Acad. Sci. USA* 76, 5124-5128.
- 3 Rutherford, A.W. and J.E. Mullet (1981) *Biochim. Biophys. Acta* 635, 225-235.
- 4 Swarthoff, T., P. Gast and A.J. Hoff (1981) *FEBS Lett.* 127, 83-86.
- 5 Schaafsma, T.J., J.F. Kleibeuker, R.J. Platenkamp and P. Geerse (1976) *in: Molecular Spectroscopy of Dense Phases. Proc. 12th Eur. Congr. Molec. Spectroscopy, Strasbourg, France, 1975*, pp. 491-494.
- 6 Norris, J.R. and J.J. Katz (1978) *in: The Photosynthetic Bacteria* (Clayton, R.K. and W.R. Sistrom, eds.) pp. 397-418, Plenum, New York.
- 7 Thurnauer, M.C., J.J. Katz and J.R. Norris (1975) *Proc. Natl. Acad. Sci. USA* 72, 3270-3274.
- 8 Blankenship, R.E., T.J. Schaafsma and W.W. Parson (1977) *Biochim. Biophys. Acta* 461, 297-305.
- 9 Tiede, D.M., R.C. Prince and P.C. Dutton (1976) *Biochim. Biophys. Acta* 449, 447-467.
- 10 Prince, R.C., D.M. Tiede, J.P. Thorber and P.L. Dutton (1977) *Biochim. Biophys. Acta* 462, 467-490.
- 11 Okamura, M.Y., R.A. Isaacson and G. Feher (1979) *Biochim. Biophys. Acta* 546, 394-417.
- 12 Gast, P. and A.J. Hoff (1979) *Biochim. Biophys. Acta* 548, 520-535.
- 13 Hoff, A.J. and P. Gast (1979) *J. Phys. Chem.* 83, 3355-3358.
- 14 Hoff, A.J. and P.J. Hore (1984) *Chem. Phys. Lett.* 108, 104-110.
- 15 Haberkorn, R. and M.E. Michel-Beyerle (1979) *Biophys. J.* 26, 489-498.
- 16 Hoff, A.J., H. Rademaker, R. van Grondelle and L.N.M. Duysens (1977) *Biochim. Biophys. Acta* 460, 547-554.
- 17 Den Blanken, H.J. and A.J. Hoff (1982) *Biochim. Biophys. Acta* 681, 365-374.
- 18 Den Blanken, H.J. and A.J. Hoff (1983) *Chem. Phys. Lett.* 98, 255-262.
- 19 Hoff, A.J. and I.I. Proskuryakov (1985) *Chem. Phys. Lett.* 115, 303-310.
- 20 Kleibeuker, J.F., R.J. Platenkamp and T.J. Schaafsma (1976) *Chem. Phys. Lett.* 41, 557-561.
- 21 Butler, W.F., R. Calvo, D.R. Fredkin, R.A. Isaacson, M.Y. Okamura and G. Feher (1984) *Biophys. J.* 45, 947-973.
- 22 Den Blanken, H.J. and A.J. Hoff (1983) *Chem. Phys. Lett.* 96, 343-347.
- 23 Angerhofer, A., J.U. von Schütz and H.C. Wolf (1984) *Z. Naturforsch.* 39C, 1085-1090.
- 24 Scholes, C.P., R.A. Isaacson and G. Feher (1971) *Biochim. Biophys. Acta* 244, 206-210.
- 25 Dismukes, G., H.A. Frank, R. Friesner and K. Sauer (1984) *Biochim. Biophys. Acta* 764, 253-271.

The relation between the electron spin polarization of the donor triplet state of the photosynthetic reaction center from *Rhodospseudomonas viridis* and the redox state of the primary acceptor

F.G.H. van Wijk, P. Gast[†] and T.J. Schaafsma

Agricultural University, Laboratory of Molecular Physics, De Dreijen 11, 6703 BC Wageningen, The Netherlands

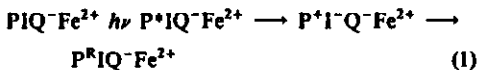
Received 20 June 1986

The hypothesis [(1986) Photobiochem. Photobiophys. 11, 95–100] that the temperature dependence of the electron spin polarization (ESP) pattern of the $\Delta m = \pm 1$ EPR spectrum of the triplet state P^R of the *Rhodospseudomonas viridis* reaction center is caused by magnetic interaction between the reduced menaquinone-iron complex Q^-Fe^{2+} and the electron spin on I^- (reduced bacteriopheophytin b), which is part of the radical pair P^+I^- (P^+ is the oxidized primary electron donor P960) has been investigated. It was found that the AEAEAE ESP pattern of the EPR spectrum detected at $T > 20$ K changes into the usual AEEAAE pattern, when Q^-Fe^{2+} is photochemically converted into $Q^{2-}Fe^{2+}$. This demonstrates that the presence of Q^- in Q^-Fe^{2+} is a necessary condition to obtain the AEAEAE ESP pattern.

Triplet state electron spin polarization Bacterial photosynthesis EPR Reaction center Redox state

1. INTRODUCTION

In bacterial photosynthetic reaction centers (RCs) the donor triplet state P^R is generated under illumination when the primary acceptor, a quinone-iron complex (Q^-Fe^{2+}), has been reduced [1–3]:



where P is the primary electron donor ($BChl_2$) and I is the intermediary acceptor ($BPhco$). At low temperature the radical pair P^+I^- (P^F) recombines exclusively forming P^R [3,4]. In high external magnetic fields this occurs via the radical pair mechanism [5,6], resulting in a triplet state with an

electron spin polarization (ESP) pattern that has been shown to be inconsistent with an intramolecular intersystem crossing (ISC) mechanism [7,8], and characteristic for photochemical activity in photosynthetic RCs. This triplet state has been detected by means of EPR spectroscopy in numerous photosynthetic species, including plant photosystem I and II, and green bacteria [1,9–12], invariably showing an AEEAAE ESP pattern (A, enhanced absorption; E, emission). However, we observed deviating ESP patterns in the $\Delta m = \pm 1$ EPR triplet spectra of P^R in isolated RCs from the purple bacterium *Rhodospseudomonas viridis* (AEAEAE) and in chromatophores of *Chromatium vinosum* (AE--EA) at temperatures above 20–25 K [13,14]. Spin-lattice relaxation within P^R or intramolecular ISC are unlikely to cause this change in the polarization pattern. The phenomenon was ascribed to a magnetic interaction between the electron spin on I^- , which is a part of the radical pair P^+I^- , and a third electron

[†] Present address: University of Chicago, Department of Chemistry, 5735 South Ellis Avenue, Searle Chemistry Laboratory, Chicago, IL 60637, USA

spin on the reduced menaquinone Q^- in the Q^-Fe^{2+} complex. This complex transmits the rapid relaxation of the high-spin Fe^{2+} to I^- .

Although SDS treatment is known to uncouple at least the iron atom from the QFe^{2+} complex [15], this method is not so well-defined as the technique of iron removal in RCs from *Rps. sphaeroides* R26 [16,17]. Therefore, a stronger proof for the involvement of Fe^{2+} and/or Q in the polarization inversion of the Y peaks of P^R in this system is desirable. Unfortunately, the iron-removal technique using $LiClO_4$ and *o*-phenanthroline does not apply to RCs from *Rps. viridis*, nor can Q be removed easily. We therefore have investigated the triplet polarization pattern as a function of the redox state of the primary acceptor. Since the *Rps. viridis* RC contains a fast donating cytochrome, it is possible to reduce doubly the quinone acceptor. This is expected to quench the magnetic interaction between the quinone-iron complex and the radical pair P^+I^- .

2. EXPERIMENTAL

RCs were isolated according to [14] and concentrated to $A_{830} = 50 \text{ cm}^{-1}$. EPR experiments were carried out as described in [14]; a typical EPR sample contained 25 μl of 0.5 M sodium ascorbate, 75 μl RCs, and 200 μl ethylene glycol. To create the doubly reduced state $Q^{2-}Fe^{2+}$, the samples were illuminated at room temperature with white light ($\sim 0.5 \text{ W} \cdot \text{cm}^{-2}$) from a 150 W xenon lamp (Eimac R150-7A) filtered through 6 cm water for varying periods of time, followed by rapid cooling to 77 K. Exposure to UV light was avoided. Reoxidation of $Q^{2-}Fe^{2+}$ was accomplished by flushing the sample with oxygen for several minutes at room temperature [18]. 2 μl ascorbate was added to these samples, which were then refrozen in the dark. Q_A to Q_B electron transfer was blocked by adding $\sim 5 \text{ mM}$ *o*-phenanthroline to the EPR samples.

3. RESULTS

The treatment of the RCs, in order to produce the $Q^{2-}Fe^{2+}$ state, is very similar to that on *Rps. sphaeroides* R26 RCs by Okamura et al. [18], and on *Rps. viridis* RCs by Prince et al. [19]. Fig. 1 presents the Q^-Fe^{2+} , I^- and light-induced triplet

EPR spectra, when the RCs had been exposed to white light at room temperature for different periods of time. Prince et al. [19] found that upon illumination under these conditions the triplet spectrum completely disappears, due to trapping of I^- , inhibiting any further charge separation. To be able to observe P^R we had to use a moderate redox potential, allowing Q^{2-} production, and simultaneously permitting reoxidation of I^- . We used ascorbate at pH 8 ($E^{o'} = 0 \text{ mV}$), so the Q^-Fe^{2+} state had to be generated by illumination, since the Q/Q^- redox couple is $\sim -150 \text{ mV}$ [20].

Upon increasing the period of illumination, the EPR signal at $g = 1.8$ of Q^-Fe^{2+} [21,22] disappears. Concurrently, the spin polarization of the Y^-/Y^+ peaks in the triplet spectrum changes from A/E into E/A (fig. 1b,c), whereas at low microwave power a $g = 2$ signal appears, due to trapping of I^- [19,23]. The $I^-Q^-Fe^{2+}$ spectra can be understood by considering the results of the experiments represented in fig. 1a-c: although the sample was not illuminated at 300 K (fig. 1a) a split signal (S in fig. 1a) is observed, due to the trapping of a small amount of I^- , competitively formed during the generation of Q^- by illumination at 10–20 K. (When the sample is left in the dark, no split signal is observed.) After 20 s of illumination at 300 K (fig. 1b), Q^{2-} is built up at the cost of Q^- and more I^- has been trapped, as is evident from fig. 1 (center). After 120 s of illumination at 300 K (fig. 1c), the sample contains four different photoproducts: (i) IQ^- , (ii) I^-Q^- , (iii) IQ^{2-} , (iv) I^-Q^{2-} . From the amplitude of the $g = 1.8$ signal an estimated fraction of less than 5% of these photoproducts were in states i and ii. Of the remaining 95%, state iii gives rise to the observed P^R triplet spectrum, whereas state iv is detected as I^- , but does not give rise to triplet formation. Formation of state iv explains the reduced amplitude of the EPR triplet spectrum. Prolonged illumination results in a lower triplet yield, due to the increased fraction of I^-Q^{2-} . The EPR triplet spectrum of fig. 1c does not show any changes in the 8–100 K temperature range, except for some decrease in amplitude of all peaks.

When the sample of fig. 1c is thawed, flushed with oxygen and refrozen in the dark, the Q^-Fe^{2+} signal reappears, and the ESP pattern of P^R at 110 K is converted into the original AEAEAE pattern. When the experiments are repeated with

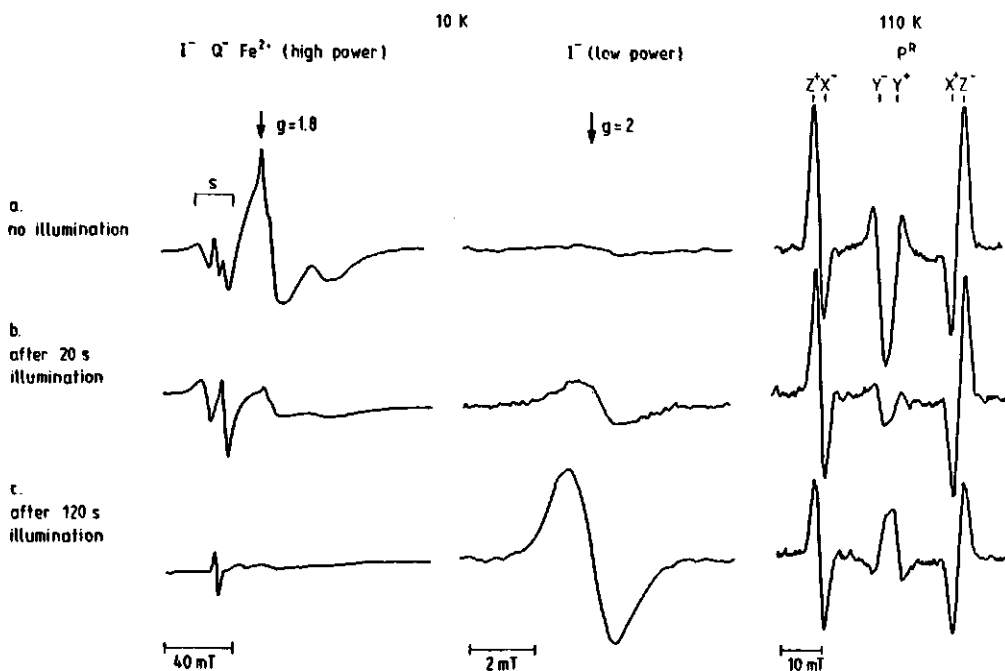


Fig. 1. Relation between electron spin polarization pattern of the EPR triplet spectrum of P^R in isolated RCs of *Rps. viridis* and the redox state of the primary acceptor. All samples contained 4 mM sodium ascorbate ($E^{0'} = 0$ mV) pH 8, 200 μ l ethylene glycol, 75 μ l RCs ($A_{430} = 50$ cm $^{-1}$) and were photochemically reduced. (a) No illumination at 300 K (only low-temperature illumination to produce Q^-), P^R spin polarization pattern: AEAEAE, s = split signal (I^-Q^-); (b) intermediate case, after 20 s of 300 K illumination; (c) after 120 s illumination, P^R polarization pattern: AEEAAE. Instrumental settings: $I^-Q^-Fe^{2+}$ spectra: 3.2 mT modulation amplitude, 5 mW, I^- (low-power) spectra: 0.4 mT modulation, 2 μ W, P^R spectra: 1 kHz light modulation, 2.5 mT field modulation, 5 mW. All spectra have the same vertical scale.

samples in which the electron transfer from Q_A to Q_B is blocked, identical results are obtained.

4. DISCUSSION

In *Rps. viridis* RCs the magnetic I^-Q^- interaction is relatively large (~ 15 – 20 mT [19]) as compared to other bacteria (e.g. *Rps. sphaeroides* ~ 0.1 – 0.5 mT [18,24], *Chromatium vinosum* ~ 6 mT [23]). Therefore, we ascribed the observed effects to a spin-spin interaction between Q^-Fe^{2+} and P^+I^- [14].

In the left wing of the Q^-Fe^{2+} spectrum in fig. 1 the I^- high-power spectrum can be recognized.

This split I^-Q^- signal (S in fig. 1) disappears concomitantly with the Q^-Fe^{2+} signal and the A/E polarization of the Y^-/Y^+ peaks, resulting in the AEEAAE ESP pattern, characteristic for the radical pair mechanism. It can be concluded that the presence of the paramagnetic species Q^-Fe^{2+} is essential to observe the AEAEAE polarized P^R triplet spectrum at $T > 20$ K. There are several possible explanations: (i) Direct magnetic (dipolar) coupling between Q^-Fe^{2+} and P^R as suggested to exist in *Rps. sphaeroides* [25]. This is unlikely, since it cannot explain the relation [14] between I^-Q^- coupling strength and the observed P^R ESP pattern of the triplet spectrum in *Rps. viridis*, C.

vinosum and *Rps. sphaeroides*. For the latter we did not observe a temperature-dependent change in polarization pattern. (ii) The presence of Q^{2-} converts the high-spin Fe^{2+} into its low-spin form and subsequently changes the interaction with P^+I^- . This indeed may explain the experimental results, if Fe^{2+} is the source of the temperature effect on the spectra of P^R . Although there is no firm proof that the spin state of Fe^{2+} does not change when the primary quinone is doubly reduced, addition of *o*-phenanthroline to the RCs, blocking the electron transfer step between Q_A and Q_B [26], does not affect our experimental results. Butler et al. [27] have observed the characteristic $g = 1.83$ EPR signal in the $Q_B^-Fe^{2+}Q_A^-$ state. Under our experimental conditions the Fe^{2+} is ligated to Q_A^- and Q_B , which together are expected to have a smaller effect on the iron spin state. Furthermore, susceptibility measurements on *Rps. sphaeroides* R26 RCs did not show any changes in the spin state of the iron on reduction of the primary acceptor [16]. It is therefore unlikely that the Fe^{2+} spin state in *Rps. viridis* RCs changes upon illumination, due to the reduction of the quinone(s). (iii) Q^- acts as a carrier of spin transitions between the high-spin Q^-Fe^{2+} and P^+I^- . The $P^+I^-Q^-Fe^{2+}$ must be considered as a multispin system, to which the conventional radical pair mechanism cannot be applied as is reflected by the observed temperature-dependent change of the P^R triplet pattern. Doubly reducing the primary quinone restores the radical pair mechanism as demonstrated by the AEEAAE polarization pattern.

The $Fe^{2+}Q^-$ complex is coupled to the P^+I^- radical pair state and causes the ESP pattern of P^R to change at higher temperatures. Consequently, monitoring the EPR triplet state not only yields information about the photochemical activity of the P-I part in the RC (i.e. AEEAAE below 15–20 K). Well above this temperature the observed ESP pattern also demonstrates that the Q_AFe^{2+} part is active in the RC. This provides a tool to check the acceptor side in RC or chromatophore preparations from *C. vinosum* and *Rps. viridis* with EPR at liquid nitrogen temperatures.

REFERENCES

- [1] Dutton, P.L., Leigh, J.S. and Seibert, M. (1971) *Biochem. Biophys. Res. Commun.* 46, 406–413.
- [2] Levanon, H. and Norris, J.R. (1982) *Mol. Biol. Biochem. Biophys.* 35, 152–195.
- [3] Hoff, A.J. (1982) in: *Triplet State ODMR Spectroscopy* (Clarke, R.H. ed.) pp.347–426, Wiley, New York.
- [4] Parson, W.W., Clayton, R.K. and Cogdell, R.J. (1975) *Biochim. Biophys. Acta* 387, 265–278.
- [5] Blankenship, R.E., Schaafsma, T.J. and Parson, W.W. (1977) *Biochim. Biophys. Acta* 461, 297–305.
- [6] Haberkorn, R. and Michel-Beyerle, M.E. (1979) *Biophys. J.*, 489–498.
- [7] Schaafsma, T.J., Kleibeuker, J.F., Platenkamp, R.J. and Geerse, P. (1976) in: *Molecular Spectroscopy of Dense Phases*, Proc. 12th Congr. Mol. Spectrosc., Strasbourg, France, 1975, pp.491–494.
- [8] Norris, J.R. and Katz, J.J. (1978) in: *The Photosynthetic Bacteria* (Clayton, R.K. and Sistrom, W.R. eds) pp.397–418, Plenum, New York.
- [9] Thurnauer, M.C., Katz, J.J. and Norris, J.R. (1975) *Proc. Natl. Acad. Sci. USA* 72, 3270–3274.
- [10] Rutherford, A.W., Paterson, D.R. and Mullet, J.E. (1981) *Biochim. Biophys. Acta* 635, 205–214.
- [11] Frank, H.A., McLean, M.B. and Sauer, K. (1979) *Proc. Natl. Acad. Sci. USA* 76, 5124–5128.
- [12] Swarthoff, T., Gast, P. and Hoff, A.J. (1981) *FEBS Lett.* 127, 83–86.
- [13] Van Wijk, F.G.H., Gast, P. and Schaafsma, T.J. (1985) in: *Antennas and Reaction Centers of Photosynthetic Bacteria* (Michel-Meyerle, M.E. ed.) p.146, Springer, Berlin.
- [14] Van Wijk, F.G.H., Gast, P. and Schaafsma, T.J. (1986) *Photobiochem. Photobiophys.* 11, 95–100.
- [15] Loach, P.A. and Hall, R.C. (1972) *Proc. Natl. Acad. Sci. USA* 69, 786–790.
- [16] Feher, G. and Okamura, M.Y. (1978) in: *The Photosynthetic Bacteria* (Clayton, R.K. and Sistrom, R. eds) pp.349–386, Plenum, New York.
- [17] Tiede, D.M. and Dutton, P.L. (1981) *Biochim. Biophys. Acta* 637, 278–290.
- [18] Okamura, M.Y., Isaacson, R.A. and Feher, G. (1979) *Biochim. Biophys. Acta* 546, 394–417.
- [19] Prince, R.C., Tiede, D.M., Thornber, J.P. and Dutton, P.L. (1977) *Biochim. Biophys. Acta* 462, 467–490.
- [20] Prince, R.C., Leigh, J.S. and Dutton, P.L. (1976) *Biochim. Biophys. Acta* 440, 622–636.
- [21] Leigh, J.S. and Dutton, P.L. (1972) *Biochem. Biophys. Res. Commun.* 46, 414–421.

- [22] Dismukes, G.C., Frank, H.A., Friesner, R. and Sauer, K. (1984) *Biochim. Biophys. Acta* 764, 253-271.
- [23] Tiede, D.M., Prince, R.C. and Dutton, P.L. (1976) *Biochim. Biophys. Acta* 449, 447-467.
- [24] Gast, P. and Hoff, A.J. (1979) *Biochim. Biophys. Acta* 548, 520-535.
- [25] De Groot, A., Lous, E.J. and Hoff, A.J. (1985) *Biochim. Biophys. Acta* 808, 13-20.
- [26] Shopes, R.J. and Wraight, C.A. (1985) *Biochim. Biophys. Acta* 806, 348-356.
- [27] Butler, W.F., Calvo, R., Fredkin, D.R., Isaacson, R.A., Okamura, M.Y. and Feher, G. (1984) *Biophys. J.* 45, 947-973.

4.4 THE ELECTRON SPIN POLARIZATION OF THE DONOR-TRIPLET STATE IN
NATIVE AND MODIFIED PHOTOSYNTHETIC REACTION CENTERS FROM
RHODOBACTER SPHAEROIDES R-26

F.G.H. Van Wijk, C.B. Beijer, P. Gast[‡], and T.J. Schaafsma

Dept. of Molecular Physics, Wageningen Agricultural University, De
Dreijen 11, 6703 BC Wageningen, The Netherlands.

[‡]: Present address: Chemistry Department, University of Chicago,
5735 South Ellis Avenue, Chicago, Illinois 60637, USA.

ABSTRACT

The electron spin polarization (ESP) pattern of the donor-triplet state (P^R) from reaction centers (RC's) of the purple bacterium Rhodobacter (formerly Rhodospseudomonas) sphaeroides R-26 was investigated. $\Delta m = \pm 1$ triplet EPR spectra were recorded of unmodified RC's as well as of RC's from which Fe^{2+} or ubiquinone was removed, or ubiquinone was substituted by menaquinone.

The relative amplitude of the Y peaks in the triplet EPR powder spectrum of P^R decreases when the temperature is increased from 8 K to 100 K in RC's with an intact quinone-iron complex. This decrease is more pronounced when the primary ubiquinone is substituted by menaquinone. These observations provide further support for the hypothesis that the observed lineshape of the P^R triplet state EPR spectrum reflects the presence of a third electron spin, magnetically coupled to I^- in the P^+I^- radical pair, as suggested by Van Wijk et al. (Photobiochem. Photobiophys. 11, 1986, 95-100). Our observations suggest that this phenomenon may be general in purple bacteria.

INTRODUCTION

The triplet state (P^R) of the primary electron donor in both plant and bacterial photosynthetic reaction centers (RC's) is generated by recombination of the electron-hole on the oxidized donor (P^+), and the unpaired electron on the reduced intermediary acceptor (I^-) under conditions that forward electron transfer is blocked, e.g. by removal or prereduction of the primary acceptor (a quinone, Q_A , in bacterial RC's) [1,2]. In high magnetic fields (i.e. for external fields, which are much larger than the magnetic interactions between the electronic and nuclear spins on P^+ , I^- , and Q_A^-) this results in an electron spin polarization (ESP) of the recombination triplet state of P [3,4]. This spin polarization has been shown to be incompatible with generation via intersystem crossing through spin-orbit coupling [5,6], and is observed in low temperature $\Delta m = \pm 1$ EPR powder triplet spectra with an AEEAAE ESP pattern (A=enhanced absorption, E=emission) [1,2]. This ESP pattern has been found in all photosynthetic species [7-10], and is now a common spectroscopic parameter which is suitable to demonstrate full photochemical activity in the photosynthetic reaction center (RC). However, recently we reported deviating ESP patterns at temperatures above ~ 20 K in RC preparations from Rhodospseudomonas viridis and chromatophores from Chromatium vinosum [11,12]. We demonstrated that the observed effect depends on the presence of a (singly) reduced primary acceptor (Q_A^-) in the native quinone-iron complex [13], indicating that the magnetic coupling between I^- and Q_A^- is involved. At $T > 20$ K T_1 processes on the high spin Fe^{2+} ($S=2$) in the $Q_A^-Fe^{2+}$ complex [14] are believed to induce rapid spin transitions on Q^- . The spin-spin coupling between I^- and Q_A^- transmits these spin transitions from Q_A^- to I^- , the latter being a part of the radical pair P^+I^- .

In order to investigate the generality of the relation between the coupling of I^- with Q^-Fe^{2+} and the ESP pattern in bacterial photosynthesis, we studied the temperature dependence of the EPR spectra of P^R in Rb. sphaeroides RC's, for which it is known [16-18] that the

magnetic coupling strength between Q_A^- and I^- is weak. Furthermore, we extracted the primary ubiquinone from these RC's and replaced it by menaquinone as present in e.g. Rps. viridis, thereby increasing the magnetic coupling between I^- and Q^- from ≤ 0.05 mT for ubiquinone [16-18] to ~ 6 mT for menaquinone [16].

MATERIALS AND METHODS

RC's from Rb. sphaeroides were isolated as described elsewhere [19], with the modification that instead of Triton X-100, Brij-58 was used as the solubilizing detergent. Iron was removed using the lithium perchlorate method first used by Tiede and Dutton [20]. The result of this procedure was tested by monitoring the emissively polarized Q_A^- EPR signal at $g=2$ [21]. Ubiquinone depleted RC's were prepared using the method given in ref [22]. To see whether reconstituted RC's contained menaquinone, we determined the kinetics of recombination of P^+ and Q_A^- at room temperature [23]. As a further evidence we used the presence of the characteristic $g=1.8$ EPR signal from Q_A^- in the $Q_A^- Fe^{2+}$ complex at 10 K [14,24,25]. EPR measurements were carried out as in ref. [12]. The home-built optical absorbance difference spectrometer was described in [26,27].

The reduction of the RC's was accomplished by addition of excess horse heart cytochrome-c and sodium ascorbate at pH 8. The samples were illuminated at room temperature with white light from a 200 W Tungsten lamp and rapidly frozen under continuous illumination.

RESULTS AND DISCUSSION

Ubiquinone-depleted RC's were reconstituted with menaquinones with isoprenoid tail lengths varying from C_{35} (MQ-7) to C_{50} (MQ-10). The reconstitution procedure was tested by monitoring the absorbance changes at 448 nm. At this wavelength the difference in visible

absorption of MQ and MQ⁻ is at a maximum. The recombination time of P⁺UQ_A⁻ at room temperature is 115 ms [23], whereas the kinetics of the P⁺MQ⁻ recombination yielded single exponential decay with τ-values of 80±5 ms (independent of the length of the MQ-tail), demonstrating the photochemical electron accepting activity of the reconstituted menaquinone. However, in several of the reconstituted RC preparations, the EPR signal of Fe²⁺Q_A⁻ at g=1.8 was not observed.

These results indicate that the reconstitution is less critical for the BPheo-a (L-branch) binding-site (probably a tryptophane [28,29]), than to the Fe²⁺ binding-site (probably a histidine [28,29]); this is not too surprising, since removal of Q_A is known to affect the protein environment of the Fe²⁺ [30]. The optical measurements at room temperature therefore cannot be taken as the sole check for native reconstitution.

An intact quinone-iron complex was demonstrated by a reconstituted RC that did show an EPR transition at g=1.8, although somewhat weaker than in untreated RC's. Only in samples where the characteristic g=1.8 signal was present, indicating that at least part of the MQ's were correctly bound to the iron, we observed a temperature dependent ESP pattern in the EPR triplet spectrum from P^R.

In the following we will use the total fractional amplitude (F) of the Y-peaks (Y⁺ and Y⁻) in the polarized EPR (first derivative) triplet spectrum: $F = 3I_y / (|I_x| + |I_y| + |I_z|)$, where $|I_i|$ denotes the sum of the absolute values of the low field and high field peak amplitudes (i=x,y,z). We choose I_y to be positive for an ABEAAE polarized triplet spectrum.

At low temperature (~5 K) F is about 1 in all samples. When the temperature is increased, differences are observed depending on the state of the quinone-iron acceptor complex. Figure 1 shows triplet spectra at 100 K. Those samples that lack the quinone (fig. 1a) or the iron (not shown, but identical amplitudes are obtained as in fig 1a) do not change their relative Y-amplitudes as a function of temperature. However, when the Q_A⁻Fe²⁺ complex is intact, the fraction of the Y peaks drops significantly from 0.9 at 8 K to 0.7 at 100 K (fig.

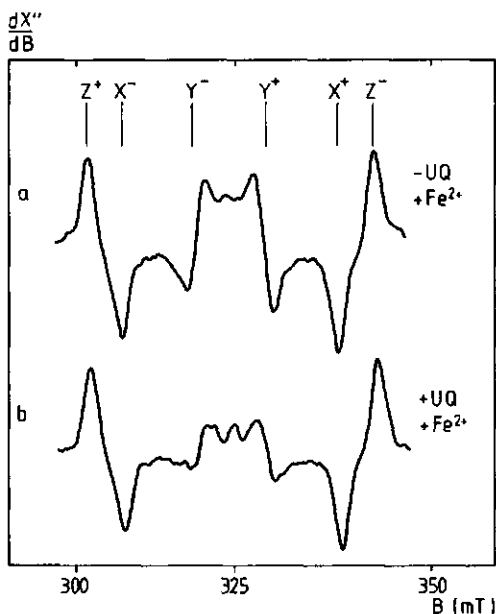


Figure 1

$\Delta m=1$ triplet EPR spectra of pR in RC's from Rb. sphaeroides R-26 at 50 K. a. RC's from which the primary ubiquinone (Q_A) is extracted; b. Native RC's. Experimental conditions: microwave power: 100 μW (9 GHz), modulation amplitude: 2.5 mT at 100 kHz; illumination: 150 W Xe, filtered through 6 cm water, light-modulation frequency: 100 Hz.

1b), whereas the X-peaks, which have very similar kinetics, do not. When the ubiquinone is replaced by menaquinone, which couples magnetically much stronger to I^- than UQ^- [16], the observed fraction is even lower: 0.5 at 100 K. The general trend of the temperature dependence of F for RC's reconstituted with MQ-9 is shown in figure 2. From earlier work [16] it is known that the magnetic coupling between I^- and $Q_A^-Fe^{2+}$ in MQ reconstituted RC's from Rb. sphaeroides R-26 is 5-6 mT. This coupling strength is also present in RC's from C. vinosum [31], from which we have observed that the triplet Y-peak amplitudes decrease with temperature until $T \approx 25$ K, above this temperature the Y-peaks have totally disappeared [12]. Since both types of RC's contain identical chromophores (BChl-a, BPheo-a, MQ, paramagnetic Fe^{2+}) with very similar magnetic interactions between the various electron

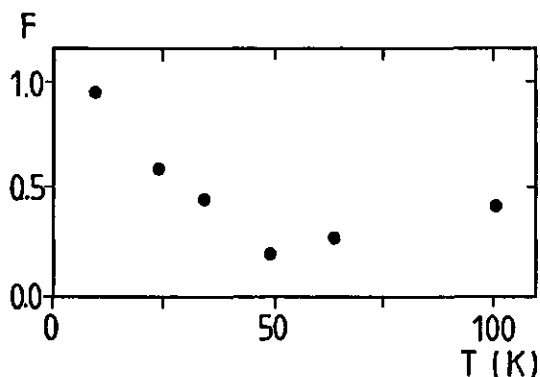


Figure 2

Temperature dependence of the fractional Y-amplitude F of the $\Delta m = \pm 1$ EPR triplet spectrum of RC's from Rb. sphaeroides R-26, from which the primary ubiquinone is substituted by menaquinone-9. F is defined in the text. EPR spectra were recorded as in figure 1.

spins, one would expect both species to exhibit a very similar temperature dependence of the lineshape of the $\Delta m = \pm 1$ P^R EPR spectrum. The reduced amplitude of the $g=1.8$ EPR signal from these reconstituted RC's with respect to that of native RC's, indicated that less than 100% of the MQ was present in an intact MQ^-Fe^{2+} complex.

Note, however, that every non-intact acceptor will yield $F=1$, thereby increasing the observed fraction of Y-peaks. Hence, the observed fractions in figure 2 represent upper limits, and therefore it cannot be excluded, that the triplet Y-peaks from reconstituted RC's which contain native MQ^-Fe^{2+} complexes, have zero amplitude at temperatures above ~ 25 K, similar to the observations for C. vinosum [12].

The observed temperature dependence of the Y-peaks in the P^R triplet spectra from Rb. sphaeroides R-26 RC's with an intact acceptor complex is similar to the observations reported earlier for Rps. viridis and C. vinosum [11-13]. I.e. whenever the acceptor ($Q_A^-Fe^{2+}$) complex in the RC is modified, and consequently the magnetic interactions in this complex are destroyed, the observed fraction F of the Y-amplitudes is larger than in RC's with intact acceptor complexes when

Table I

Species	Acceptor	$J_{I^-Q^-}$ (mT)	ESP ^a	F ^{a,b}	ref.
<u>Rps. viridis</u>	$MQ^- - Fe^{2+}$	15 - 20	AEAEAE	-1.3	12
<u>Rps. viridis</u> ^c	$MQ^- \blacksquare Fe^{2+}$	15 - 20	AEEAAE	1.4	12
<u>Rps. viridis</u>	$MQ^= - Fe^{2+}$	0	AEEAAE	0.9	13
<u>C. vinosum</u>	$MQ^- - Fe^{2+}$	6	AE--AE	0.0	12
R-26 ^d	$UQ^- - Fe^{2+}$	≤ 0.05	AEEAAE	0.7	e
R-26'	$UQ^- - .$	≤ 0.05	AEEAAE	1.0	e
R-26''	$. - Fe^{2+}$	0	AEEAAE	1.0	e
R-26'''	$MQ^- - Fe^{2+}$	5 - 6	AEEAAE	≤ 0.5	e

a: 100K

b: $F = 3I_y / (|I_x| + |I_y| + |I_z|)$, I_x denotes the amplitude of $X^- + X^+$ etc.

c: incubated with SDS, destroying the $MQ^- Fe^{2+}$ coupling (no $g=1.8$ signal), and probably keeping the I^-Q^- coupling intact (intact electron transfer).

d: Rb. sphaeroides R-26

e: this work.

observed at the same temperature. Table I summarizes the observed ESP patterns and the fractional Y-amplitude for several bacterial RC's and chromatophores. The minimum value of F in figure 2 at $T \sim 50$ K was not observed in samples of Rps. viridis and C. vinosum. At this moment, the origin of this difference is unclear.

In conclusion, these results provide further support for the existence of a relation between the magnetic coupling of the $Q_A^- Fe^{2+}$ complex with I^- , and the observed temperature dependence of the lineshape of the triplet EPR spectrum of p^R . This effect seems to be a general phenomenon in bacterial RC's, its extent is determined by the strength of the coupling between I^- and $Q_A^- Fe^{2+}$.

ACKNOWLEDGEMENTS

We thank dr. J.F.H. Snel (Dept. of Plant Physiological Research, Wageningen) for the use of the time-resolved absorption spectrophotometer. We acknowledge a kind gift of vitamins K₂ (menaquinones) from F. Hoffmann-La Roche & Co, Switzerland.

REFERENCES

1. Levanon, H, and J.R. Norris (1978) Chem. Rev. 78, 185-198.
2. Hoff, A.J. (1982) in Molecular Biology, Biochemistry and Biophysics, vol. 35, pp 80-153.
3. Thurnauer, M.C., J.J. Katz, and J.R. Norris (1975) Proc. Natl. Acad. Sci. (USA) 72, 3270-3274.
4. Blankenship, R.E., T.J. Schaafsma, and W.W. Parson (1977) Biochim. Biophys. Acta 461, 297-305.
5. Schaafsma, T.J., J.F. Kleibeuker, R.J. Platenkamp, and P. Geerse (1976) in Molecular Spectroscopy of Dense Phases. Proc. 12th Eur. Congr. Molec. Spectroscopy, Strassbourg, France, 1975, pp 491-494.
6. Norris, J.R., and J.J. Katz (1978) in The Photosynthetic Bacteria (R.K. Clayton and W.R. Sistrom, eds.) pp 397-418, Plenum, New York.
7. Dutton, P.L., J.S. Leigh, and M. Seibert (1971) Biochem. Biophys. Res. Comm. 46, 406-413.
8. Frank, H.A., M.B. McLean, and K. Sauer (1979) Proc. Natl. Acad. Sci. (USA) 76, 5124-5128.
9. Rutherford, A.W., J.E. Mullet (1981) Biochim. Biophys. Acta 635, 225-235.
10. Swarthoff, T., P. Gast, and A.J. Hoff (1981) FEBS Lett. 127, 83-86.
11. Van Wijk, F.G.H., P. Gast, and T.J. Schaafsma (1985) in Antennas and Reaction Centers of Photosynthetic Bacteria. Proc. Int.

- Workshop Feldafing, F.R.G. (Michel-Beyerle, ed.), p. 146, Springer, Berlin.
12. Van Wijk, F.G.H., P.Gast, and T.J. Schaafsma (1986) *Photobiochem. Photobiophys.* 11, 95-100.
 13. Van Wijk, F.G.H., P.Gast, and T.J. Schaafsma (1986) *FEBS Lett.* 206, 238-242.
 14. Butler, W.F., R. Calvo, D.R. Fredkin, R.A. Isaacson, M.Y. Okamura, and G. Feher (1984) *Biophys. J.* 45, 947-973.
 15. Woodbury, N.W., W.W. Parson, M.R. Gunner, R.C. Prince, and P.L. Dutton (1986) *Biochim. Biophys. Acta* 851, 6-22.
 16. Okamura, M.Y., R.A. Isaacson, and G. Feher (1979) *Biochim. Biophys. Acta* 546, 394-417.
 17. Gast, P., and A.J. Hoff (1979) *J. Phys. Chem.* 83, 3355-3358.
 18. Hoff, A.J., and P. Gast (1979) *Biochim. Biophys. Acta* 548, 520-535.
 19. Wraight, C.A. (1979) *FEBS. Lett.* 93, 283-288.
 20. Tiede, D.M., and P.L. Dutton (1981) *Biochim. Biophys. Acta* 637, 278-290.
 21. Gast, P., and A.J. Hoff (1979) *Biochim. Biophys. Acta* 548, 520-535.
 22. Okamura, M.Y., R.A. Isaacson, and G. Feher (1975) *Proc. Natl. Acad. Sci. (USA)* 72, 3491-3495.
 23. Hsi, E.S.P., and J.R. Bolton (1974) *Biochim. Biophys. Acta* 347, 126-133.
 24. Feher, G. (1971) *Photochem. Photobiol.* 14, 373-388.
 25. Dutton, P.L., J.S. Leigh, and D.W. Reed (1973) *Biochim. Biophys. Acta* 292, 654-664.
 26. Van Kooten, O., A.G.M. Gloudemans, and W.J. Vredenberg (1983) *Photobiochem. Photobiophys.* 6, 9-14.
 27. Snel, J.F.H. (1985) Thesis, Wageningen, The Netherlands.
 28. Deisenhofer, J., O. Epp, K. Miki, R. Huber, and H. Michel (1985) *Nature* 318, 618-624.
 29. Michel, H., O. Epp, and J. Deisenhofer (1986) *EMBO J.* 5, 2445-2451.
 30. Butler, W.F., D.C; Johnson, H.B. Shore, D.R. Fredkin, M.Y. Okamura, and G. Feher (1980) *Biophys. J.* 32, 967-992.

31. Tiede, D.M., R.C. Prince, and P.L. Dutton (1976) *Biochim. Biophys. Acta* 449, 447-467.

4.5 SUMMARY AND CONCLUSIONS

This Chapter describes the observed temperature dependence of the shape of the $\Delta m = \pm 1$ EPR spectra of the donor triplet state (P^R) in RC-containing preparations of Rps. viridis, Rb. sphaeroides R-26, and C. vinosum.

SDS-treatment of chromatophores of Rps. viridis destroys the magnetic interaction between electron spins located on the high-spin Fe^{2+} and Q_A^- (together constituting the quinone-iron complex). In such SDS-treated samples the radical pair electron spin polarization (ESP) pattern of the triplet EPR spectrum from P^R (AEEAAE) is observed at all temperatures between 8-120 K, despite the fact that a third electron spin (Q_A^-), magnetically coupled to I^- , is present.

In addition, an AEEAAE polarization pattern is monitored, when the primary quinone is doubly reduced ($Q_A^-Fe^{2+}$), independently of the temperature at least up to 120K. Conversion of $Q_A^-Fe^{2+}$ to the singly reduced state ($Q_A^-Fe^{2+}$) also restores the temperature dependence of the P^R triplet state spin polarization.

The magnitude of the effect of a change of temperature on the ESP and the strength of the magnetic interaction between Q_A^- and I^- appear to be related. The strongest effect is observed in Rps. viridis with a magnetizing coupling strength of 10 - 20 mT. In C. vinosum the effect is smaller, in accordance with a coupling strength of 6 mT. In RC's from Rb. sphaeroides R-26 the magnetic coupling is very weak: 0.01 - 0.05 mT. A modest temperature dependence of the lineshape was observed, which is absent in RC's with a modified acceptor side (i.e. either Fe^{2+} or Q_A^- removed).

In Rb. sphaeroides R-26 the abovementioned relation was shown to exist by substituting ubiquinone in the quinone-iron complex, by menaquinone-9, thereby increasing the magnetic interaction between I^- and Q_A^- . This reconstitution resulted in a more prominent change in the lineshape of P^R with temperature.

In conclusion:

The temperature dependence of the ESP pattern, or more correctly

the lineshape of the donor-triplet EPR powder spectrum in bacterial RC's depends on:

1. the magnitude of the $I^- - Q_A^-$ magnetic interaction;
2. the presence of an intact $Q_A^-Fe^{2+}$ complex.

This knowledge is of practical interest: the lineshape of the p^R EPR spectrum at $T > 30$ K reflects the structural status of the acceptor in the RC. A defect acceptor side always results in an AEEAAE ESP pattern, independent of the temperature, whereas for an intact acceptor side the fractional amplitude of the Y-transitions in the EPR $\Delta m = \pm 1$ powder spectrum decreases with temperature, eventually leading to sign-reversal of the Y^-/Y^+ transitions. Thus, if another than an AEEAAE ESP pattern in the EPR spectrum of p^R is observed, this does not imply that the RC-containing preparation is not photochemically active, although the inverse statement does hold.

Our results indicate that the magnetic coupling between I^- and Q_A^- , exclusively observed at low temperatures (split EPR signal at $T < 20$ K), persists up to almost room temperature.

Rapid T_1 processes, located on the high-spin Fe^{2+} are thought to be the source of the temperature effect on p^R polarization. Thus, the Fe^{2+} acts as a relaxation source, the singly reduced quinone acts as a relaxation carrier between source and radical pair. This hypothesis is consistent with the observation that both Fe^{2+} and Q_A^- are required to observe the temperature dependence.

The experimental result that the steady-state peak intensities for magnetic fields parallel to the X, and Y canonical axis are governed by almost identical decay constants, and the finding that only the Y-peaks are affected by the temperature, may be ascribed to anisotropic magnetic interactions between Q_A^- and I^- , and/or Q_A^- and Fe^{2+} .

Because the experiments, described in this Chapter, reflect steady-state spin polarizations, it can not be concluded whether the initial spin polarizations are identical to the observed polarizations. For that purpose time-resolved EPR experiments were carried out, the results of which are described in the succeeding Chapter.

CHAPTER V

TRIPLET STATE SPIN DYNAMICS IN REACTION CENTERS FROM RHODOPSEUDOMONAS VIRIDIS AS STUDIED BY TIME-RESOLVED EPR

5.1 INTRODUCTION

The primary donor triplet state (P^R) in photosynthetic reaction centers (RC's) can be used as an internal probe to monitor (changes in) the environment of the donor (P). Furthermore, since this triplet state is exclusively generated via the charge separated state P^+I^- , usually denoted as P^F , I denotes the intermediary electron acceptor, (a B_{Pheo}-b in Rps. viridis), its electron spin polarization (ESP) in high magnetic fields is determined by the spin dynamics within P^F [1-4].

When the primary electron acceptor (Q_A) is removed, or reduced prior to illumination, the forward electron transfer reaction is blocked, increasing the lifetime of P^F from ca. 200 ps [5-7] to 10-20 ns [7,8,20]. The increased lifetime allows rephasing of the spins in P^F . At sufficiently low temperature ($T < 20$ K) [9], the charge separated state (P^+I^-) recombines exclusively into a triplet spin configuration, generating P^R in an $m_s = 0$ spin state. The corresponding ESP pattern as recognized in the $\Delta m = \pm 1$ triplet EPR spectrum [1-4], exhibits an AEEAAE (A=enhanced absorption, E=emission) pattern. This ESP pattern is a general phenomenon in photosynthesis [10-13], and demonstrates the photochemical activity at the donor side of the RC, since the AEEAAE pattern is characteristic for generation of P^R via the radical pair mechanism [1,2], which determines the spin dynamics in P^F at high magnetic field strengths.

Recently, we observed that this ESP pattern is reversibly converted into AEAEAE when the temperature is increased from $T < 20$ K to

T>20 K for RC's isolated from Rps. viridis [14,15]. A similar, albeit less pronounced temperature dependent change was found in the triplet lineshape in RC-containing preparations from C. vinosum [15] and Rb. sphaeroides R-26 [16]. The extent of the change depends strongly on the magnitude of the magnetic interaction between I^- and Q_A^- . Furthermore, it was observed that when Q_A is doubly reduced ($Q_A^=$) destroying the abovementioned magnetic interaction, the change in lineshape of the P^R EPR spectrum disappeared [17]. Finally, when the magnetic interaction between the paramagnetic ion $Fe^{2+}(S=2)$ and Q_A^- is destroyed (e.g. by adding SDS, or removing Fe^{2+} and/or Q_A) again no change in lineshape is observed [15,16].

From these results we concluded that the temperature dependence of the ESP in P^R , as monitored by EPR, is caused by rapid electron spin T_1 -processes of Fe^{2+} ; Q_A^- acts as a relaxation carrier between Fe^{2+} and I^- in the RP state P^F .

In order to investigate the effect of a third electronic spin on the spin dynamics in P^F , resulting in a temperature dependence of the recombination statistics, we studied the kinetic response of the $\Delta m=\pm 1$ triplet EPR transitions of P^R using pulsed optical excitation. The initial ESP pattern, observed immediately after generation of P^R reflects the relative populating rates from the -multi- spin state P^F , and thus yields more direct information about the temperature dependence of the spin processes in P^F than steady state measurements. (In the following P^F denotes the total (spin) state $P^+I^-Q_A^-Fe^{2+}(S=2)$ and includes all interactions within this state.)

Furthermore, since the observed decay constants of P^R are known to increase by spin-lattice relaxation [18,19], the time-resolved EPR results provide also information on the spin-lattice relaxation processes within P^R . Optical studies already revealed that the decay rate constants of P^R are independent of the temperature in the range 0-150 K [21]. At T>150 K the triplet decay becomes faster.

The rate of the back electron transfer reaction $P^+Q_A^-$ to P^*Q_A was studied by several groups in RC's from Rb. sphaeroides R-26 [22,23]. As a result it was concluded that, at least at higher temperatures, a back reaction from P^R into P^F (or a relaxed state of P^F) might be

involved, increasing the rate of the $P^+Q_A^-$ recombination process, and thus also the P^R decay rate constants. Studies on the effect of a magnetic field on the triplet state lifetime, led to the same conclusion [24].

These studies were carried out in Rb. sphaeroides. Whether thermal repopulation of the initial radical pair also occurs in RC's from Rps. viridis, may be concluded from the EPR transients at various temperatures. Our findings include:

1. the temperature dependence ($T < 125$ K) of the change in the relative populating rates of P^R from P^F for all three canonical orientations of the magnetic field;
2. the temperature dependence of the relaxation rate within P^F . The results are discussed using the framework of a kinetic model, yielding good quantitative comparison with experiment for $T < 40$ K. Spin relaxation seems to take place in another state (P^X), and not in P^R itself. P^X is probably identical to P^F (or a relaxed form).

The non-zero $P^R \leftrightarrow P^F$ transition probability is discussed in terms of the peculiar property of Rps. viridis that the energy of the S_1 state of the antenna is lower than that of P-960 [25].

The abovementioned model is consistent with the idea that in Rps. viridis cells or chromatophores T-T energy transfer might be the usual pathway for the light energy to enter the RC, from where the $P^R \rightarrow P^F$ process generates the stable charge separated state $P^+Q_A^-$ in an initial triplet radical pair spin configuration.

5.2 MATERIALS AND METHODS

Cells of Rps. viridis were grown anaerobically as described in [26,27], RC's were isolated as described in [28], with a slight modification as described in [29].

EPR samples were prepared as described in [15], using ascorbate to reduce the cytochromes and the primary donor, followed by rapid freezing in the dark. Photoreduction generated the PIQ_A^- state in the

RC's.

The time-resolved EPR measurements were carried out using a novel method as described in [30]. Briefly, the standard phase-sensitive detector of the EPR spectrometer (Varian E6), was bypassed, and replaced by a modified broad-band phase-sensitive detector (B-PSD) (Brookdeal), with sub-microsecond time-resolution. A high-pass filter at the input of the B-PSD was employed (-3dB point at 100 kHz), replacing the tuned amplifier, which is standard present in lock-in detectors. The low-pass filter at the output of the B-PSD was removed. The magnetic field modulation frequency was 200 kHz, which slightly improves the fidelity of the obtained transient as compared to the more usual 100 kHz modulation frequency. EPR signals were averaged randomly with respect to the modulation frequency, averaging out the rectified sine waves from the output of the B-PSD. A LeCroy 3500 signal analyzer was used to digitize and average the EPR transient signals, optically triggered by the exciting laser flash. The overall time-resolution of the time-resolved set-up, employing the 200 kHz B-PSD method was 750 ± 150 ns, with a frequency response from 0 to 1 MHz.

Typically 5000 transients were averaged per run to obtain a satisfactory S/N ratio.

Excitation was from a Q-switched Nd:YAG pulse laser (JK HY-200), frequency doubled (532 nm, 30 mJ/pulse) pumping a home built high-gain broadband tunable pulsed dye laser [31]. A mixture of Rhodamine 6G and Rhodamine 101 (1:1) in methanol was used to obtain laser flashes with $\lambda=612$ nm (3 nm FWHM), 1 - 2 mJ/pulse and a pulse duration of 10 ns. Excitation repetition rate was 21 Hz, running freely from the EPR magnetic field modulation frequency (200 kHz, see above). The laser beam entered the EPR cavity (Varian, rectangular E-231 operating in TE₁₀₁ mode) through a light tube in the front of the cavity, taken from an optical transmission cavity.

The intense laser flash generates a spurious transient in the EPR cavity, originating from heating of the side walls by scattered light. This artefact is partly subtracted by the magnetic field modu-

lation method, since its amplitude does not depend on the magnetic field position, as the true EPR signal from P^R . However, part of the signal remains, but can be further reduced by the averaging process. The phase of the artefact (present in the first few μs after the laser flash) is more or less random, whereas the phase of the EPR signal is always the same. Therefore, the laser flash artefact is substantially reduced with respect to the amplitude of the EPR signal. For those transients where the first few microseconds are less important (i.e. for transients with relatively long decay rates), the signal at the input of the B-PSD was blocked during the first 5 microseconds by a microswitch, driven by the laser excitation. In later experiments the interior of the cavity was covered by carbon paper (except the back and front side), reducing the light-induced spurious transient by a factor 5 - 10, but reducing the loaded Q-factor of the cavity. However, the net improvement of S/N ratio by this method was ca. a factor 2 - 5. Further details are given in [32].

Exponential functions were fitted using the method described by McLachlan [33], employing a Rainbow 100 microcomputer interfaced to the LeCroy 3500 signal analyzer. For transients consisting of two exponentials this method was extended by an iterative subtraction of the calculated exponential from the experimental transient to calculate the residual exponential.

5.3 RESULTS

Figure 1 shows the EPR transients at 100 K recorded in the peaks of the first derivative $\Delta m = \pm 1$ triplet spectrum as indicated by arrows in the inset. The spectra were recorded using the pretrigger facility of the signal analyzer. Therefore the laser flash arrives at 1/8th of the horizontal (time) axis. Note the entirely different signal amplitude at $t = 0 \mu s$ of the X, Y, and Z transients.

In order to investigate whether the observed changes in ESP pattern originate in P^E , the decay rates from the spin levels of P^E to

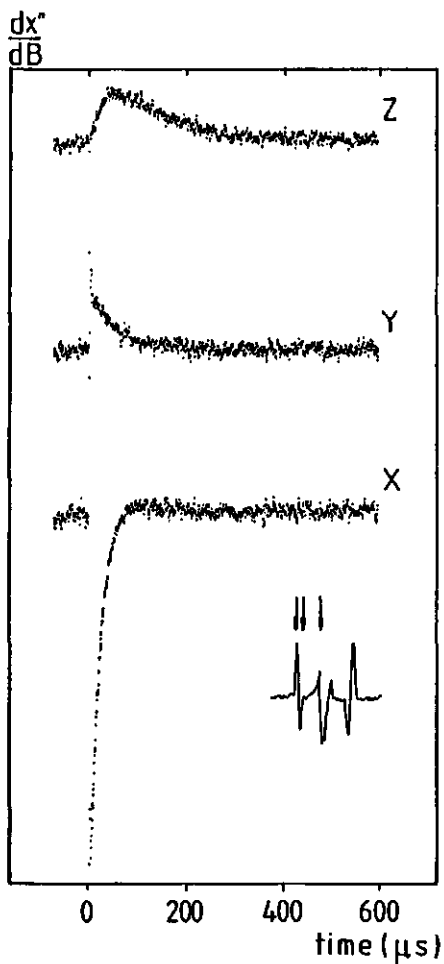


Figure 1

EPR transients from P^R in RC's from *Rps. viridis* detected at 100 K. The transients are recorded at the peak positions of the steady state $\Delta m = \pm 1$ triplet EPR spectrum as indicated by the arrows in the inset: from left to right: Z^+ , X^- , and Y^- . Experimental conditions: microwave power: 200 μW , magnetic field modulation frequency: 200 kHz., modulation amplitude: 2.5 mT, excitation: 21 Hz, 12 ns pulse duration, 2 mJ/pulse, excitation wavelength: 612 nm. Sample: $A_{830} = 40 \text{ cm}^{-1}$. 100 μl RC's in 200 μl ethyleneglycol. Photoreduction by 1 mM sodium ascorbate.

those of P^R should be determined. These are $\approx 10^8 \text{ s}^{-1}$ [7], and are too fast to be recorded by our spectrometer. However, the initial ESP pattern of P^R , corresponding to the ESP pattern as recognized in the first microsecond of the EPR transients in figure 1, contains the same information, since the spin-lattice relaxation of the P^R spin levels does not contribute at a μs timescale (see below). The initial spectrum exhibits an -EAEA- ESP pattern, where "-" denotes zero amplitude for the Z-transitions. The transients of the three corresponding high field transitions are not shown in figure 1, but these are identical to those shown. The time-integrated ESP pattern, corresponding to spectra as observed under continuous illumination is AEAEAE, in accordance with our previous results [14,15].

The transients at 100 K exhibit several differences with those in figure 1.

i) At 5 K the initial ESP pattern (transient amplitude for X, Y, and Z at $t < 1 \mu\text{s}$) is AEEAAE, whereas at 100 K -EAEA- is found;

ii) the observed decay rate constants obtained by a two-exponential fit of the EPR transients of the X- and Z peak have increased, but the observed decay rate constant of the Y-transition has decreased;

iii) at $T < 5 \text{ K}$ all transients show single exponential decay (not shown) at sufficiently low microwave power [19]. At 100 K, however, four out of six transients follow a two-exponential decay (Y^- , Y^+), even at very low microwave power, the ones which follow single exponential decay, represent decay from the T_{\pm} spin levels of P^R .

All these features can be explained by invoking a temperature dependent change in the populating channel, i.e. in the spin dynamics of the RP state P^+I^- .

Our temperature study of the steady state EPR spectra showed the disappearance of the Y peaks around $19 \pm 3 \text{ K}$ [15]. Figure 2 shows the transients detected at 17 and 40 K of the two EPR transitions, which change most strongly with temperature: Y, and Z (the relative X-peak amplitudes of the EPR transients hardly change with temperature). As is evident from this figure, the initial ESP pattern yields an AEEAAE pattern, however, time-integration of the Y transient yields about

Z

Y

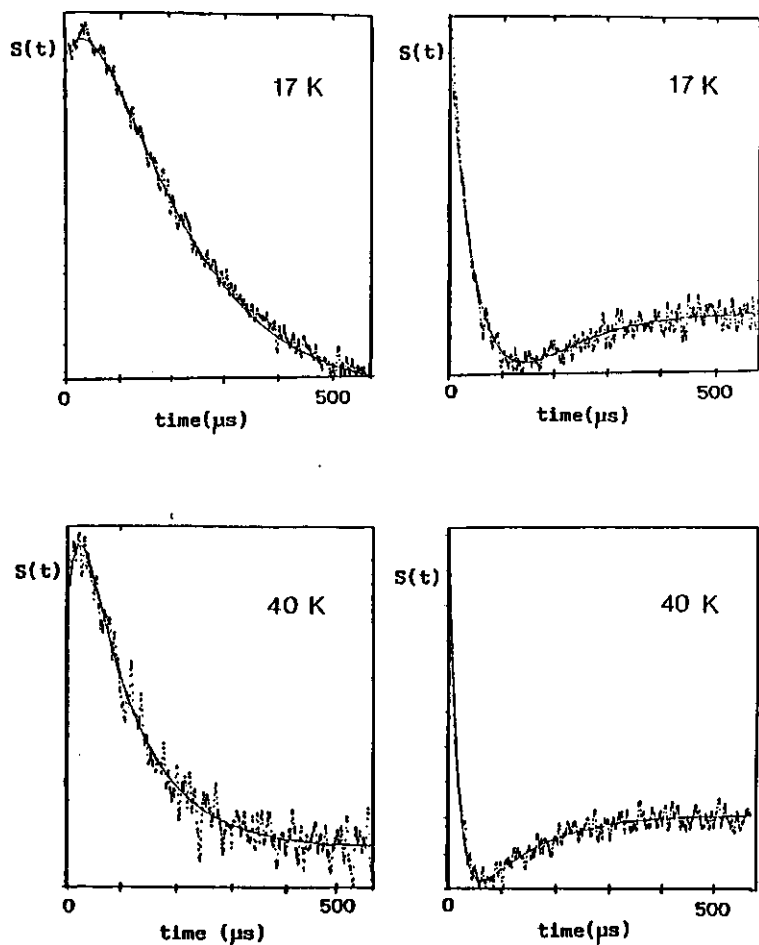


Figure 2

EPR transients from p^R in RC's from *Rps. viridis* detected at 17 K and 40 K. Conditions were identical to those given at fig. 1. Solid lines represent fitted curves.

zero amplitude at 17 K, and a net absorptive signal at 40 K. Time-integration of the Z-transient yields a net absorptive signal for both temperatures. These observations are in agreement with the steady state ESP pattern at the same temperatures.

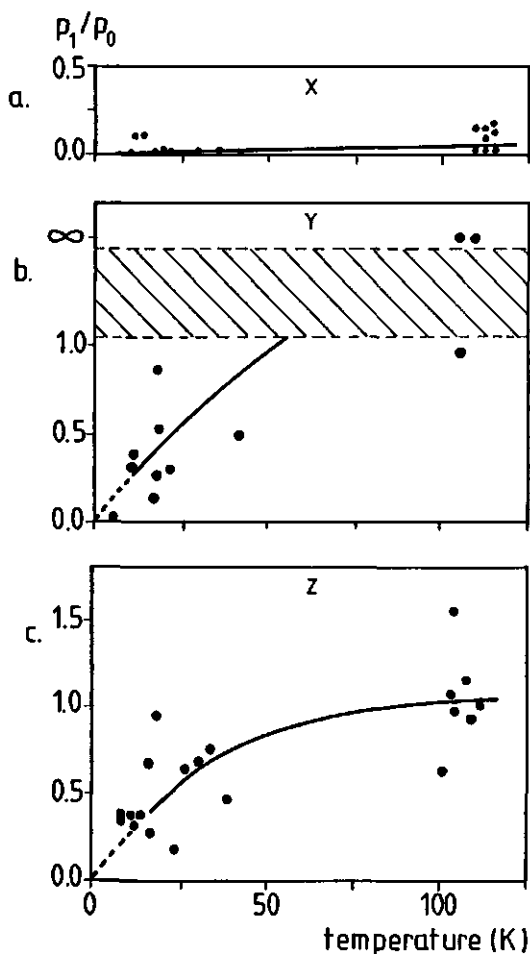


Figure 3

Ratio of amplitudes of the exponential decay constants making up the experimental transients. P_1 denotes the amplitude assigned to the populating channel of the T_{\pm} spin levels of p^R , P_0 denotes the populating channel assigned to the T_0 spin level of p^R .

a: transients detected in the X transitions of the $\Delta m = \pm 1$ triplet EPR spectrum; b: idem in the Y transitions, when the T_0 spin level is not populated (around 100 K), the P_1/P_0 ratio becomes infinity. Due to the limited accuracy of the experiments the region between 1 and ∞ has been hatched; c: transients detected in the Z transition of the steady state EPR spectrum.

From these correspondences we conclude that the transients, as we have measured them, represent the time-dependent equivalent of the previously observed steady state spectra, even though the excitation procedure is entirely different, and the intense laser flash induces a spurious transient signal (see the previous section).

Figure 3 shows the temperature dependence of the ratio of amplitudes in the first μs of the exponential components of the EPR transients. This ratio represents the relative populating rate from P^F to P^R . Ratios larger than unity represent preferential populating of the T_{\pm} sublevels of P^R . The spread in the measured p_1/p_0 ratio is rather large, since the flash artefact affects the initial amplitudes of the exponentials constituting the EPR transient.

Especially for small contributions of one of the exponential components, the fit becomes relatively less accurate with respect of the initial amplitude. For B/Y two of the three transients follow a single exponent, leading to $p_1/p_0 \rightarrow \infty$. Considering the S/N ratio, p_1/p_0 ratios of 3 - 6 are most likely. This ratio is supported by the observation that for $T < 40$ K, the experimental results compare rather well (within experimental error) to those for the Z-peak, although the difference of p_1/p_0 at 100 K is significant (see also fig. 1).

To investigate whether the change of the observed decay rate constant is due to an increase of the spin-lattice relaxation rate

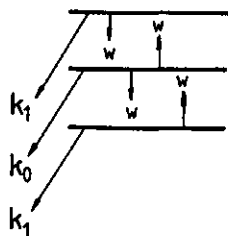


Figure 4

Kinetic scheme for P^R . k_1 and k_0 denote decay rate constants from P^R to the singlet ground state of P-960. w denotes the relaxation rate constant. More details are given in the text.

within P^R , the experimental data was used to fit various intramolecular relaxation models, of which only the model given in figure 4 yielded satisfactory results, shown in figure 5a-c. In the calculations to get this figure, the decay rate constant values at $T=4$ K were assumed not to change with temperature in the experimental range ($4 < T < 120$ K). Thus, the increase in observed decay rate must entirely be due to the spin-lattice relaxation process. A quadratic dependence of the relaxation rate (w in fig. 5) on the temperature in the first 40 degrees Kelvin was found. The drawn line in fig. 5a, 5b, and 5c represents the calculated relaxation rate. The dots represent measured relaxation rates.

Due to the fact that the decay rate constants from T_+ and T_- are identical for P^R , the transient EPR signal from this state is composed of a maximum of two exponential decay rates: one represents the decay from the T_{\pm} levels of P^R , the other from the T_0 level (k_1 and k_0 in figure 4). The mean decay rate constant $\langle k \rangle$ for a 1:1:1 spin distribution over $|T_+\rangle$, $|T_0\rangle$, and $|T_-\rangle$, given by: $\langle k \rangle = (k_0 + 2 k_1)/3$, would be observed in full thermal equilibrium, i.e. when the relaxation process is much faster than the decay rates. In the intermediate case, when the relaxation rate is of the order of the decay rate, both exponential decays are increased, due to the increased equalizing of the population difference between the two observed levels. The slowest observed decay rate increases until the mean decay rate constant $\langle k \rangle$ value is reached, whereas the faster observed decay rate constant continuously increases with temperature. This compares with what we experimentally found. The observed decay rate (k_0 for all transitions at $T \approx 5$ K, (i.e. without SLR) increases with temperature, and the transients start to follow a two-exponential decay.

In figure 5a, and 5b the faster observed decay rate was used to calculate the relaxation rate w , since at low temperature (when almost exclusive T_0 populating occurs) only k_0 is observed, which is larger than k_1 for the X and Y transitions. The theoretical relaxation rate (using the empirical relation: $w \sim T^2$), therefore is expected to increase 'forever' with temperature. However, the experimental results

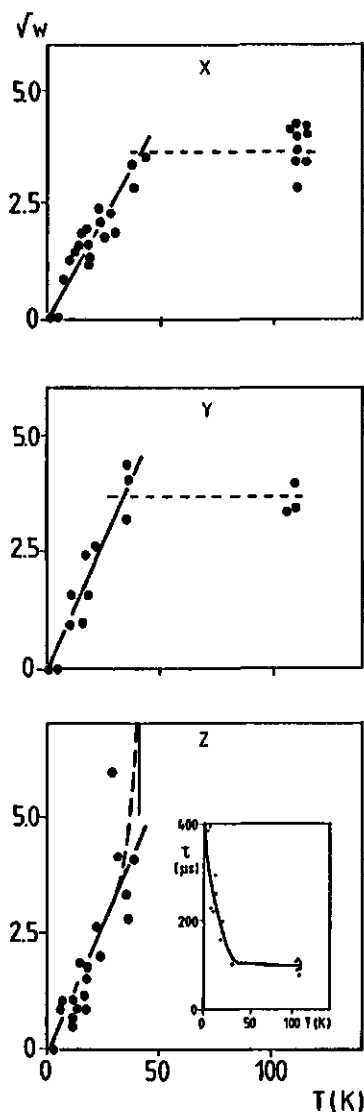


Figure 5

The relation rate $w^{\frac{1}{2}}$ (w denotes spin-lattice relaxation rate, expressed in ms^{-1}) and temperature as measured at the canonical magnetic field positions (B/X, Y, and Z). The dots represent experimental values for w , using the theory given in the Appendix. The solid line represents a fit, using the empirical relation: $w = aT^2$. For B/X $a = 0.010 \pm 0.001$, for B/Y, and B/Z $a = 0.012 \pm 0.001$ was used to fit the experimental data. The inset gives the temperature dependence of the decay time τ present in the transients. More details are given in the text.

show that above 35 - 40 K no further increase in observed decay rate occurs. For the Z transition the situation looks different: $k_0(Z)$ is smaller than $k_1(Z)$, thus the observed decay rate is expected to increase until the mean decay rate $\langle k \rangle$ is reached, becoming independent of the relaxation rate at higher temperatures. This happens at $T > 40$ K (see inset in figure 5c). The extraction of the experimentally observed relaxation rate from the observed decay rate (the dots in fig. 5c), yielded values close to infinity at temperatures above 40 K. (The method of extracting the relaxation rate w from the observed EPR decay rates is given in the Appendix).

The similarity between a, b and c in figure 5 is that at a temperature of about 35 K the decay kinetics of P^R shows that the relative population of the P^R sublevels becomes independent of temperature in a steady state, and thus independent of a further increase of the relaxation rate. Moreover, this high-temperature equilibrium distribution over the sublevels of P^R , is not a Boltzmann distribution, as the time-integrated and steady-state [15] ESP pattern demonstrate.

At 40 - 100 K the observed decay rates are given in Table I.

Table I.

transition	$k_1(\text{ms}^{-1})$	%	$k_2(\text{ms}^{-1})$	%
X	55 ± 5	95 ± 5	9 ± 2	5 ± 5
Y	60 ± 5	10 ± 20	14 ± 6	90 ± 20
Z	50 ± 10	50 ± 10	11 ± 2	50 ± 10

5.4 DISCUSSION

First we will discuss experimental results with respect to the fate of P^R in the first microsecond after generation of P^R . Since this period is short with respect to the lifetimes and spin-lattice

relaxation (SLR) times of P^R , as shown in this Chapter, we are observing the relative populating rates of the P^R spin levels. These are directly related to the spin dynamics of P^F , because any process affecting the probabilities to find a particular spin configuration within P^F , must also result in a change of populating rates of P^R , since $P^F \rightarrow P^R$ transitions are spin conserving. Transient EPR eliminates to a great extent unwanted effects due to processes within P^R .

In the second part of the discussion we will take a closer look at the time development of the EPR transients of P^R and their dependence on temperature.

Decay from P^F

As we are about to demonstrate, the transients in figure 1 provide evidence that the initial ESP of P^R results from the spin dynamics in the precursor state P^F . For Rps. viridis this is the multi-electron spin system composed by the electron spins on P^+ , I^- , and in the $Q_A^-Fe^{2+}$ complex. We suggested in previous papers [14-17], that the rapid SLR in the paramagnetic Fe^{2+} ion is the source of the temperature dependence of the ESP pattern of the $\Delta m = \pm 1$ triplet EPR spectra of P^R . This relaxation is transferred to the 'traditional' P^+I^- radical pair by the unpaired spin on the reduced primary acceptor (Q_A^-). It is noteworthy that this relaxation process does not impose a Boltzmann equilibrium population distribution on the substates of P^F , since such a distribution, at 100 K, would have been monitored as almost zero signal intensity at $t=0 \mu s$ (i.e. in the first microsecond after generation of P^R). The transient of the Y-transitions of P^R clearly shows an inverted population distribution with respect to the low temperature distribution (mainly T_0 populated). Therefore, it must be concluded that, in the temperature region of the experiments ($5 K < T < 120 K$), the spin dynamics at high magnetic field in the state P^F is affected by the relaxation processes of Fe^{2+} in such a way, that the correlation time of the Q_A^- electron spin in the quinone-iron complex never becomes much shorter than the lifetime of P^F , otherwise

a fully relaxed state would have been monitored by P^R , nor much longer than the lifetime of P^F , otherwise no temperature effect would have been observed.

Simple calculations, based on the model presented in Chapter II, involving the Zeeman-, and the spin exchange interaction between I^- and Q_A^- , neglecting all other, much smaller, interactions (see Chapter II), show that, upon entering P^F from the excited singlet state of P, the probability for recombination of P^+ and I^- in the T_+ or T_- spin state of P^R varies much faster with time than the probability for recombination in the T_0 state, although the net amplitude of the latter is much larger. This may provide a clue to understand the unexpected phenomenon of inversion in the recombination probabilities of the multi-electron spin state P^F in *Rps. viridis*, for this discriminates in time domain the T_{\pm} probabilities from the T_0 probability.

These calculations also show that, at low temperature, when the spin-lattice relaxation of the Fe^{2+} center can be neglected, some mixing of T_+ with T_0 , and the singlet state S occurs in P^F (in the presence of the spin on Q_A^-), due to the magnetic interaction between I^- and Q_A^- . The same holds for mixing of T_- with T_0 and S. Thus, even at low temperature, the T_+ and T_- substates of P^R are populated, albeit not enough to affect the ESP pattern of the $\Delta m=1$ EPR triplet spectrum from P^R , which is in accordance with the experimental observations [15].

The effect of temperature dependent electron-spin relaxation of Q_A^- , as a result of its strong magnetic coupling with the Fe^{2+} ion, can be qualitatively understood as follows.

We define an average correlation time τ_e , during which a Q_A^- spin state α or β persists. Then, evolution of any spin state of P^F can only take place during a period τ_e . On average, at $t=\tau_e$, the phases of all P^F spin states, mutually connected by non-zero matrix elements of the static Hamiltonian, are assumed to be reset. During the lifetime τ of P^F the probability P for a transition between a spin level of P^F and the corresponding level of P^R , taking into account spin

conservation for all three electron spins involved in this transition, is given by:

$$P \sim \int_{t=0}^{\tau_e} |c_i(t)|^2 \exp \left\{ -\frac{t}{\tau} \right\} dt \quad (1)$$

where i denotes any of the P^F spin states $|i\rangle$; $|c_i(t)|^2$ has the form $a_i + \sum b_{ij} \cos(\omega_{ij}t)$, with the constants a_i (>0), b_{ij} (<0), and the angular frequency ω_{ij} appropriate for spin state $|i\rangle$ (see Chapter II). From an analysis of eqn. (1) it follows that if $\tau_e < \tau < 1$ and $\omega\tau_e < 1$, the value of the integral in (1) increases with $\omega\tau_e < 1$, i.e. for a particular value of τ_e , the probability for a $P^F \rightarrow P^R$ transition is higher for a more rapidly varying spin state in P^F , than for a slower one.

Referring to figure 3 of Chapter II, it is easy to see that for sufficiently short values of τ_e , the rapidly oscillating probability $|c_i(t)|^2$ (where $|i\rangle = |T_+\rangle$ or $|T_-\rangle$), results in a higher populating rate for the $m_s = \pm 1$ spin levels of P^R , than for the $m_s = 0$ level. For the latter the probability $|c_i(t)|^2$ (where $|i\rangle = |T_0\rangle$) of the corresponding P^F level varies more slowly. This may provide a qualitative explanation for the relative increase of the ratios of the T_+/T_0 populating rates as a result of a reduction of τ_e at increasing temperature (fig. 3).

A large number of spin flips on Q_A^- , each 'resetting' a particular P^F spin configuration with another, results in a non-zero probability to go from a given spin configuration into any other spin configuration (see Chapter II). The spin flips of Q_A^- have two distinct effects (Abragam [46]): a flip of spin 3 alone induces an equal (i.e. Boltzmann) distribution over all 8 spin levels of P^F , increasing the relative probability to detect a T_+ spin configuration within P^F , and equalizing this probability with that for an S or T_0 spin configuration. Simultaneously, the coupled flip flop transitions of spins 2 and 3 induce the preferential probability to find T_+ and T_- in P^F , described above, since only the flip flop term in the relaxation process induces $S, T_0 \leftrightarrow T_+$ transitions.

It can be shown, that generation of P^F in a triplet P^+I^- radical pair spin configuration, creates much more favourable conditions for preferential populating into the T_{\pm} spin states. The effect of the foregoing is, that the T_{\pm} recombination probabilities are already affected by τ_e values which may be much larger than for singlet creation of P^F , (analogous to the case given above). Then, relaxation effects on the T_{\pm}/T_0 populating ratio are expected to show up at lower temperature (i.e. smaller τ_e) than for continued resetting of P^F in the singlet RP state. From the discussion given above, it is evident, that the distinction between the evolution of the initial creation of P^F in a singlet or triplet spin configuration is destroyed by the resetting process during the lifetime of P^F . Generally, this results in a relaxing of the restrictions imposed on τ_e , allowing values much longer than $\approx 10^{-10}$ s.

For the multi level P^F system the quantitative effects of relaxation can only be calculated numerically.

Such calculations are currently carried out by Hore and Hunter in Oxford, using the three-electron, one-proton Hamiltonian previously described [34].

Preliminary results, incorporating a stochastic third electron spin state into this Hamiltonian, and invoking both exchange and dipolar spin-spin interactions between I^- and Q_A^- , indeed show that the populating rate from P^F to P^R can be larger for the T_{+} and T_{-} sublevels, than for the T_0 sublevel of P^R [35], supporting our hypothesis concerning the role of spin flips in the quinone iron complex with respect to the observed triplet EPR ESP pattern. Also the anisotropy in the temperature dependent change of the ESP pattern could be reproduced in the calculated spectra, by employing a dipolar interaction between I^- and Q_A^- . At this moment we cannot exclude, however that anisotropic relaxation (see fig. 1) arises from the anisotropy in the $Fe^{2+} Q_A^-$ spin-spin coupling.

Decay from P^R

The kinetics of P^R show an unexpected temperature dependence:

- i) The SLR rate is found to be relatively slow in Rps. viridis as compared to e.g. Rb. sphaeroides [18,19]. In the latter $1/T_1$ is about 250 ms^{-1} at 100 K, whereas in Rps. viridis this rate is ca 10 ms^{-1} .
- ii) the temperature dependence of the relaxation rate reaches a plateau around 40 K.
- iii) the relaxation rate shows a quadratic dependence on temperature in the first 40 K.

The model we used to get rate equations to fit the experimental data is shown in figure 4. Note the absence of a relaxation channel between the T_+ and T_- substates of P^R . Furthermore, it is remarkable that both exponentials present in the transient yield a decay constant which does not vary in the temperature range 40 K - 100 K. One of these exponentials has a rate constant close to the mean triplet decay rate $\langle k \rangle$. This indicates that the population distribution over the P^R spin levels does not change anymore during the observation time, i.e. during the average decay time $\langle k \rangle^{-1}$ of P^R . However, at this temperature the ESP pattern is far from Boltzmann equilibrium. We therefore conclude that the relaxation does not take place within P^R , but in another state, connected to P^R . If the other state relaxes fully above 40 K, then no further effect is expected to be observable in P^R . However, the relaxation process within the other state must not impose a Boltzmann distribution on P^R .

If the projection of this other state, which we shall call P^X , on the P^R triplet axes does not yield the original spin state, e.g. because spin scrambling occurs in P^X , and hence the transition probabilities from P^X to the three substates of P^R are different, then relaxation in P^X would impose a non-Boltzmann equilibrium spin distribution on P^R , as will be shown below.

What is the nature of P^X ?

Recently, Woodbury et al. [22] proposed the existence of a second, more relaxed, RP state below the unrelaxed RP state, which we have so far

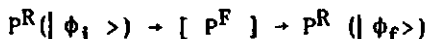
discussed. Chidsey et al. [24] invoked back transitions from P^R into P^F to explain their optical, temperature dependent magnetic field effects in RC's from Rb. sphaeroides. Our results also suggest the involvement of the charge separated state P^F (more relaxed or not) at higher temperature in the kinetic pathway of P^R : Since P^F does not consist of a pure triplet state, repopulating from P^R into a P^F triplet spin configuration (analogous to generation of P^F from P^* in the singlet spin configuration), is followed by spin scrambling within P^F . Spin-rephasing is fast, because the g-value differences between $g_{1,2}$ and g_3 are substantial, and quite different from the situation in the 'pure' radical pair. Once in P^F , the history of the spins may be lost due to the spin transitions caused by the Fe^{2+} . The recombination probabilities, (again) generating P^R , are only determined by the magnetic interactions within P^F , i.e. a replay of the processes leading to the first populating process of P^R , yet different, since P^F is now born from a T_0 or a T_+ state in P^R , instead of from the singlet state P^* (see Chapter II).

Using experimental values for the exchange interaction between the spins on I^- and Q_A^- , and g-value differences [36], we can calculate the approximate probabilities for recombination in any of the three spin states of P^R , upon recombination in P^F . Thus, we consider the process:

Table II

$\phi_i \backslash \phi_f$	T_+	T_0	T_-
T_+	0.95	0.05	0.00
T_0	0.12	0.76	0.12
T_-	0.00	0.05	0.95

Relative recombination probabilities for creation of $|\phi_f\rangle$ within P^F during its lifetime, taken to be 15 ns, upon entering P^F in the spin state $|\phi_i\rangle$; $J_{23}=20$ mT, $g_{1,2}-g_3=28$ mT. More details are given in the text.



$|\phi_i\rangle$ denotes the initial spin state, $|\phi_f\rangle$ denotes the final spin state. The results are given in Table II. These results were obtained using the static Hamiltonian, i.e. no relaxation of $Fe^{2+}Q_A^-$. Using this static Hamiltonian, only 2 - 3 % T_+ and T_- is obtained, entering p^F in the singlet spin configuration, also demonstrating that the spin flips in the iron-quinone complex are a prerequisite to explain the observed change in the initial ESP pattern of figure 1.

A kinetic scheme for the mechanism described above is given in figure 6, and leads to the relatively simple model given in figure 4. It is evident from the observed relaxation rates (see fig. 5), that the jump rate from p^R into p^F is much slower than the lifetime of p^F . Thus, the rate of transition between a p^R substate and p^F vice versa is entirely determined by the upward jump rate (w). It can be shown, using the qualitative model for the three-electron spin state p^F , outlined above, that only mixing between T_+ and T_0 , or T_- and T_0 occurs (the singlet state is also involved, but since at lower temperatures the probability of recombination into the singlet state is negligible, this process is not taken into account). Therefore, upon entering the state p^F in any of the three triplet spin configurations, no effective mixing of T_+ with T_- can occur (see also Table II). This explains the absence of the relaxation channel between these two states in figure 4, used to fit the experimental transients. In the kinetic model for the $p^R \leftrightarrow p^F$ interaction as given in figure 6, it is easily recognized that the model of figure 4 can be extracted from it, if $a - d \gg p$ (and thus $\gg w$).

The rate equations from the kinetic scheme in figure 6 can be solved using the approximation that the transitions between p^R and p^F are much faster than the decay rates from p^R to the singlet ground state. This is not exactly true, but for $T > 40$ K a reasonable approximation. Solving the rate equations, yields the result that the ratio of T_+/T_0 populations (equal to T_-/T_0) is independent of w , and thus of the temperature. Furthermore, this ratio is not unity. The EPR signal $S(t) = n(T_-) - n(T_0)$ is given by:

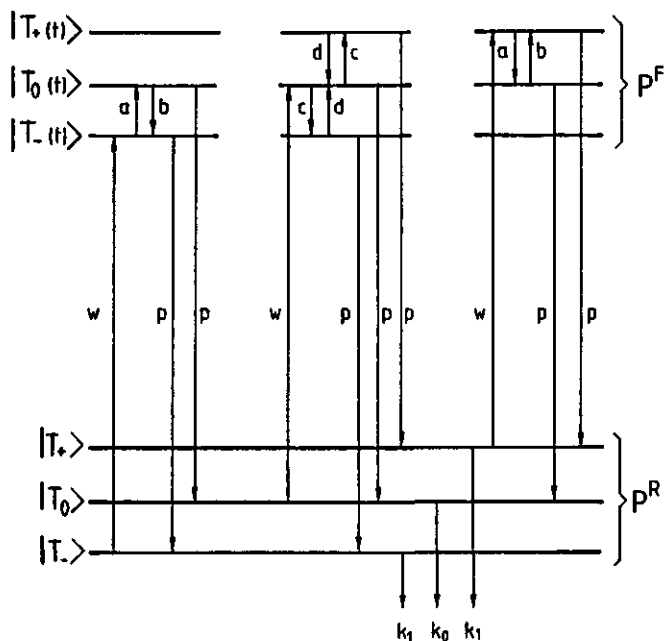


Figure 6

Kinetic scheme to model the coherent and stochastic processes within P^F (rate constants a - d), and the transitions between P^F and P^R (rate constants p and w); k_1 and k_0 represent the usual decay rate constants of P^R . The time dependent probabilities to find any spin configuration in P^F (T_+ , T_- , or T_0) depend on the spin configuration in which P^F is born. The three schemes of P^F represent the three different ways by which P^F can be generated from P^R . From left to right: generation in T_- , T_0 , and T_+ . More information is given in the text.

$$S(t) = N [c(b+p) - a(c+d+p)] \quad (2)$$

where N is a proportionality constant, and the rate constants a-d, p are referring to figure 6. From the experimental results, we know that the initial amplitude in the Y^- EPR transient is absorptive (emissive for $n(T_+) - n(T_0)$, i.e. Y^+).

The approximate values of the rate constants a - d in fig. 6, can be derived from the results in Chapter II. The g-value difference

between the spins on P^+ and I^- , with that of the spin on Q_A^- , induces rephasing of the spins in P^F , analogous to the RPM. This rephasing frequency is of the order $10^9-10^{10} \text{ s}^{-1}$, using experimental values for the g-value difference and the magnetic interaction between I^- and Q_A^- . Thus, the constants a-d in figure 6, are at least one order of magnitude larger than the lifetime of P^F (p in fig. 6). Furthermore, the numbers summarized in Table II can be used to estimate the relative magnitudes of a-d in the absence of spin relaxation within P^F . It is easily seen, using Table II, that then $b=20a$, and $d=6.3c$. By further taking $a=c \approx 10p$, an absorptive EPR signal is predicted using eq. 2. Furthermore, in steady-state, i.e. after many cycles of $P^R \leftrightarrow P^F$ during the P^R lifetime, the ratio of T_+ population over that of T_0 in P^R approaches approximately 3:1, i.e. a strong non-Boltzmann distribution.

When spin-relaxation within P^F is taken into account, the recombination kinetics change with temperature, just as described in the first part of this Discussion. Thus, the numbers in Table II will change, resulting in a different steady state ratio of T_+ population over that of T_0 .

The quadratic dependence on temperature of the observed relaxation rate within P^R (i.e. the jump rate from P^R to P^F in our model) is unusual. Neither Orbach, nor Raman processes show this kind of dependence on temperature [39]. Also the direct relaxation process, which is rare as the sole relaxation mechanism, has a different temperature dependence from what we observed.

De Groot et al. [40] reported a possible interaction between P^R and Q_A^- in RC's of Rb. sphaeroides. The existence of such an interaction was deduced from similar kinetical behaviour of the polarized Q_A^- EPR signal [41-43], and the decay time of P^R . In the RC's studied by De Groot et al., the magnetic coupling between Q_A^- and Fe^{2+} was destroyed. If the magnetic coupling is still intact, as in our experiments, the observation implies an indirect magnetic coupling between the paramagnetic Fe^{2+} and P^R . If this interaction is also present in Rps. viridis, the jump rate from P^R to P^F is also governed by T_1

processes on the Fe^{2+} . SLR of P^{R} may then reflect the Fe^{2+} relaxation, or part of it.

The $\text{P}^{\text{R}} \leftrightarrow \text{P}^{\text{F}}$ mechanism may also provide understanding of the fact that the photosynthetic system of Rps. viridis is able to function using an unusual energy scheme.

The lowest excited singlet state of the antenna system is higher in energy than the corresponding state of P-960. This can be understood, if we assume that P^{F} , necessary for light-driven photosynthesis, is generated from P^{R} and not, as is usual, from the excited singlet state P^* . The RC triplet is certainly lower than the antenna excited singlet state, and possibly lower than the lowest triplet state of the antenna chromophores.

In this respect the following intriguing observations may be relevant: The sign of transitions in the ODMR spectra of Rps. viridis chromatophores [37] is the same as that in ODMR spectra from RC's [38]. In all other studied photosynthetic species the sign of the ODMR transitions in spectra of chromatophores or cells, containing both antennas and RC's, is opposite to the sign of these transitions in ODMR spectra of preparations exclusively containing RC's. The sign inversion in chromatophores and cells is explained by singlet-singlet energy transfer between antenna and the primary donor in the RC [44,45]. In Rps. viridis however, the sign for both types of preparations is identical [38].

If it is assumed that the energy from the antenna system is transferred to the RC by a triplet-triplet energy-transfer mechanism, it is straightforward to show that the sign of the ODMR transitions will be the same for RC's with and without antennas. The charge separation, according to the model given above, would now have to occur via the $\text{P}^{\text{R}} \rightarrow \text{P}^{\text{F}}$ back reaction, also yielding the $\text{P}^+\text{Q}_\text{A}^-$ charge separated state. At low temperatures, under conditions where the ODMR experiments are performed, this back reaction is very slow (less than 1 ms^{-1}). It should thus be noticeable in time-resolved low temperature optical absorption measurements.

Also, the initial ESP pattern of P^{R} in antenna containing prepara-

tions, detected at low temperature, and exclusively generated via an antenna triplet state, would be different from the AEEAAE pattern. This would be a second independent check for this model.

Conclusions

We have measured the EPR transients in the three canonical transitions of the $\Delta m=1$ triplet spectrum of Rps. viridis RC's. We established with microsecond time-resolution, that the initial amplitude of these transitions at 100 K is inverted for the Y-peaks, zero for the Z-peaks, and not affected (thus firmly emissively polarized) for the X-peaks with respect to the low ($T < 10$ K) initial amplitudes. This demonstrates that the populating channel, i.e. the multi electron spin state P^F , is responsible for the temperature dependent changes.

The decay rate constants after correcting for SLR contributions from P^R for all three canonical axes do not change with temperature from 4 K to 100 K. The observed increase in decay rate constants is explained invoking a relaxation mechanism via a state in which spin-scrambling occurs, probably P^F , or a relaxed form of it, between which we cannot discriminate. At a temperature of 40 K and higher the relaxation rate does not affect the observed decay rates anymore, although its magnitude is of the same order as that of the decay rate constants of P^R . We speculate that above 40 K the initial ESP and the steady-state ESP approach each other, reducing the effect of the relaxing process.

The proposed reversible jump mechanism between P^F and P^R in Rps. viridis is consistent with a lower energetic S_1 state in the antenna, than the corresponding state of P-960. Creation of P^F from P^R is in line with P^R being populated by T-T energy transfer from the antenna. The latter mechanism also explains the absence of the sign reversal in ODMR spectra of cells, and chromatophores as compared with purified RC's.

5.5 APPENDIX

Calculation of the P^R spin-lattice relaxation rate

From the rate equations of the model schematically given in figure 4, it is easy to extract the secular equation in w :

$$(3\lambda - 2k_1 - k_0)w^2 + (-4\lambda^2 + 2\lambda(3k_1 + k_0) - 2(k_1^2 + k_0k_1))w + \lambda^3 - \lambda^2(2k_1 + k_0) + \lambda(k_1^2 + 2k_0k_1) - k_0k_1^2 = 0 \quad (A1)$$

where λ is the experimentally measured decay rate constant.

Substituting one λ in (A1), using the values for k_0 and k_1 values at 4 K, two possible values for w are found (for the Z-EPR transients a single w is found using A1).

The solutions of λ are of the form:

$$\lambda_1 = k_0 + f_1(w, k_0, k_1)$$

$$\lambda_2 = k_1 + f_2(w, k_0, k_1)$$

For $T \rightarrow 0$ K, $f_i \rightarrow 0$ ($i=1,2$). Thus, by extrapolating the observed λ 's to $T \rightarrow 0$ K, one can decide which w to take, since only one of the two possible w -values has the correct limiting value (k_0) for $T \rightarrow 0$ K.

From A(1) and the abovementioned limiting condition, we can derive a unique, analytical relation between w and λ ; since the dependence of λ on T is experimentally obtained, the temperature dependence of w is found (see fig. 5).

5.6 REFERENCES

- [1] T.J. Schaafsma, J.F. Kleibeuker, R.J. Platenkamp, and P. Geerse (1976) in: *Molecular Spectroscopy of Dense Phases*, Proc. 12th Congr. Mol. Spectrosc, Strasbourg, France, 1975, pp. 491-494.
- [2] J.R. Norris, and J.J. Katz (1978) in: *The Photosynthetic Bacteria* (R.K. Clayton, and W.R. Sistrom, eds.) pp. 397-418, Plenum, New York.

- [3] M.C. Thurnauer, J.J. Katz, and J.R. Norris (1975) Proc. Natl. Acad. Sci. USA 72, 3270-3274.
- [4] R.E. Blankenship, T.J. Schaafsma, and W.W. Parson (1977) Biochim. Biophys. Acta 461, 297-305.
- [5] M.G. Rockley, M.W. Windsor, R.J. Cogdell, and W.W. Parson (1975) Proc. Natl. Acad. Sci. USA, 2251-2255.
- [6] C.C. Schenck, W.W. Parson, D. Holten, and M.W. Windsor (1981) Biochim. Biophys. Acta 635, 383-392.
- [7] D. Holten, M.W. Windsor, W.W. Parson, and J.P. Thornber (1978) Biochim. Biophys. Acta 501, 112-127.
- [8] A.J. Hoff (1982) in: Triplet State ODMR Spectroscopy (R.H. Clarke, ed.) pp. 367-425.
- [9] W.W. Parson, and T.G. Monger (1976) Brookhaven Symp. Biol. 28, 195-212.
- [10] P.L. Dutton, J.S. Leigh, and M. Seibert (1971) Biochem. Biophys. Res. Comm. 46, 406-413.
- [11] A.W. Rutherford, D.R. Paterson, and J.E. Mullet (1981) Biochim. Biophys. Acta 635, 205-214.
- [12] H.A. Frank, M.B. McLean, and K. Sauer (1978) Proc. Natl. Acad. Sci. USA 76, 5124-5128.
- [13] T. Swarthoff, P. Gast, and A.J. Hoff (1981) FEBS Lett. 127, 83-86.
- [14] F.G.H. Van Wijk, P. Gast, and T.J. Schaafsma (1985) in: Antennas and Reaction Centers of Photosynthetic Bacteria (M.E. Michel-Beyerle, ed.), p. 146, Springer, Berlin.
- [15] F.G.H. Van Wijk, P. Gast, and T.J. Schaafsma (1986) Photobiochem. Photobiophys. 11, 95-100.
- [16] F.G.H. Van Wijk, C.B. Beijer, P. Gast, and T.J. Schaafsma, submitted to Photochem. Photobiol.
- [17] F.G.H. Van Wijk, P. Gast, and T.J. Schaafsma (1986) FEBS Lett. 206, 238-242.
- [18] A.J. Hoff, and I.I. Proskuryakov (1985) Chem. Phys. Lett. 115, 303-310.
- [19] P. Gast, and A.J. Hoff (1978) FEBS Lett 85, 183-188.

- [20] M.W. Windsor, and D. Holten (1980) *Phil. Trans. R. Soc. Lond.* A298, 335-349.
- [21] V.A. Shuvalov, and W.W. Parson (1981) *Biochim. Biophys. Acta* 638, 50-59.
- [22] N.W. Woodbury, W.W. Parson, M.R. Gunner, R.C. Prince, and P.L. Dutton (1986) *Biochim. Biophys. Acta* 851, 6-22.
- [23] M.R. Gunner, D.E. Robertson, and P.L. Dutton (1986) *J. Phys. Chem.* 90, 3783-3795.
- [24] C.E.D. Chidsey, L. Takiff, R.A. Goldstein, and S.G. Boxer (1985) *Proc. Natl. Acad. Sci. USA* 82, 6850-6854.
- [25] A.S. Holt, and R.K. Clayton (1965) *Photochem. Photobiol.* 4, 829-831.
- [26] C.A. Wraight (1977) *Biochim. Biophys. Acta* 548, 309-327.
- [27] D. Budil, Argonne Natl. Lab. USA, personal communication.
- [28] H.J. Den Blanken, and A.J. Hoff (1982) *Biochim. Biophys. Acta* 681, 365-374.
- [29] F.G.H. Van Wijk, R.M.D. Verhaert, C. Laane, P. Gast, and T.J. Schaafsma, submitted.
- [30] P.A. De Jager, and F.G.H. Van Wijk (1987) *Rev. Sci. Instrum.*, in press.
- [31] A. Van Hoek, and F.G.H. Van Wijk (1987) *Applied Optics*, in press.
- [32] F.G.H. Van Wijk (1987) Thesis, Wageningen agricultural Univ., The Netherlands.
- [33] L.A. McLachlan (1977) *J. Magnet. Reson.* 26, 223-228.
- [34] A.J. Hoff, and P.J. Hore (1984) *Chem. Phys. Lett.* 108, 104-110.
- [35] P.J. Hore, pers. comm.
- [36] R.C. Prince, D.M. Tiede, J.P. Thornber, and P.L. Dutton (1977) *Biochim. Biophys. Acta* 462, 467-490.
- [37] F.G.H. Van Wijk, T.J. Schaafsma, and H. Michel (1983) *Adv. Photosynth. Res., Proc. Int. Congr. Photosynth.* 6th 2, 173-176.
- [38] H.J. Den Blanken, A.P.J.M. Jongenelis, and A.J. Hoff (1983) *Biochim. Biophys. Acta* 725, 472-482.
- [39] A. Abragam, and B. Bleaney (1970) in *Electron Paramagnetic Resonance of Transition Ions*.

- [40] A. De Groot, E.J. Lous, and A.J. Hoff (1985) *Biochim. Biophys. Acta* 808, 13-20.
- [41] P. Gast (1982) Thesis, Univ. Leiden, The Netherlands.
- [42] A.J. Hoff, P. Gast, and J.C. Romijn, *FEBS Lett.* 73, 185-190.
- [43] P. Gast, and A.J. Hoff (1979) *Biochim. Biophys. Acta* 548, 520-535.
- [44] A.J. Hoff, and H.G. De Vries (1978) *Biochim. Biophys. Acta* 681, 32-40.
- [45] J. Hala, G.F.W. Searle, T.J. Schaafsma, A. Van Hoek, P. Pancoska, K. Blaha, and K. Vacek (1986) *Photochem. Photobiol.* 44, 527-534.
- [46] A. Abragam (1961) in *The Principles of Nuclear Magnetism*, pp. 305-313, Oxford Univ. Press, London.

CHAPTER VI

PHOTO-ACTIVITY AND STABILITY OF THE REACTION CENTER PROTEIN FROM THE PHOTOSYNTHETIC BACTERIUM RHODOPSEUDOMONAS VIRIDIS IN REVERSED MICELLES

6.1 ABSTRACT

The membrane bound reaction center protein complex (RC) of the photosynthetic bacterium Rhodopseudomonas viridis has been incorporated into a reversed micellar solution containing 1.0 M AOT (sodium bis (2-ethyl-hexyl) sulfosuccinate) in 3-methylpentane. The stability of the RC was investigated by optical absorption spectroscopy and the electron spin polarization pattern of the EPR spectrum of the primary electron donor (P-960). No changes in the absorption spectrum were observed over a period of 30 days when the RC's were kept in the dark at 4°C. Photochemical activity was demonstrated by light-induced cytochrome oxidation and donor-triplet formation at various temperatures. It was found that the spin polarization pattern of the donor triplet EPR spectrum depends on the [H₂O]/[AOT] ratio. Increasing this ratio from 0.2 to 2 results in a change in the photoactivity of the acceptor side. This irreversible change blocks forward electron transport. Full activity of the RC's is obtained at [H₂O]/[AOT] ratios lower than 0.4. The incorporated protein is highly sensitive to pH variations. Based on these results a model of the incorporated protein complex in the reversed micelles is presented.

6.2 INTRODUCTION

Membrane-bound proteins such as the reaction center protein complex (RC) from photosynthetic bacteria are solubilized by dispersion in a buffered aqueous solution containing a small amount ($\leq .1\%$) of detergent [1].

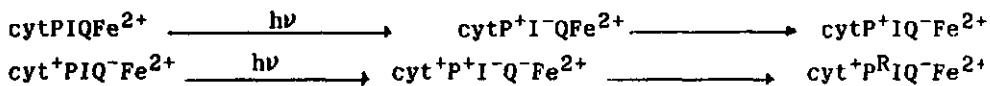
The stability and activity of the proteins depend on the detergent but is in general excellent. In this respect detergents provide suitable membrane-mimetic systems. Furthermore, the ability of detergents in apolar media to form microemulsion droplets in the presence of water [2] has been employed to incorporate isolated proteins [3-6], protecting them from the bulk organic solvent. The encapsulated proteins can thus be used to compose artificial biocatalytic systems [7,8], or to study the physical properties of the entrapped water, which has some properties of water at biological interfaces [9]. Recently, also hydrophobic proteins have been successfully incorporated into microemulsion droplets [10], including the photosynthetic RC [11]. In this experiment soybean phospholipids were used instead of the commonly used synthetic detergents, and hexane as the organic bulk phase. This resulted in good stability of the protein, in spite of some irreversible changes at the quinone acceptor side of the protein; however, photochemistry was demonstrated when excess quinone was added. We report here on the photochemical properties of the RC from the purple bacterium Rhodospseudomonas viridis incorporated into a reverse microemulsion containing the synthetic detergent Aerosol-OT (AOT) and 3-methylpentane (3-MP) as the organic bulk phase, because this solution forms a clear glass at low temperatures.

The photosynthetic RC from Rps. viridis is a useful probe to study the protein-reversed micellar system, since its architecture is known from X-ray crystallography [12,13]. Furthermore, the RC is intensively studied [14], and its spectroscopic properties are sufficiently known and suitable to monitor the structural stability and photochemical activity [15-17].

The RC protein complex with a molecular weight of 37 kD [35] consists

of a hydrophilic cytochrome complex, tightly bound to the hydrophobic LM complex in which the photochemical chromophores are embedded. A third subunit (also hydrophilic) is linked to the LM complex opposite to the cytochrome complex [13].

Upon illumination at low temperature and under moderate redox conditions, the following reactions take place in the RC:



cyt denotes a c-type cytochrome, P denotes the primary electron donor P-960 (BChl-b dimer), I the intermediary electron acceptor (BPheo-b), and QFe²⁺ denotes the menaquinone high spin iron complex. P^R denotes the triplet state of P-960, and is generated by recombination of P⁺ and I⁻, if forward electron transfer is blocked. It has been shown [18,19], that the recombination of this radical pair results in an anomalous electron spin polarization (ESP) of P^R, inconsistent with inter system crossing [20]. The EPR spectrum of this anomalously polarized state of P^R exhibits the characteristic AEEAAE polarization pattern (A denotes enhanced absorption, E denotes emission).

In *Rps. viridis*, however the state P⁺I⁻Q⁻Fe²⁺ must be considered as a multi spin system, in which the magnetic coupling between I⁻ and Q⁻ causes a temperature dependent change in the ESP pattern of P^R. At T < 20 K the AEEAAE pattern is observed whereas at T > 20 K an AEAEAE ESP pattern is monitored, when the Q⁻Fe²⁺ complex is intact [21]. If this complex is inactivated the AEEAAE ESP pattern is also observed. Thus, the ESP pattern of P^R provides a sensitive tool to check the acceptor side of the RC [17]. We have used this tool together with optical measurements to probe the RC properties in RM's.

In spite of the very high detergent concentration of 70 % (w/v), which is equivalent to a concentration of 1.0 M after solvation of the detergent in the organic solvent, it was found that the protein complex is stable at very low water to detergent ratio (w₀).

Since the RC is an efficient pump of electrons, and the reverse microemulsion system bears potent biotechnological application [8,9], the interactions between the protein complex and the detergent/organic solvent system are considered in some detail, resulting in a model that explains most of our results.

Note that throughout this paper both the expressions "reversed micelles" and "(reverse) microemulsions" are used without discrimination.

6.3 MATERIALS AND METHODS

Isolation

RC's from *Rps. viridis* were isolated using a simplified method from ref [22] in which the sucrose gradient centrifugation was omitted. Instead, the LDAO-treated chromatophores were, after a short spin, directly loaded onto a DEAE-sephasel column, followed by extensive washing with buffer (10 mM Tris/HCl, pH 8.0, 0.1 % LDAO, 1 mM EDTA). The RC's were removed from the column with 0.05 M NaCl in buffer and concentrated to $A_{830} = 60 \text{ cm}^{-1}$ or in a second batch to 30 cm^{-1} .

Incorporation

As reversed micellar solution AOT (Aldrich) with 3-MP [2] was chosen for its ability to form a very clear glass at low temperatures (110 K) [24] for $w_0 < 4$. The final concentration in the organic phase of AOT was 1 M (70% w/v). The water content of the vacuum dried AOT, as well as the 1.0 M stock solution were measured by the Karl Fischer method [23] conducted on a Metrohm Herisau Automat E 547. The residual water content was 0.21 [H₂O]/[AOT]. w_0 values given in this paper refer to moles water added to the system.

To obtain a high degree of reproducibility, it is essential to

pay special attention to the method of incorporation of the RC's. The best method turned out to be to inject the RC's slowly under the reversed micelle solution contained in a 1 ml Eppendorff microtube. This ensured that the contact between RC's and organic phase was kept to a minimum. After this the biphasic solution was sonicated vigorously for several hundreds of milliseconds (typically 0.7 s) at maximum power (150 W Branson sonifier, equipped with microtip), resulting in a clear solution. Before each sonication the solutions and the microtip of the sonifier were cooled to 0-5°C. The whole procedure was carried out in dim green light. For the EPR experiments, the reversed micelle/RC solution was immediately transferred into a standard quartz EPR tube, and rapidly frozen in the dark to 77 K.

Redox potential and pH

The redox potential in the samples was determined by mixing the RC's with a buffer solution containing the redox chemicals. For most of the experiments stock solutions of 1M Tris/HCl, 0.5 M ascorbate pH 8.0 were used. For the redox potential of 440 mV a 4:1 mixture of potassium Fe^{3+}/Fe^{2+} cyanide was used. The final concentration of the buffer in the waterpool of the reversed micelles was 80 mM. In all cases the redox chemicals were in thousand fold excess compared to the RC's.

The pH in the system is determined by the same buffer solution that contains the redox chemicals. For pH 7, 8, and 9 Tris/HCl was used, for pH 6.5 sodium phosphate buffer was taken. No effect of the kind of buffer was observed.

Ionic strength.

The ionic strength in the RM solution was varied using an appropriate stock solution of NaCl in water. First a low w_0 microemulsion was prepared, without salt, but including the protein. Then high salinity water, or pure water was added, and by a second sonication mixed with the RC-microemulsion. Microemulsions with $w_0 = 5$ were not comple-

tely clear and did not form glasses upon rapid freezing.

EPR experiments were performed as in ref [21]. Light-absorption spectra were recorded with a Uvikon 810 for $\lambda < 700$ nm, or with a Beckman DU G2400 for $\lambda > 700$ nm. Optical absorption-difference spectroscopy was performed at the Department of Biophysics at Leiden University, with a home-built spectrophotometer [25]. The viscosity of the microemulsion was measured with an Ubbelohde type viscometer at 20°C in a thermostatted waterbath. Optical birefringence measurements were conducted on a Zeiss research microscope (6.3x planachromate).

6.4 RESULTS

To test the stability of the RC's from Rps. viridis in AOT and in 3-MP separately, the RC's (25 μ l) were first incubated in a 2 ml aqueous AOT solution (2% AOT in 10 mM Tris/HCl pH 8.0) at room temperature in the dark. Already after one hour, a strong increase in the absorption at 680 nm was observed, indicating degradation of the BChl-b of the protein. When the RC's were injected into a solution of 3-MP (25 μ l RC-solution in 2.5 ml 3-MP), most of the BChl-b was extracted from the protein after two minutes of incubation. However, when the RC-solution was injected into a reversed micellar solution of 1.0 M AOT (70% w/v in 3-MP), no damage to the RC's was observed, based on the absorption spectrum (Fig. 1a). Many methods of incorporating the RC's into the micellar solution were tried, before good reproducibility of the spectroscopic results were obtained, including negligible increase of absorption at 680 nm. The best method is the one described in the previous section. Although also good results were obtained when the RC's are injected into the reversed micelles during sonication, the latter method was found less reproducible. No effect of the period of sonication on the activity of the RC's was observed (0.1 - 1.0 s), when the total energy (period x power) was kept constant.

As figure 1a shows, the absorption peaks around 960, 830, 790,

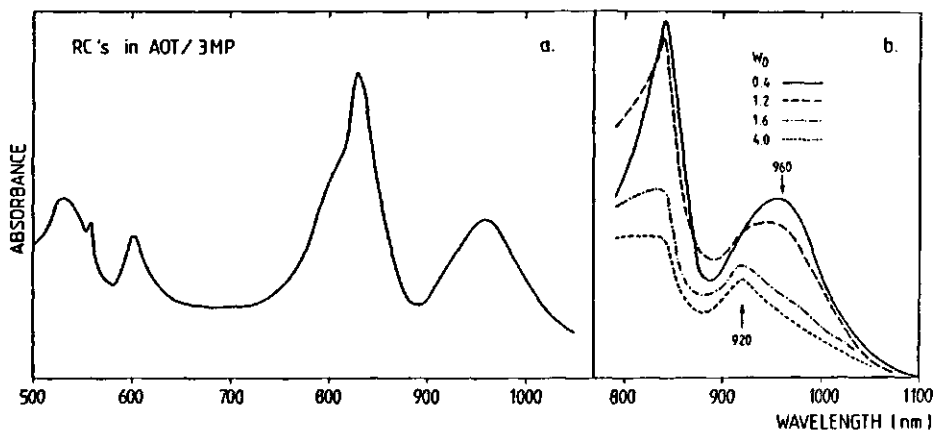


Figure 1.

a. Absorption spectrum of RC's from *Rps. viridis* incorporated in a reversed micellar solution, consisting of 1.0 M AOT in 3-methylpentane.

b. Effect of increasing w_0 $[H_2O]/[AOT]$ on the absorption spectrum of RC's in the AOT/3-MP reversed micellar solution.

600, 550, and 530 nm are identical to the normal spectrum of this type of RC's [15]. No change in the absorption spectrum was found over a period of 30 days when the RC's were kept in the dark at 4°C; when kept at room temperature in the dark, the ratio A_{600}/A_{680} increased to 2.5 after 7 days, whereas no absorption increase at 680 nm was found for RC's in Tris/LDAO.

The stability under illumination was slightly less for the RC's in the microemulsion than for RC's in Tris/LDAO. After one hour of strong illumination with a 150 W Xenon lamp (about 0.5 W/cm²) at room temperature, the ratio A_{680}/A_{600} was ≈ 1 in the microemulsion, whereas no 680 nm absorption band was observed in the RC absorption spectrum in Tris/LDAO solution.

These results are only valid for solutions with $w_0 < 0.4$. Figure 1b shows the effect of increasing w_0 values on the RC absorption spectrum. For $w_0 > 0.4$, the absorption band of P-960 shifts to 920 nm, and the 830 nm absorption diminishes, whereas the 790 nm absorption proportionally increases. The shift of the 960 nm band to 920 nm could be

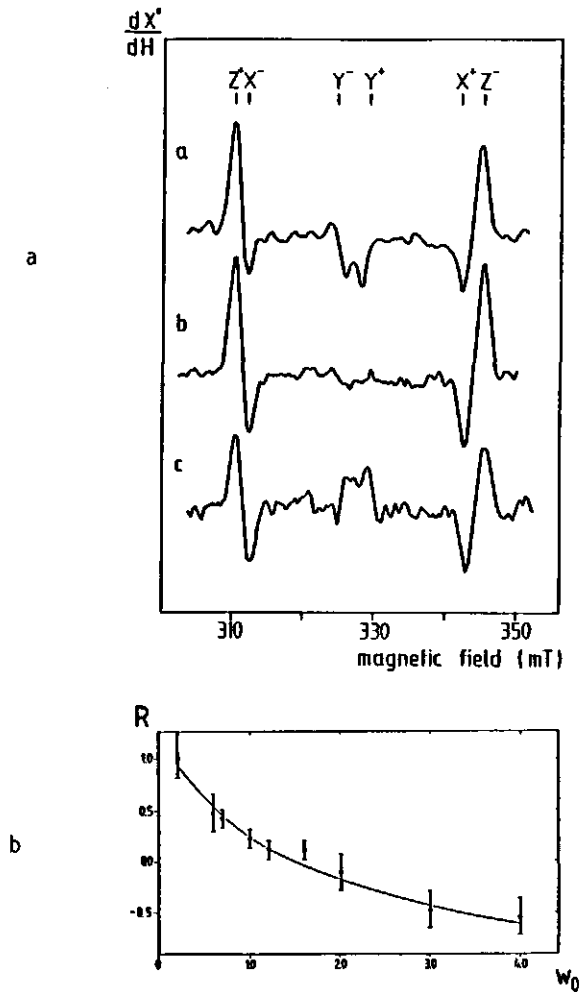


Figure 2.

2a. Effect of w_0 ($[H_2O]/[AOT]$) on the EPR electron spin polarization pattern of the donor triplet state (P^R) at 110 K. a. $w_0 = 0.7$; b. $w_0 = 1.6$; c. $w_0 = 3.0$. Experimental conditions: microwave power: 3.5 mW, magnetic field modulation amplitude: 2 mT_{pp}, central magnetic field: 327.5 mT, illumination: 150 W Xenon lamp filtered through 5 cm water and glass, light modulation frequency: 500 Hz.

2b. Ratio (R) of the Y^- peak over the amplitude of the Z^+ peak relative to this ratio in ethyleneglycol/Tris/LDAO versus w_0 . Error bars represent 90% confidence and increases at relatively low w_0 (due to low protein concentration), and at high w_0 (due to low triplet yield). Positive values of R represent absorptive Y^- signals.

the analogue of the shift of the 865 nm band to 855 nm in Rps. sphaeroides, when the quinone acceptors are extracted [26].

The photoactivity of the RC's in the microemulsion was examined with low temperature EPR spectroscopy and room temperature optical absorption difference spectroscopy. The primary photo-induced charge separation activity upon illumination was demonstrated by the observation of the anomalous electron spin polarization (ESP) pattern (AEEAAE [18,20]) of the $\Delta m = \pm 1$ EPR triplet spectrum of $^3P-960$ (P^R) at 10 K (not shown). Even at 0°C P^R could still be observed with EPR under continuous illumination in the liquid micellar solution of low w_o , due to the low dielectric losses in the EPR cavity. As described in the Introduction the ESP pattern of P^R at 110 K is a sensitive probe to monitor structural changes at the acceptor side of the RC [17]. The relation between ESP pattern of P^R and w_o is shown in figures 2a and 2b. In figure 2a the P^R triplet spectra from RC's in the AOT/3-MP solution are given for various w_o values. For $w_o = 1.6$ the triplet yield (amplitude of the Z peaks) is equal to that of RC's in a $w_o = 0.7$ reversed micellar medium, whereas the triplet yield

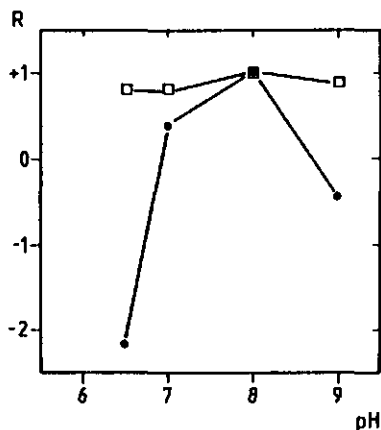


Figure 3.

pH dependence of the ratio (R) of the amplitude of the Y^- peak over the amplitude of the Z^+ peak from the triplet EPR spectra, scaled to unity at pH 8.0 in ethyleneglycol/Tris/LDAO in reversed micelles with $w_o = 1.0$. Positive values denote absorptive Y^- peaks.

Table 1

w_0	Salinity	Relative triplet yield a)	ESP pattern b)
< 0.4	low	+	+
0.4 - 2	low	+	+/-
0.4 - 2	high	++	-
~ 5	low	+/-	-
~ 5	high	++	-

a): + denotes triplet yield of the order at $w_0 < 0.4$

b): + denotes AEAEAE ESP pattern

+/- decreased y-amplitudes

- AEEAAE ESP pattern

Relation between activity of the RC and the ionic strength of the waterpool of the microemulsion.

Low salinity implies that no NaCl was added. High salinity refers to 0.5 M to 3.5 M NaCl in the waterpool of the RC/microemulsion. Activities of donor and acceptor side are related to the amplitude of the triplet peaks (donor side), and ESP pattern of the EPR triplet spectrum from P^R (acceptor side).

drops at higher w_0 values. Clearly the central Y-peaks of the spectrum change sign at increasing w_0 , this sign reversal is irreversible. Figure 2b shows the w_0 dependence of the fraction (R) of the ratio of Y^-/Y^+ amplitudes divided by this ratio of amplitudes from RC's in an ethyleneglycol glass. R is strongly pH dependent in the microemulsion, whereas only small variations in R are observed for RC's in ethyleneglycol (fig.3).

The ESP pattern of P^R is also affected by changes in the ionic

strength (Table 1). In this Table the triplet yield at high ionic strength is compared to that at low ionic strength at the same w_0 value. The ESP pattern provides the information about the activity of the donor and acceptor.

To test whether electron transfer between the intermediary acceptor I and the first quinone acceptor still occurs, in spite of the change in magnetic interaction between these two species [15,17,21], the effect of different redox potentials of the RC-solution was monitored. A redox potential of +440 mV was chosen, just between the $E^{0'}$ values of the primary donor P-960 ($E^{0'} = +500$ mV [27]) and the high potential cytochrome that donates an electron to the (light-induced) oxidized primary donor P^+ ($E^{0'} = +340$ mV [28,29]).

Since the RC's are frozen in the dark, the first absorbed photon produces the state P^+I^- , or $P^+Q_A^-$. Because the electron donating cytochrome is already oxidized, no subsequent rereduction of P^+ takes place. Then either P^+I^- recombines to generate exclusively P^R (at low temperature), due to the malfunction of the Q_A acceptor, or P^+Q^- recombines (much slower) without P^R formation. The results for both RC's in the ethyleneglycol glass and in the frozen microemulsion are shown in figure 4. The triplet yield of RC's in ethyleneglycol decreases with a factor 6 when exposed to the high redox potential. However, the AEAEAE ESP pattern is not affected. A large EPR signal is detected around $g=2$, due to the generation of light-induced P^+ radicals. When the RC's are incorporated into the reversed micelles with relatively high w_0 ($w_0 = 3$) the triplet yield even increases slightly at high redox potential. The relative amplitude of the Y-peaks also increases at high redox potential; no radical signal is observed, and a pronounced AEEAAE ESP pattern is detected, indicative for active primary charge separation at the donor side.

To test whether secondary charge separation at the donor side occurs in the RC's in reversed micelles, light-induced cytochrome oxidation was monitored by absorption difference spectroscopy around 555 nm at room temperature. The results are shown in figure 5, and clearly show cytochrome oxidation [30]. The kinetics of the absorption changes

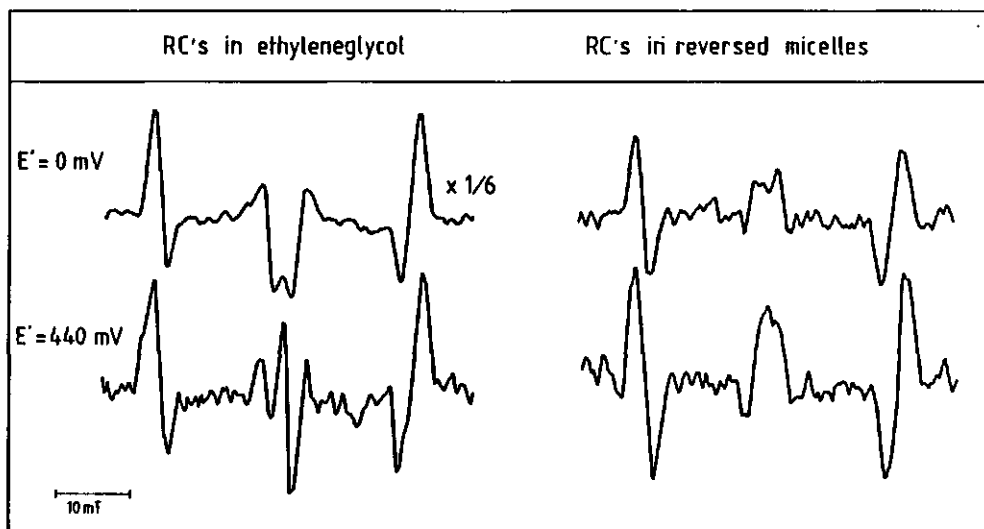


Figure 4.

Effect of redox potential on the EPR electron spin polarization pattern and triplet yield of P^R . Samples were prepared at room temperature in dim light and frozen in the dark. $E' = 0$ mV: 35 mM sodium ascorbate pH 8.0; $E' = 440$ mV: 35 mM potassium ferri/ferrocyanine, pH 8.0. $w_0 = 3.0$ of the reversed micelle solution. Spectra have the same vertical scale (note the reduction factor of the upper left spectrum). EPR settings as in figure 2.

(fig. 5, inset) are almost identical for RC's in AOT/3-MP and in Tris/LDAO solution. Identical absorption changes were found in a sample that was kept at 4°C for 30 days in the dark.

The viscosity and optical birefringence of the AOT/3-MP solution were measured in order to investigate the nature of the observed w_0 effects. It was found that the viscosity steadily increases from 3.0 cp at $w_0 = 0$ to 4.3 cp at $w_0 = 2$, and 9.8 cp at $w_0 = 4$, independent of the presence of the protein complex. No static optical birefringence was observed for w_0 values in the range from 0 to 2.

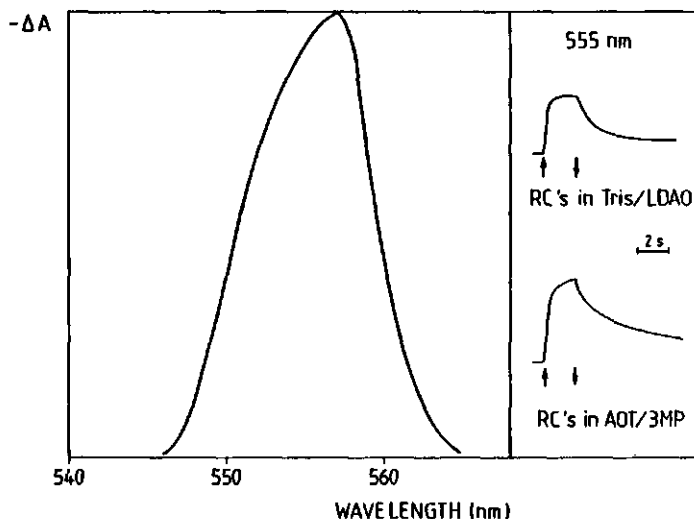


Figure 5.

Absorption difference spectrum of RC's in AOT/3-MP reversed micelles around 555 nm. Conditions: light excitation with an RG780 cut-off filter; room temperature; sodium ascorbate was added to the RC solution. Inset: kinetic traces of the absorption change at 555 nm for RC's in Tris/LDAO solution and in 1.0 M AOT/3-MP, $w_0 = 0.4$.

6.5 DISCUSSION

We have demonstrated the stability and photoactivity of the RC's from *Rps. viridis* in a microemulsion under the condition that w_0 is kept below ca. 0.4 at 0°C and at low temperature (110K) without the necessity of adding any quinone as was reported to be necessary for *Rps. sphaeroides* RC's [11]. In spite of the fact that both components of the reversed micelle solution, AOT and 3-MP, when used separately, inactivate the protein complex very rapidly, a combination of both components has almost no effect on the protein. The developed injection method is very successful and yields reproducible spectroscopic results. It may well be that this technique can also be applied to incorporate other (hydrophobic) proteins into reversed micelle solution, which are otherwise inactivated or denatured.

Light-induced P^R formation and cytochrome oxidation [30] demonstrates that the primary charge separation and charge stabilization at the donor side takes place. A slight difference in the transients of the absorption changes at 555 nm between RC's in Tris/LDAO and RC's in AOT/3-MP was observed (fig.3, inset). These differences indicate partial inactivation of the primary quinone acceptor in AOT/3-MP [11]. This observation is consistent with the shift of the 960 nm band to 920 nm at high w_0 values [26], and the reversal of the Y peaks in the P^R triplet EPR spectrum at high w_0 . Even at a w_0 value of 0.4 the amplitude of the Y-peaks reflect some strain at the quinone acceptor side.

Although the acceptor side seems to be mostly affected by the alien environment, the electron transfer from the reduced intermediary acceptor to the quinone may still occur. To test this possibility the redox potential was raised to a value (440 mV) where the majority of the cytochromes is oxidized (E^0 cyt/cyt $^+$ = 340 mV [28,29]), and at the same time, most of the primary donors are not (E^0 P/P $^+$ = 500 mV [27]). Figure 4 shows that the triplet yield at 440 mV in the ethyleneglycol glass has dropped significantly, due to light-induced P^+Q^- radical formation instead of P^R formation. In contrast, in the reversed micelles the triplet yield is at least equal to that at 0 mV, because apparently no secondary P^+ reduction is necessary to produce P^R . This demonstrates that indeed the electron transfer step from I^- to Q_A is effectively blocked in RC's in the microemulsion, since any accumulation of P^+Q^- during the illumination would have resulted in a decreased triplet yield. Therefore, the quinone acceptor itself must be affected by high w_0 . Nevertheless, the charge separation step ($P^* \rightarrow P^+I^-$) still occurs as the AEEAAE ESP pattern demonstrates. The slightly higher triplet yield at 440 mV as compared to 0 mV in the microemulsion is probably caused by the total absence of rereduction of P^+ within the lifetime of the radical pair P^+I^- (10 - 20 ns) in a blocked forward electron transfer situation.

To understand why the w_0 value is such a crucial factor for the activity of the incorporated RC, the AOT/3-MP solution was studied in

more detail. Because the concentration of the protein is very small (typically 10 μM) as compared to the number of micelles ($\approx 25 \text{ mM}$) at all w_0 values used in our experiments [31], we have verified whether a phase transition of the AOT/3-MP imposes a structural change in the incorporated RC's. Neither the results of the viscosity measurements, nor those of the birefringence point to the occurrence of a phase transition in the range of w_0 values used in our experiments. The increase in viscosity at higher w_0 can be explained by the increase in volume fraction of the microemulsion droplets, due to the increased amount of enclosed water [31]. At the very high detergent concentration which was used, in combination with the very low w_0 values necessary for good stability, the chemical potential of the AOT molecules probably changes drastically upon increasing the w_0 value. This change in chemical potential might explain the observed w_0 dependencies as will be discussed hereafter.

Before the proteins are incorporated into the microemulsion droplets, the protein complex was already solubilized by the detergent LDAO. This detergent was also used in the isolation procedure of the RC's. It is known, that when the anionic SDS is used instead of the non ionic LDAO, the quinone-iron complex is damaged [15], and the AEAEAE ESP pattern of p^R is changed into AEEAAE [21]. AOT is also an ionic detergent, and the effects on the EPR spectra for $w_0 > 0.4$ strongly resemble those obtained after SDS treatment of the protein.

The results summarized in Table 1 show the dependence of the relative triplet yield and ESP pattern on the ionic strength. It indicates that electrostatic forces play an important role in the stability of the incorporated RC, since at high ionic strength charges are shielded in the aqueous phase. From table 1 it is clear that the charge separation, located at the donor side in the RC is stabilized at high ionic strength, as demonstrated by the increased relative triplet yield, whereas the acceptor side is drastically modified, as shown by the pronounced AEEAAE ESP pattern of p^R . At $w_0 = 5$ the AOT/3-MP microemulsion does not form a clear glass at 110 K. Nevertheless, the sodium chloride stabilized RC's showed an enhanced

triplet yield, as compared to RC's at low ionic strength at the same w_0 -value.

On the other hand, for $w_0 > 0.4$, Table 1 shows that both donor and acceptor side are stable at low ionic strength. Increasing the ionic strength does not affect the relative triplet yield, but the amplitude of the γ -peaks decreases in the triplet spectrum, indicating that the magnetic interactions between I^- and Q_A^- , and/or Q^- and Fe^{2+} are reduced. Under these conditions the electron transfer rate from I^- to Q_A^- is not yet affected, otherwise an increase in triplet yield would have been observed. This was probably the case for the intermediate w_0 -values (0.4 - 2.0 in Table 1).

The effects of SDS treatment, and our observations can be understood when the following model is invoked. In aqueous solution the hydrophobic part of the RC is covered with LDAO molecules, which make the surface of this part of the protein also polar. Thus the solubilized protein is completely surrounded by water and ions. Sonication for a short period of the RM solution leaves this water layer intact, whereas water which is not tightly bound to the RC, is captured in microemulsion droplets. At low w_0 values the size of the microemulsion droplets is much smaller than the size of the protein (13 x 7 x 3 nm [32]), and during the sonication several reversed micelles are required to provide the number of detergent molecules necessary to cover the small water layer around the protein [4]. The water layer around the RC is very thin and thus highly structured, so that a high degree of dissociation of the AOT molecules is unlikely. Probably the LDAO molecules around the hydrophobic part of the RC are exchanged with the vast excess of AOT molecules. This situation is depicted in figure 6, left hand part. Thus, the thin water layer around the protein does not change significantly after mixing at low w_0 . In order to understand the observed w_0 dependence, consider that at higher w_0 values the extra water is put in the microemulsion droplets. Then the AOT molecules in these droplets would be in a different environment with respect to those surrounding the protein, and the consequent difference in chemical potential forces water molecu-

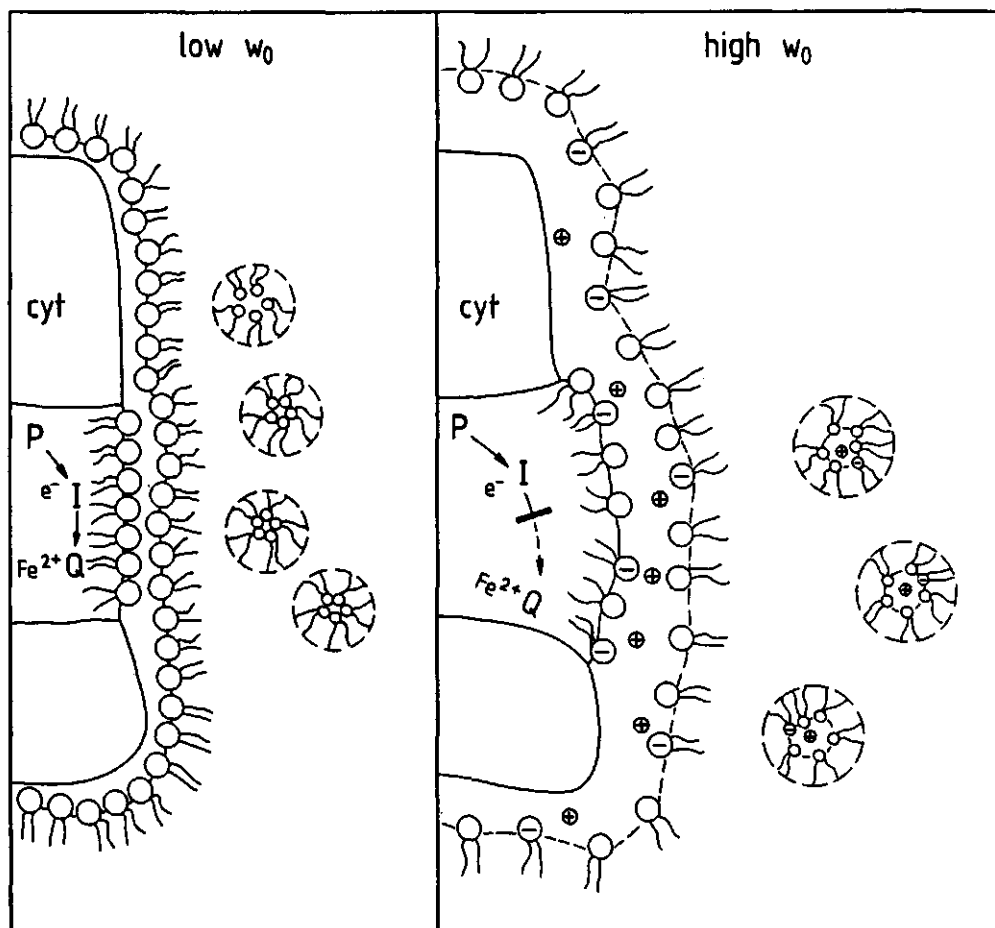


Figure 6.

Schematic model of RC incorporated into an AOT/3-MP microemulsion. For clarity the polar head groups of the AOT molecules are enlarged to a different extent for the AOT molecules surrounding the RC and those within the reversed micelle. The dimensions of the protein moiety and those of the microemulsion droplets are proportional. P. denotes the primary electron donor, I denotes the intermediary electron acceptor, and Q the first quinone acceptor. Left hand side: closely packed AOT/water layer surrounding the protein; right hand side: less structured water layer around the protein. Further explanation is given in the text.

les from the microemulsion droplets into the water layer surrounding the protein. In equilibrium the result is a slightly more liquid-like water layer, allowing increased dissociation of the AOT molecules. The polar head groups of the dissociated AOT molecules which are adsorbed to the protein create a repulsive force which opens the protein structure (fig. 6 right hand part). This environment of the RC's becomes more comparable to that of SDS solubilized RC's in aqueous systems. Apparently, the weakest spot in the LM unit is located at the quinone-iron complex, which is also the most polar group within this unit. This model explains almost all observed effects. However, the pH effect (fig. 3) is not fully understood. At the high detergent concentrations which were used, a change in pH affects the properties of AOT and thus the chemical potential. To explain the observed maximum in figure 3 a single effect might not be sufficient, e.g. the titration of an (AOT-induced) exposed amino acid in the LM moiety may be involved. Although a high ionic strength affects the structure of the microemulsion, its effect can be understood using our model. Clearly the donor side is stabilized. The destabilization of the acceptor side indicates that direct electrostatic interactions between the ions and the acceptor are also involved; not merely the direct effect of the repulsive force leading to the distortion of the protein matrix of the LM complex.

In conclusion, we demonstrated the stability and the photochemical activity of RC's from *Rps. viridis* in relation to the w_0 value of the AOT/3-MP microemulsion. The dependencies on w_0 can be explained qualitatively by considering the chemical potential of the detergent. Further, the RC/microemulsion system exhibits efficient charge separation under controlled conditions and it is a potential candidate as an electron donor in artificial systems. At low w_0 intermediates are produced at ca -100 mV [34] (the Q^- state) with a lifetime of > 10-100 ns. At high w_0 -values charge separation produces intermediates with an $E' = -400$ mV [29] and a lifetime of 10 - 20 ns (I^-) [33], instead of the usual 200 ps [33].

R.M.D. Verhaert, dr. C. Laane, dr. P. Gast and dr. T.J. Schaafsma have considerably contributed to this research, in the framework of a cooperative project supported in part by the Netherlands Technology Foundation contract nr. WTN 33.0559.

We acknowledge useful discussions concerning the protein-detergent interactions with dr. A.M. Cazabat (Paris). PG thanks dr. J. Amesz (Leiden) for the use of the absorption difference spectrophotometer. Mr. Ruud Spruijt assisted in the isolation of RC's.

6.6 REFERENCES

1. Gingras, G. (1978) in *The Photosynthetic Bacteria* (Clayton, R.K. and Sistrom, W.R., eds.) Plenum Press, New York, pp. 119-131.
2. Eicke, H.F. (1982) in *Microemulsions, I* (Dobbs, I.D., ed.) Plenum Press, New York, pp. 17-32.
3. Wolf, R., and Luisi, P.L. (1979) *Biochem. Biophys. Res. Comm.* 89, 209-217.
4. Chatenay, D., Urbach, W., Cazabat, A.M., Vacher, M., and Waks, M. (1985) *Biophys. J.* 48, 893-898.
5. Luisi, P.L., Meier, P., Imre, V.E., and Pande, A. (1984) in *Reverse Micelles* (Luisi, P.L., and Straub, B.E., eds.) Plenum Press, New York, pp. 323-358.
6. Martinek, K., Levashov, A.V., Klyachko, N.L., Pantin, V.I., and Berenzin, I.V. (1981) *Biochim. Biophys. Acta* 657, 277-294.
7. Hilhorst, R., Laane, C., and Veeger, C. (1982) *Proc. Natl. Acad. Sci. (USA)* 79, 3927-3930.
8. Hilhorst, M.H. (1984) Thesis, Agricultural Univ. Wageningen, The Netherlands.
9. Gierasch, L.M., Thompson, K.F., Lacy, J.E., and Rockwell, A.L. (1984) in *Reverse Micelles* (Luisi, P.L., and Straub, B.E., eds.) Plenum Press, New York, pp. 265-277.
10. Delahodde, A., Vacher, M., Nicot, C., and Waks, M. (1984) *FEBS*

- Lett. 172, 343-347.
11. Schönfeld, M., Montal, M., and Feher, G. (1980) *Biochemistry* 19, 1535-1542.
 12. Deisenhofer, J., Epp, O., Miki, K., Huber, R., and Michel, H. (1984) *J. Mol. Biol.* 180, 385-398.
 13. Deisenhofer, J., Epp, O., Miki, K., Huber, R., and Michel, H. (1985) *Nature* 318, 618-624.
 14. Hoff, A.J. (1982) in *Molecular Biology, Biochemistry and Biophysics* vol. 35 (Fong, F.K., ed.) Springer Verlag, Berlin, pp. 80-151.
 15. Prince, R.C., Tiede, D.M., Thornber, J.P., and Dutton, P.L. (1979) *Biochim. biophys. Acta* 462, 467-490.
 16. Hoff, A.J. (1982) in *Tripet State ODMR Spectroscopy* (Clarke, R.H., ed.) John Wiley & Sons, New York, pp. 367-425.
 17. Van Wijk, F.G.H., Gast, P., and Schaafsma (1986) *FEBS Lett.* 206, 238-242.
 18. Thurnauer, M.C., Katz, J.J., and Norris, J.R. (1975) *Proc. Natl. Acad. Sci. (USA)* 72, 3270-3274.
 19. Blankenship, R.E., Schaafsma, T.J., and Parson, W.W. (1977) *Biochim. Biophys. Acta* 449, 447-467.
 20. Schaafsma, T.J., Kleibeuker, J.F., Platenkamp, R.J., Geerse, P. (1976) in *Molecular Spectroscopy of Dense Phases*, Proc. 12th Eur. France, 1875, pp. 491-494.
 21. Van Wijk, F.G.H., Gast, P., and Schaafsma, T.J. (1986) *Photo-biochem. Photobiochem. Photobiophys.* 11, 95-100.
 22. Den Blanken, H., and Hoff, A.J. (1982) *Biochim. Biophys. Acta* 681, 365-374.
 23. Anon. (1966) *Moisture determination by the Karl Fisher Reagent*, 2nd ed., Dorset British Drug House, Ltd., Dorset, England.
 24. Heyman, M.G.J., Horikx, J.J.L., Nauta, H., and Levine, Y.K. (1984) *Radiat. Phys. Chem.* 23, 661-666.
 25. Visser, J.W.M. (1975) Thesis, Univ. of Leiden, The Netherlands.
 26. Debus, R.J., Feher, G., and Okamura, M.Y. (1985) *Biochemistry* 24, 2488-2500.

27. Prince, R.C., and Dutton, P.L. (1976) *Arch. Biochem. Biophys.* 172, 329-334.
28. Thornber, J.P., and Olson, J.M. (1971) *Photochem. Photobiol.* 14, 329-341.
29. Prince, R.C., Leigh, J.S., and Dutton, P.L. (1976) *Biochim. Biophys. Acta* 440, 622-636.
30. Case, G.D., Parson, W.W., and Thornber, J.P. (1970) *Biochim. Biophys. Acta* 223, 122-128.
31. Day, R.A. Robinson, B.H., Clarke, J.M.R., and Doherty, J.V. (1979) *J. Chem. Soc. Faraday Trans. I*, 75. 132-139.
32. Deisenhofer, J., Michel, H., and Huber, R. (1985) *Trends Biochem. Sci.* 6, 243-248.
33. Holten, D., Windsor, M.W., Parson, W.W., and Thornber, J.P. (1978) *Biochim. Biophys. Acta* 501, 112-126.
34. Cogdell, R.J., and Crofts, A.R. (1972) *FEBS Lett.* 27, 176-178.
35. Deisenhofer, J. (1986), Oral presentation at CECAM Workshop on Structure and Dynamics of Photoreaction centers in Photosynthesis, 1986, Orsey, France.

SUMMARY

In this work the temperature dependence of the lineshape, and more specifically, the electron spin polarization pattern of the $\Delta m = \pm 1$ triplet EPR (Electron Paramagnetic Resonance) spectra from several photosynthetic purple bacteria has been investigated.

In Chapter I a general introduction is presented to photosynthesis, focussing on the structure of the protein complex, known as the reaction center (RC), and the processes in this RC. All investigations presented in this work are related to processes and magnetic interactions within this RC. At the end of Chapter I the triplet state (P^R) of the primary electron donor (P) is introduced, and also the way it is generated, i.e. in sufficiently high magnetic fields via the radical pair mechanism.

In Chapter II the theoretical background is presented to support the explanations given in later chapters in order to understand the experimental results. First it is proven that the observed temperature dependence of the triplet lineshape cannot be caused by intramolecular spin-lattice relaxation. Then the radical pair state P^F is generalized to a three electron spin state, coupled to the paramagnetic Fe^{2+} ion in the RC. Solving the secular equations exactly for a Hamiltonian which contains all relatively strong magnetic interactions, the time-evolution of P^F is obtained, resulting in the break-down of the exclusive $S-T_0$ mixing, which is characteristic for the radical pair mechanism. The effect of spin transitions on the Fe^{2+} is considered phenomenologically. The theory developed in this Chapter is used, and in some respects extended in Chapter V.

In Chapter III time-resolving equipment and experimental techniques are described, as far as employed in this work. The design and construction of a high-gain, broad-band tunable pulsed dye laser is reported. Furthermore, a novel time-resolving EPR tech-

nique is described, which is based on broad-band phase-sensitive detection. The technique is able to detect EPR transients with frequency components from 0 Hz - 1 MHz and a low initial S/N ratio, which makes it very suitable for the purpose of detecting the time-evolution of the triplet state in photosynthetic RC's. Furthermore, a means is described to reduce the light-induced transient artefact distorting time-resolved EPR signals, because of the high-power laser flash.

In Chapter IV the results are presented from a number of studies on the lineshape of EPR spectra, reflecting steady state populations of P^R , as a function of: i) temperature, ii) redox potential, iii) SDS incubation, or iv) modification of the electron acceptor side in the RC. The results were interpreted as follows: The lineshape reflects the population distribution over the spin levels of P^R . This distribution is determined by the processes in the precursor state P^F . The relaxation processes of the paramagnetic Fe^{2+} are transferred by the unpaired electron spin of the reduced primary quinone. The latter is magnetically coupled to the familiar radical pair in the RC. Thus the primary quinone acts as a relaxation carrier within P^F .

In Chapter V the explanation presented in the preceding Chapter, is considered with respect to its time-evolution. Time-resolved EPR measurements established that the (temperature dependent) lineshape, as observed under steady-state conditions, is already present in the first microsecond after excitation at 100 K. This indicated that the processes within P^F favour recombination of P^+ with I^- (I denotes the intermediary acceptor) into P^R into a T_+ or T_- spin configuration for magnetic fields parallel to the Y triplet axis of P^R . Using the theoretical results of Chapter II, the preferential T_{\pm} recombination probability was qualitatively explained.

Once P^R has been generated, the time-evolution of the EPR triplet signals shows a remarkable temperature dependence. Spin-lattice relaxation seems to be dependent on temperature only for $T < 40$ K. A model is proposed to explain this unusual temperature dependence. In this model transitions from P^R back into P^F are invoked. The values of the P^R decay rate constants at 4 K are found to be in-

dependent of temperature up to at least 120 K. Furthermore, the relaxation rate as measured as an increased triplet decay is found to be proportional with the square of the temperature.

In Chapter VI the use of the lineshape of P^R triplet EPR spectra was demonstrated in a series of experiments in which the RC's from Rhodopseudomonas viridis were incorporated into a reversed micellar solution (water in oil). One of the results is that under very strict conditions the RC maintains its native structure. Damage to the acceptor side (which turned out to be the most fragile part of the RC) is reflected by pronounced changes in the lineshape of the EPR spectrum, monitored at ~ 100 K.

SAMENVATTING

In dit werk is de temperatuursafhankelijkheid onderzocht van de lijnvorm, en meer in het bijzonder, van het electron spin polarisatie patroon, van de $\Delta m = \pm 1$ triplet EPR (Electron Paramagnetische Resonantie) spectra afkomstig van verscheidene fotosynthetiserende purper bacteriën.

In Hoofdstuk I wordt een algemene inleiding gegeven op de fotosynthese. Speciaal de structuur van een complex van eiwitten, bekend als het reactiecentrum (RC), en de processen die zich daarin afspelen worden beschouwd. Alle onderzoeken die in dit werk gepresenteerd zijn, hebben te maken met die processen en met magnetische interacties die in dit RC plaats hebben. Aan het eind van Hoofdstuk I wordt de triplet toestand (P^R) van de primaire elektron donor (P) geïntroduceerd, alsmede de manier waarop deze toestand wordt gemaakt; nl. via het radikaal-paar mechanisme, mits er een voldoende groot extern magnetisch veld aanwezig is.

In Hoofdstuk II wordt de theoretische achtergrond gegeven die nodig is om de verklaringen van experimentele resultaten, die in latere hoofdstukken aan de orde komen, te ondersteunen. Eerst wordt bewezen dat de gevonden temperatuursafhankelijkheid van de triplet lijnvorm niet veroorzaakt kan worden door intramoleculaire spin-rooster relaxatie. Vervolgens wordt de radikaal-paar toestand (P^F) generaliseerd tot een radikaal-trio, n.l. een drie elektron toestand, gekoppeld met het paramagnetische Fe^{2+} ion in het RC.

De seculaire vergelijkingen worden exact opgelost voor een Hamiltoniaan die alle relatief sterke magnetische wisselwerkingen beschrijft. Daarmee kan het gedrag van P^F in de tijd worden beschreven. Dit resulteert hierin, dat de exclusieve S- T_0 menging, karakteristiek voor het radikaal-paar mechanisme, niet meer geldt. Het effect van spin overgangen, gelokaliseerd op het Fe^{2+} , op P^F wordt fenomenolo-

gisch beschouwd. De theorie die in dit Hoofdstuk ontwikkeld is, wordt gebruikt en enigszins uitgebreid in Hoofdstuk V.

In Hoofdstuk III worden tijdsoplossende apparatuur en experimentele technieken beschreven (voor zover toegepast in dit werk). Er wordt een beschrijving gegeven van het ontwerp en de bouw van een breedbandige, afstelbare gepulste kleurstof laser. Verder wordt een nieuwe tijdsoplossende EPR techniek beschreven. Deze techniek is gebaseerd op breedbandige fase-gevoelige detectie. Er kunnen kortlevende EPR signalen (transients) met frekwentiekomponenten van 0 Hz - 1 MHz en met lage initiële S/N verhouding mee gedetecteerd worden. Dit maakt deze techniek geschikt voor o.a. het detecteren van triplet signalen van RC's.

Verder wordt in dit Hoofdstuk een methode beschreven om de lichtgeïnduceerde stoorsignalen van de hoogvermogen laserflits in de EPR trilholtte te onderdrukken.

In Hoofdstuk IV worden de resultaten gepresenteerd van een aantal studies betreffende de veranderingen in lijnvorm in EPR spectra van P^R in steady-state als functie van: i) temperatuur, ii) redox potentiaal, iii) SDS incubatie, of iv) modificatie van de elektron acceptorkant van het RC. De resultaten werden als volgt geïnterpreteerd: De lijnvorm weerspiegelt de bevolkingsverdeling over de spinnivo's van P^R . Deze verdeling wordt bepaald door de processen die zich afspelen in de precursor-toestand P^F . De spin-relaxatieprocessen gelokaliseerd op het paramagnetische Fe^{2+} worden doorgegeven door de ongepaarde elektronspin van het gereduceerde primaire chinon. Deze laatste is magnetisch gekoppeld met het bekende radikaal-paar in het RC; aldus opereert het primaire chinon als een relaxatie-'carrier' binnen P^F .

In Hoofdstuk V wordt de hierboven gegeven verklaring beschouwd m.b.t. het gedrag in de tijd van P^R . Tijdsopgeloste EPR metingen toonden aan dat de (temperatuursafhankelijke) lijnvorm, zoals die reeds was waargenomen onder steady-state condities, al aanwezig is in de eerste microseconde na excitatie bij 100 K. Dit gaf aan dat de processen die zich binnen P^F afspelen, leiden tot een preferentiële rekombinatie van P^+ met I^- (I staat voor de intermediaire acceptor)

tot p^R , in een T_+ , of T_- spinconfiguratie, d.w.z. bij magneetvelden evenwijdig aan de triplet Y-as. Deze voorkeur voor T_+ en T_- kon kwalitatief worden verklaard m.b.v. de resultaten uit Hoofdstuk II. Zodra p^R ontstaan is, toont het tijdsverloop van de EPR signalen van p^R een opmerkelijke temperatuursafhankelijkheid. De spin-rooster relaxatie snelheid lijkt slechts afhankelijk te zijn van de temperatuur voor $T < 40$ K. Er wordt een model voorgesteld dat deze ongebruikelijke temperatuursafhankelijkheid kan verklaren. In dit model zijn overgangen van p^R terug naar p^F betrokken.

De waarden van de p^R -snelheidskonstanten bij 4 K zijn onafhankelijk van de temperatuur tot tenminste 120 K.

In Hoofdstuk VI tenslotte, wordt het nuttig gebruik van de lijnvorm van p^R triplet EPR spectra gedemonstreerd in een reeks experimenten waarin de RC's van Rhodopseudomonas viridis werden geïncorporeerd in omgekeerde micellaire oplossingen (water in olie). Eén van de resultaten is dat slechts onder strikte condities het RC zijn native structuur behoudt. Beschadigingen aan de acceptorkant (dit blijkt de zwakste plaats van het RC te zijn) zijn waarneembaar als een duidelijke verandering in de lijnvorm van het p^R EPR spectrum bij ~ 100 K.

CURRICULUM VITAE

Fred van Wijk werd 24 maart 1956 geboren te Apeldoorn. In 1974 legde hij het eindexamen Atheneum-B af aan de Rijksscholengemeenschap 'Noord-Kennemerland' in Alkmaar. Na een korte periode Industriële Vormgeving aan de Technische Hogeschool in Delft te hebben gestudeerd, begon hij in 1975 aan de studie Moleculaire Wetenschappen aan de Landbouwhogeschool te Wageningen.

Zijn afstudeervakken waren: Theoretische Natuurkunde (bijvak), Moleculaire Fysica (hoofdvak) en Biochemie (hoofdvak). Zijn praktijk-tijd bracht hij door in Groot-Brittanie aan het laboratorium van Shell-Research in Sittingbourne, bij de afdeling 'Fermentation and Microbiology'.

In 1982 studeerde hij af aan de Landbouwhogeschool en begon direct daarna bij de vakgroep Moleculaire Fysica aan het onderzoek dat tot dit werk zou leiden.